PAUL SCHERRER INSTITUT

PSI Bericht Nr. 05-03
February 2005
ISSN 1019-0643

Nuclear Energy and Safety Research Department
Laboratory for Waste Management

Modelling the Transport of Solutes and Colloids in the Grimsel Migration Shear Zone

Georg Kosakowski and Paul Smith

PAUL SCHERRER INSTITUT

PSI Bericht Nr. 05-03
February 2005
ISSN 1019-0643

Nuclear Energy and Safety Research Department
Laboratory for Waste Management

Modelling the Transport of Solutes and Colloids in the Grimsel Migration Shear Zone

Georg Kosakowski, PSI, Switzerland
Paul Smith, SAM, United Kingdom

Paul Scherrer Institut
5232 Villigen PSI
Switzerland
Tel. +41 (0)56 310 21 11
Fax +41 (0)56 310 21 99
www.psi.ch

Preface

The Laboratory for Waste Management of the Nuclear Energy and Safety Research Department at the Paul Scherrer Institut is performing work to develop and test models as well as to acquire specific data relevant to performance assessments of planned Swiss nuclear waste repositories. These investigations are undertaken in close co-operation with, and with the partial financial support of, the National Cooperative for the Disposal of Radioactive Waste (Nagra). The present report is issued simultaneously as a PSI Bericht and a Nagra Technical Report.

Abstract

This report describes modelling of the transport of solutes and colloids in an experimental system comprising an artificial dipole flow field in a water-conducting shear zone at Nagra's Grimsel Test Site (GTS) in the central Swiss Alps. The modelling work forms part of the Colloid and Radionuclide Retardation Project (CRR), which includes a series of field transport experiments and a supporting laboratory programme, as well as modelling studies. Four independent groups representing different organisations or research institutes have conducted the modelling, with each group employing its own modelling approach or approaches. Only the work conducted at the Paul Scherrer Institute (PSI) is described in the present report.

Bentonite, which is widely considered as a potential backfill material for a range of radioactive and chemotoxic wastes, could conceivably provide a source of colloids that could then influence the transport of radionuclides released from a geological repository for radioactive waste. The main objective of CRR is to enhance understanding of the *in situ* retardation of radionuclides in the presence of bentonite colloids, in a system analogous to the near-field/geosphere interface of a geological repository.

The field transport experiments were carried out by injecting various cocktails of tracers, some of which included bentonite colloids, into the injection borehole of the dipole and measuring the resulting breakthrough curves. Modelling work was carried out in order to assist in the planning of the main experimental runs and to contribute to the interpretation of the results. Three model variants are used in the present study, namely a 1-D advection-dispersion model, similar to that developed in support of the earlier GTS Migration Experiment (MI), a 2-D advection-dispersion model, and a non-Fickian dispersion model: the CTRW (continuous time random walk) model. The 1-D and 2-D models treat dispersion as a diffusion-like process that obeys Fick's laws. They also include the retardation mechanisms of matrix diffusion of solutes and solute sorption on matrix pore surfaces. Colloids are excluded from matrix pores in all the model variants. The CTRW model allows a more general treatment of dispersion, but does not currently include matrix diffusion, and so was only applied to the transport of colloids.

The modelling of preliminary tests carried out in advance of the main CRR experimental runs showed that the 1-D and 2-D advection-dispersion models with matrix diffusion provide similarly good fits for tracers conveyed as aqueous species, using reasonable and consistent sets of parameter values. They were less successful at modelling colloid breakthrough, and various explanations for this have been considered. Of these, the occurrence of non-Fickian dispersion is considered the most likely. The CTRW model, which allows for non-Fickian dispersion, indeed provides an adequate fit in the case of colloids with a consistent set of parameters.

On the basis of the modelling of the preliminary tests, predictions of the breakthrough of Am, Pu, Np, U and Cs, both with and without the addition of bentonite colloids to the injection cocktail, were made for the main experimental runs in advance of the experiments being carried out. The experimental measurements confirm the model assumption that at least part of the injected inventories of Am, Cs, Pu and Th migrates in association with bentonite colloids. Furthermore, discrepancies between predictions and measurements that Am, Pu and Th are transported in colloidal form, even when no bentonite colloids are added to the injection cocktail. The addition of bentonite colloids, however, increases the recovery of these tracers. The characterisation of colloids in the injection cocktails, which was not available at the time that the model predictions were made, enables improved agreement to be obtained between model calculations and measured breakthrough curves.

The CRR experiment and the present modelling study have a number of limitations. For example, there is the possibility that non-Fickian dispersion affects the transport of solutes as well as colloids. It is not, however, possible to discriminate between the impact of this non-Fickian dispersion and matrix diffusion effects by modelling the breakthrough curves. If non-Fickian dispersion of solutes takes place, then this has implications for the derivation of parameter values for safety assessment (and especially sorption coefficients) from field tracer transport experiments. In particular, values derived using advection-dispersion models with matrix diffusion and with dispersion modelled using Fick's laws need to be viewed with caution.

The modelling approaches used in the present study may not be directly applicable to safety assessment problems and the direct implications of the results of this study for safety assessment are limited. It can, however, be said that the study has demonstrated the high degree of mobility of bentonite and other colloids in a system that is at least in some ways comparable to those of interest in safety assessment, and has shown that bentonite colloids can *at least potentially* affect the transport of some safety relevant radionuclides over longer temporal and spatial scales than those addressed here.

Zusammenfassung

Dieser Bericht beschreibt die Modellierung von Transportversuchen mit Kolloiden und gelösten Stoffen in einem künstlichen Dipol-Fliessfeld innerhalb einer wasserführenden Scherzone des Grimsel-Felslabors der Nagra in den zentralen Alpen. Die Feldversuche wurden wurden ergänzt durch ein experimentelles Laborprogramm und Modellierungsstudien im Rahmen des „Colloid and Radionuclide Retardation Project" (CRR). Vier Modellierungsgruppen verschiedener Organisationen und Forschungsinstitute trugen jeweils mit einem anderen Ansatz zur Modellierung bei. Dieser Bericht beschreibt nur die Modellrechnungen die am Paul Scherrer Institut (PSI) durchgeführt wurden.

Bentonit wird als Material zur Umhüllung von radioaktiven und toxischen chemischen Abfällen in Betracht gezogen. Es könnte eine Quelle für Kolloide sein, die den Transport von Radionukliden aus einem geologischen Tiefenlager für radioaktive Abfälle beeinflussen. Das Hauptziel des CRR-Projekts war deshalb ein verbessertes Verständnis der Retardierung von Radionukliden in der Anwesenheit von Bentonit-Kolloiden in einem System, das vergleichbar ist mit der Nahfeld/Geosphären Grenze eines geologischen Endlagers.

Bei den Feldexperimenten wurden Mischungen aus Tracern, bei einigen Versuchen zusammen mit Bentonit-Kolloiden, in das Injektionsbohrloch des Dipols eingebracht und die resultierenden Durchbruchskurven im Extraktionsbohrloch wurden aufgezeichnet. Die Modellierungsarbeiten sollten einerseits die Planung dieser Experimente unterstützen und andererseits zur Auswertung der Ergebnisse beitragen. Drei Modellvarianten wurden in der vorliegenden Studie eingesetzt: ein eindimensionales Advektions-Dispersions Modell, ähnlich zu dem Modell, das schon früher im Rahmen des GTS Migrationsexperimentes (MI) entwickelt wurde, ein zweidimensionales Advektions-Dispersions Modell und das „continuous time random walk" (CTRW) Modell. Die ein- und zweidimensionalen Modelle behandeln die Dispersion als einen der Fickschen Diffusion äquivalenten Prozess, während das CTRW-Modell auch „Nicht-Ficksche" Diffusion beschreiben kann. Weiterhin werden, allerdings nur bei den ein- und zweidimensionalen Modellen, als Retardierungsmechanismen die Diffusion von gelösten Stoffen in eine poröse Gesteinsmatrix (Matrixdiffusion) und die Sorption an den Oberflächen der Poren in der Gesteinsmatrix berücksichtigt. Für die Kolloide wird in allen Modellvarianten angenommen, dass Sie nicht in die poröse Gesteinsmatrix diffundieren. Das CTRW Modell erlaubt eine allgemeinere Berücksichtigung der Dispersion, zur Zeit jedoch noch keine explizite Berücksichtigung der Matrixdiffusion. Es wurde deshalb nur für die Berechnung des Kolloidtransports eingesetzt.

Bei der Modellierung einiger Vorversuche, die als Vorbereitung für die beiden CRR Injektionsversuche durchgeführt wurden, ergaben sowohl die eindimensionalen, als auch die zweidimensionalen Advektions-Dispersions-Matrixdiffusions Modelle eine gleichwertig gute Beschreibung der experimentellen Durchbruchskurven der gelösten Stoffe mit einem sinnvollen und konsisten Satz an Materialparametern. Beide Modelle waren weniger erfolgreich in der Beschreibung der Durchbruchskurven der Kolloide. Verschiedene Erklärungen für dieses Phänomen wurden untersucht. Das Auftreten eines Nicht-Fickschen Transports der Kolloide wird als am wahrscheinlichsten betrachtet. Da das CTRW-Modell den Nicht-Fickschen Transport explizit berücksichtigt, ermöglicht es eine sehr gute Beschreibung der Kollid-Durchbrüche mit einem konsistenten Satz an Materialparametern.

Ausgehend von den Vorversuchen wurden Vorhersagen für den Durchbruch von Am, Pu, Np, U and Cs in den Hauptversuchen vorgenommen, sowohl mit, als auch ohne Zusatz von Bentonit-Kolliden im Injektionscocktail. Die experimentellen Messungen bestätigten die Modell-

annahme, dass zumindest ein Teil des Inventars an Am, Cs, Pu und Th zusammen mit den Bentonit-Kolloiden transportiert wurde. Darüber hinaus zeigen die Unterschiede zwischen Vorhersage und Messung, das Am, Pu und Th in kolloidaler Weise transportiert wurden, auch wenn keine Bentonit-Kollide im Injetkonscocktail vorhanden waren. Das Zufügen von Bentonit-Kolloiden zum Injektionscocktail erhöhte allerdings die Rückgewinnung dieser Tracer. Die Berücksichtigung der Charakterisierung der Kolloide im Injecktionscocktail, die zum Zeitpunkt der Vorhersageerstellung noch nicht vorlag, erhöht die Übereinstimmung zwischen den Modellrechnungen und den gemessenen Durchbruchskurven.

Das CRR Experiment und die in dieser Studie beschriebene Modellrechnungen zeigen eine Reihe von Beschränkungen. Es ist zum Beispiel möglich, dass sowohl der Transport von gelösten Stoffen, als auch der von Kolloiden von Nicht-Fickscher Dispersion beeinflusst wird. Jedoch ist es nicht möglich die Diffusion in eine poröse Gesteinsmatrix (Matrixdiffusion) von Nicht-Fickscher Dispersion nur durch die Modellierung der Durchbruchskurven zu unterscheiden. Wenn Nicht-Ficksche Dispersion auch den Transport von gelösten Stoffen beeinflussen sollte, hat das auch Auswirkungen auf die Ableitung der Materialparameter für Sicherheitsanalysen (speziell Verteilungskoeffizienten) aus Transportversuchen. Deshalb sind Parameter, die auf Advektions-Dispersions-Matrixdiffusions-Modellen beruhen und unter Anwendung des Fickschen Gesetzes bestimmt wurden, mit Vorsicht zu betrachtet.

Die in dieser Studie angewendeten Modellansätze und auch die beschriebenen Ergebnisse sind nicht direkt für Rechnungen im Rahmen von Sicherheitsanalysen anwendbar. Es wurde jedoch gezeigt, daß die Mobilität von (Bentonit-) Kolloiden in der Scherzone zumindest vergleichbar ist mit der Mobilität in Systemen, die für Sicherheitsanalysen relevant sind. Bentonit-Kolloide können *zumindest potentiell* den Transport von Radionukliden auch über längere Entfernungen und Zeiträume beschleunigen.

Résumé

Ce rapport décrit la modélisation du transport des solutés et des colloïdes dans un système expérimental qui comporte un champ d'écoulement généré par un dipôle artificiel dans une zone de cisaillement conductrice d'eau et qui fut mis en place au Laboratoire Souterrain de Grimsel (GTS Nagra) au milieu des Alpes suisses. Le travail de modélisation fait partie du projet Retardement des Colloïdes et des Radionucléides (CRR); celui-ci comprend une série d'expériences de terrain, des études complémentaires en laboratoire, ainsi que des exercices de modélisation. Quatre groupes indépendants représentant différentes organisations ou instituts de recherche ont contribué à la modélisation, chaque groupe employant sa/ses propre(s) approche(s). Seul le travail mené à l'Institut Paul Scherrer (PSI) est décrit dans le présent rapport.

La bentonite est fréquemment considérée comme matériau de remblaiement pour les déchets radioactifs et chimiques. Hors ce même matériau pourrait être la source de colloïdes et affecter le transport des radionucléides issus d'un dépôt géologique pour déchets radioactifs. Le projet CRR a pour but principal de mieux comprendre le retardement des radionucléides *in situ*, en présence de colloïdes de bentonite, dans un système analogue à celui qu'on trouve dans un dépôt géologique, à l'interface du champ proche et de la géosphère.

Les expériences de transport ont été réalisées en injectant différents cocktails de traceurs, dans la tige d'injection du dipôle et en mesurant les courbes de percée résultantes ; certains de ces cocktails comprenaient des colloïdes de bentonite. Les exercices de modélisations ont d'une part accompagné la planification des expériences principales, d'autre part ils ont contribué à l'interprétation des résultats. Trois types de modèles ont été utilisés dans la présente étude, à savoir un modèle 1-D d'advection-dispersion similaire à celui développé antérieurement pour l'expérience de Migration GTS (MI), un modèle 2-D d'advection-dispersion, et un modèle de dispersion non fickienne CTRW (continuous time random walk). Les modèles 1-D et 2-D traitent la dispersion comme un processus de diffusion obéissant à la loi de Fick ; ils considèrent également la diffusion des solutés dans la matrice ainsi que la sorption des solutés à la surface de la matrice poreuse comme mécanismes de retardement. Dans tous les trois modèles les colloïdes n'ont pas accès à la matrice poreuse. Quant au modèle CTRW, il permet de traiter la dispersion de manière plus générale, mais il ne considère pas, présentement, la diffusion dans la matrice ; il n'a donc été appliqué qu'au transport des colloïdes.

Lors de la modélisation des tests préliminaires qui ont servi à la préparation des principales expériences du projet CRR, les modèles 1-D et 2-D d'advection-dispersion comprenant la diffusion dans la matrice ont bien su reproduire l'évolution des traceurs transportés comme espèces aqueuses en utilisant un set de paramètres raisonnable et consistant. La percée des colloïdes, par contre, n'a pas pu être simulée de façon satisfaisante avec ces mêmes modèles. Différentes explications ont été proposées, parmi elles, la dispersion non fickienne semble la plus probable. En effet le modèle CTRW capable de simuler la dispersion non fickienne reproduit adéquatement le transport des colloïdes avec un set de paramètres consistant.

Grâce aux exercices de modélisation préliminaires, les courbes de percée de l'Am, du Pu, du Np, de l'U et du Cs obtenues lors des expériences principales ont pu être prédites pour les deux cas de l'addition ou non de colloïdes de bentonite au cocktail d'injection. Les mesures expérimentales confirment l'hypothèse du modèle, à savoir qu'au moins une partie des inventaires de l'Am, du Cs, du Pu et du Th injectés migre en association avec les colloïdes de bentonite. Les écarts entre prédictions et mesures révèlent, de plus, que l'Am, le Pu et le Th sont transportés sous forme de colloïdes, même lorsqu' aucun colloïde de bentonite n'a été ajouté au

cocktail d'injection. L'addition de colloïdes de bentonite augmente pourtant la récupération de ces traceurs. La caractérisation des colloïdes dans les cocktails d'injection qui n'était pas disponible au moment des prédictions a même permis d'affiner le modèle et d'ajuster les calculs aux courbes de percée mesurées.

Toutefois, l'expérience CRR et la présente étude de simulation comptent un certain nombre de limitations. Il est par exemple possible que la dispersion non fickienne affecte le transport des solutés comme celui des colloïdes. La modélisation des courbes de percée ne permit pas de discriminer entre l'effet de la dispersion non fickienne et celui de la diffusion dans la matrice. Si effectivement il y a dispersion non fickienne, la valeur des paramètres qui ont été déduits pour l'analyse de sûreté à partir des expériences de traçage s'en trouvent affectés (spécialement les coefficients de sorption). C'est pourquoi il faut considérer avec une précaution particulière les valeurs qui ont été déduites de modèles d'advection-dispersion s'ils considèrent la diffusion dans la matrice et la dispersion fickienne.

Les approches de modélisation utilisées dans la présente étude ne sont pas directement applicables à des questions d'analyse de sûreté et les implications directes des résultats de cette étude pour l'analyse de sûreté sont limitées. On peut cependant dire que l'étude a démontré que la bentonite et d'autres colloïdes pouvaient être très mobile dans un système pour le moins comparable à ceux qui sont considérés pour l'analyse de sûreté. De cette étude il ressort également que les colloïdes de bentonite *pourraient possiblement* affecter le transport des radionucléides relevants pour la sûreté sur des échelles temporelle et spatiale plus étendues que celles étudiées ici.

Table of Contents

List of Tables

List of Figures

1 Introduction

1.1 Scope and purpose of the present work

The present document provides a description of modelling work carried out by the Paul Scherrer Institute (PSI) to analyse *in situ* experiments carried out at the Grimsel Test Site (GTS) within the framework of the Colloid and Radionuclide Retardation Project (CRR). The modelling work takes as its starting point earlier modelling studies carried out by PSI in the context of the GTS Migration Experiment (MI), and develops and modifies the earlier models to take account of the effects of bentonite colloids added to the experimental radionuclide injection cocktails. A number of alternative modelling approaches have been developed for some aspects of the system. In some cases, it was possible to make model predictions in advance of particular experimental runs in order to check the feasibility of the planned experiments and to test particular modelling hypotheses.

1.2 Background to CRR

A major field of research over the last few decades has been the development and *in situ* testing of predictive models for the transport of radionuclides in fractured rock. The joint Nagra (Swiss National Cooperative for the Disposal of Radioactive Waste), JNC[1] (Japan Nuclear-Cycle Research Institute, Japan) and PSI Migration Experiment (MI) at the GTS, Switzerland (Frick et al., 1992; Smith et al., 2001) and the international TRUE experiments at Äspö, Sweden (Winberg et al., 2000) are prominent examples.

At the GTS, work on the development and *in situ* testing of predictive models has been ongoing for more than 15 years. MI concentrated on the characterisation of a shear zone in crystalline rock and basic investigations of the transport of non-sorbing and sorbing solute tracers in dipole flow fields (see McKinley et al., 1988; Alexander et al., 1992, 2003a; Frick et al., 1992; Smith et al., 2001 for details). More recently, Nagra and JNC began the Excavation Experiment (EP), described in detail in Alexander et al. (1996, 2003b), Ota et al. (2001) and Möri (2001), which focused on the detailed investigation of the structure of the shear zone. Breakthrough curves were recorded in the same way as in MI, using a cocktail of various radionuclide tracers. The tracer experiments were stopped before all of the injected radionuclides were completely recovered and a specially developed resin was injected into the shear zone to stabilise the rock and prevent disturbance of the *in situ* radionuclide distribution. Subsequently, this part of the shear zone was excavated with a triple-barrel drilling technique. The core analysis provided 3-D information on the small-scale network of fractures in the shear zone. Although it was known that the shear zone is highly heterogeneous, the main result of the core analyses was that open channels in the fractures control water flow to a very high degree. Furthermore, penetration of radionuclides into the porous rock matrix within and around the fractures was confirmed (Möri, 2001, Möri et al., 2004).

CRR can be viewed as a continuation of MI and EP insofar that it uses a similar experimental set up in order to investigate the influence of bentonite colloids on radionuclide transport through the shear zone. The project is conducted in the framework of Phase V of the GTS investigations and the funding partners are ANDRA[2] (France), BMWA/FZK-INE[3] (Germany),

---

1 Formerly PNC (Power Reactor and Nuclear Fuel Development Corporation)

2 Agence Nationale pour la Gestion des Déchets Radioactifs, Fontenay-aux-Roses, France

3 Bundesministerium für Wirtschaft und Arbeit (formerly BMWi), Forschungszentrum Karlsruhe, Institut für Nukleare Entsorgung, Karlsruhe, Germany

ENRESA[4] (Spain), JNC (Japan), Nagra (Switzerland) and the US DoE/SNL[5] (USA). The main objective of CRR is to enhance understanding of the *in situ* retardation of radionuclides in the presence of bentonite colloids, in a system analogous to the near-field/geosphere interface of a deep geological repository (see Alexander et al., 2004, for details). Bentonite is widely considered as a potential backfill material in the disposal of a range of radioactive and chemotoxic wastes. Over the course of time, bentonite backfill could conceivably be eroded and provide a source of colloids that could influence the transport of substances released from the repository. The effects of bentonite colloids on geosphere performance has been identified as an issue requiring further study in, for example, in the Swedish SR 97 safety assessment (SKB, 1999) and in comments[6] from the Swiss regulators, HSK (HSK, 1998).

1.3 The CRR *in situ* experiments

In order to carry out the CRR *in situ* experiments, several boreholes were drilled from a tunnel into the roughly planar experimental shear zone. Fig. 1-1 shows the intersection of the tunnel and the boreholes with the idealised shear zone plane. For this study, only experiments in dipole 3, between the boreholes BOMI 08 and BOMI 10, and in dipole 1, between the boreholes BOCR 02 and BOMI 10, were evaluated. For these experiments, borehole BOMI 10 was always used as the withdrawal well, with a typical water extraction rate, Q_w, of 150 mLmin^{-1}. Boreholes BOMI 08 and BOCR02 were used for injection of the tracers, with a typical water injection rate, Q_i, of 10 mLmin^{-1}. With the ratio $Q_w/Q_i = 15$, a full recovery of conservative tracers was achieved. Groundwater injected during the experiments was collected beforehand from the experimental shear zone and stored under a cover gas (N_2) to minimise any possible changes in chemical composition, before being re-injected into the shear zone during the experiments (Frick et al., 1992)

Once a steady flow field had been attained, 10-minute step-function inputs of single tracers or colloids, or cocktails of tracers and colloids, were added to the injected water. The tracers that were used in the various experimental runs are shown in Tab. 1-1. A number of preliminary runs were carried out on the two dipoles with a limited number of tracers leading up to two main runs:

run #31, involving a cocktail of conservative and sorbing tracers, and

run #32, involving bentonite colloids, in addition to a cocktail of conservative and sorbing tracers.

The measurements and the resulting breakthrough curves are summarised in Möri (2004).

---

4 Empresa Nacional de Residuos Radioactivos SA, Madrid, Spain

5 US Dept. of Energy / Sandia National Laboratories, Albaquerque, USA

6 HSK (1998) noted that "....the generation of colloids at the boundary of the bentonite package cannot be excluded...." and "...colloid-facilitated transport of strongly sorbing radionuclides at the near-field/far-field boundary remains very much an open question....".

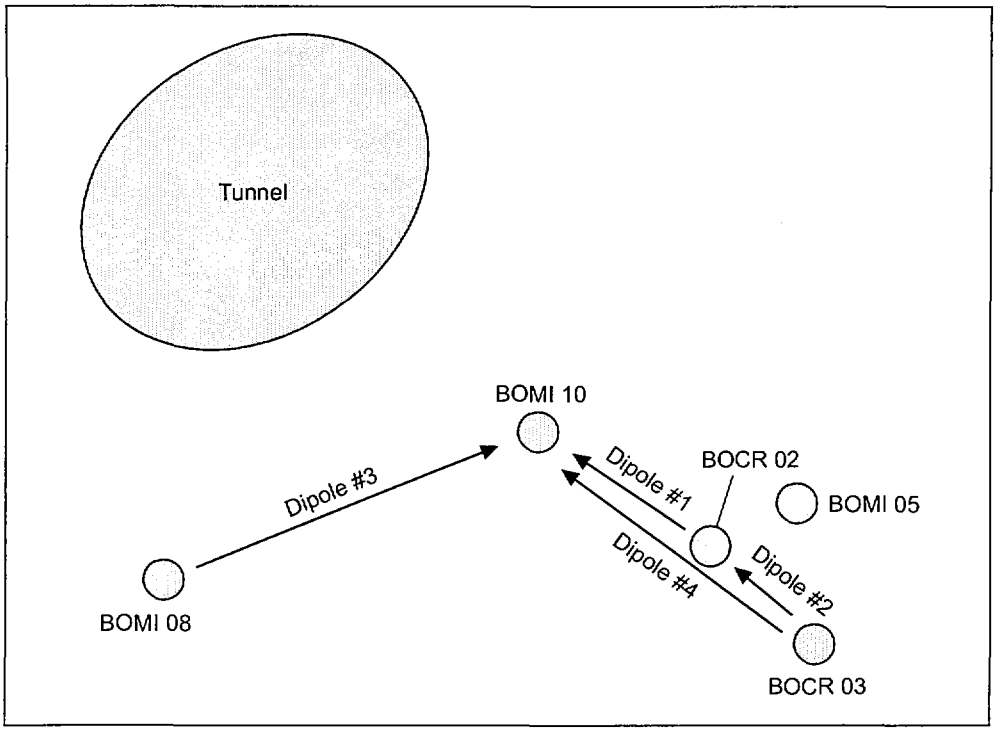

Fig. 1-1: The plane of the experimental shear zone (AU96), with the intersections of the tunnel and boreholes. Only experiments in dipole 1 and 3 are evaluated in this report. The distances between the boreholes in dipoles 1 and 3 are 2.5 m and 5 m, respectively.

Tab. 1-1: Tracer runs in dipole 1 and 3 investigated in this study.

Dipole	**Experiment no.**	**Tracer composition**
1	Run #13	uranine
1	Run #14	Th, Tb, Hf
1	Run #21	uranine, Br, Sr
1	Run #28, #29, #30, #33, #34, #35	uranine, I
1	Run #31	I, Sr, Th, U, Np, Pu, Am
1	Run #32	bentonite colloids, I, Sr, Cs, Tc, Th, U, Np, Pu, Am
3	Run #6	uranine
3	Run #6a	bentonite colloids
3	Run #7	uranine
3	Run #7a	bentonite colloids, Th, Tb, Hf
3	Run #15	Th, Tb, Hf
3	Run #16	uranine

The experiments employed uranine[7] and iodine as conservative (i.e. non-retarded) tracers (see comments in Smith et al., 2001). These were used as a reference for investigating the transport behaviour of more complex sorbing tracers, bentonite colloids and mixtures of sorbing tracers and bentonite colloids.

In the case of experiments involving bentonite colloids, several techniques were applied in order to measure colloid breakthrough, namely:

- laser induced breakdown detection (LIBD) (Hauser et al., 2002),
- a single particle monitor (PDS) and a single particle spectrometer (LPS) (Degueldre et al., 1996), and
- (in run #32) particle correlation spectroscopy (PCS) (Möri, 2004).

Furthermore, as an additional method to detect the bentonite colloid breakthrough, aluminium concentrations in the groundwater collected at the withdrawal well were measured with inductively coupled plasma mass spectrometry (ICP-MS) as a tracer for the injected bentonite colloids. Although the bentonite aluminium content was shown to swamp any natural background signature, it is not possible to differentiate directly between bentonite colloids and the background population of natural colloids[8] in the shear zone with the methods utilised. The measured colloid breakthrough curves are therefore a superposition of the concentrations of both colloid populations. The background population of natural colloids was, however, determined independently with LIBD, PDS, LPS and Al measurements, and could be subtracted from the breakthrough curves in order to obtain bentonite colloid breakthrough curves[9].

The injected bentonite suspension was also investigated using PDS, LPS and ICP-MS in order to measure the size distribution of the injected bentonite colloids for later comparison with the eluted colloid size distribution (Möri, 2004).

1.4 CRR modelling studies

Four modelling groups were set up to analyse the results of the CRR *in situ* experiments. The present report deals only with the work of the PSI group and all four groups are covered together in Guimera et al. (2004).

1.5 Overview of the present report

Chapter 2 gives a description of the methodology adopted in the PSI modelling study. It describes three alternative models used to analyse and predict the results of the tracer tests, namely a 1-D advection-dispersion model, a 2-D advection-dispersion model, and a non-Fickian dispersion model: the CTRW (continuous time random walk) model. It describes assumptions and procedures that are common to all the models, including certain assumptions about geological structure, flow and transport processes, and the procedure to generate breakthrough curves of radionuclides that are conveyed partly as aqueous solutes, and partly sorbed on colloids, as well as the distinguishing features of the three models. Then the computer codes that

---

7 The migration behaviour of uranine in this shear zone is well known from previous experiments (see, for example, Frick et al., 1992; Hadermann and Heer, 1996).

8 Information on natural colloids in the shear zone was already available at the time of CRR (see Degueldre et al. 1990, 1996, Möri, 2004 for an overview). The colloids consist mainly of amorphous silica with small amounts of mica and calcium silicates (Smith et al., 2001)

9 It should, however, be noted that measurement of the background colloids is fraught with difficulty (see comments in Möri, 2004) and so some degree of uncertainty in these data must be accepted for the time being.

are used to solve the governing equations of the three models are identified. Finally, the procedure used in applying the models to the analysis and prediction of the CRR tracer test results is explained.

Chapter 3 presents the results obtained using the models described in the previous chapter. It describes fitting of the breakthrough curves of preliminary tests carried out in advance of the main CRR experimental runs, which shows that the 1-D and 2-D advection-dispersion models with matrix diffusion provide similarly good fits for tracers conveyed as aqueous species. Assuming, however, that colloids do not undergo matrix diffusion, the non-Fickian dispersion model is required in order to provide an adequate fit in the case of colloids. It also describes predictions of breakthrough for the main experimental runs, and compares the predictions and measurements for the breakthrough of Am, Pu, Np, U and Cs with and without the addition of bentonite colloids to the injection cocktail, and suggests reasons for the discrepancies between predictions and measurements.

Chapter 4 presents a review of the model concepts and parameters used in the analyses and predictions of Chapter 3, in the light of the measured data from the main runs, and describes some modifications that improve agreement between theoretical and measured breakthrough curves. It describes some general observations that strongly suggest that at least part of the injected inventories of Am, Cs, Pu and Th migrates in association with colloids. It also discusses the specific influence of bentonite colloids on transport. It is noted that Am, Pu and Th (and also Tb and Hf) are transported in colloidal form, even when no bentonite colloids are added to the injection cocktail, but the addition of bentonite colloids increases the recovery of these tracers. It is also noted that the characterisation of colloids in the injection cocktails (not available at the time that the model predictions were made) enables improved agreement to be obtained between model calculations and measured breakthrough curves. Finally, it describes how a minor adjustment of one of the parameters of the non-Fickian dispersion model improves agreement in the tailing part of the colloid breakthrough curves.

Chapter 5 describes the reasons why advective and hydrodynamic dispersion processes, as represented by the non-Fickian dispersion model, are a likely explanation for the inability of the 1-D and 2-D advection-dispersion models to fit colloid breakthrough adequately. Possible factors affecting the tailing of colloid breakthrough curves are reviewed, including the influence of (i), diffusion processes (and, in particular, the possibility of matrix diffusion of colloids), (ii), the influence of the injection process (i.e. discrepancies between the assumed injection function and the actual injection function), (iii), the finite width of the dipole flow field, (iv), the interaction of colloids with fracture walls, and (v), the velocity profile across the fracture, which could have different effects on the breakthrough of colloids and solutes (i.e. differences in Taylor dispersion). (i) - (iv) do not provide an adequate explanation of the observed tailing. The possible effects of differences in Taylor dispersion remain, however, an open issue. Finally, evidence that supports the influence of non-Fickian dispersion on the tailing of colloid breakthrough curves is presented.

Chapter 6 describes some unresolved problems associated with the CRR experiment and discusses the limitations of the modelling approach as used in the present study. These include, (i), the counter-intuitive correlation between extraction flow rate and peak arrival time, which is currently unexplained, but is probably a result of the heterogeneous characteristics of the shear zone, (ii) the problem of non-uniqueness of the fits, i.e. different sets of parameters could, in some cases, fit particular breakthrough curves equally well, (iii), the filtration of colloids, which is currently not included in the modelling approaches presented here, although some inferences regarding the most likely mechanisms can be made from experimental observations, (iv), the possibility that non-Fickian dispersion may be an important mechanism for the transport of

aqueous solutes, as well as colloids, which has implications for the interpretation of tracer transport experiments, and (v), various other artefacts that may have arisen because of the simplified nature of the models.

Finally, Chapter 7 presents some conclusions and discusses the implication of the present study for repository safety assessment studies.

2 Methodology

This chapter gives a description of the methodology adopted in the PSI modelling study. In Section 2.1, it describes three alternative models used to analyse and predict the results of the tracer tests, namely a 1-D advection-dispersion model, a 2-D advection-dispersion model, and a non-Fickian dispersion model: the CTRW (continuous time random walk) model. In Section 2.2, it describes assumptions and procedures that are common to all the models, including certain assumptions about geological structure, flow and transport processes, and the procedure to generate breakthrough curves of radionuclide tracers that are conveyed partly as aqueous solutes, and partly sorbed on colloids. In Sections 2.3 to 2.5, the distinguishing features of the three models are explained in more detail. In Section 2.6, the computer codes that are used to solve the governing equations of the three models are identified. Finally, in Section 2.7, the procedure used in applying the models to the analysis and prediction of the CRR tracer test results is explained.

2.1 The use of alternative models

In the present study, three different models are used, which will be referred to as:

- the 1-D advection-dispersion model,
- the 2-D advection-dispersion model, and
- the non-Fickian dispersion or CTRW model.

The first model is essentially the same as the model developed by Heer and Hadermann (1996) and applied in the MI project by PSI (see also Umeki et al., 1995). Heer and Hadermann (1996) found that they could describe the transport of tracers in the MI *in situ* experiments with a double porosity model. They represented the shear zone as a set of parallel open fractures ("flow porosity") embedded in highly porous fault gouge ("matrix porosity"). Transport was considered to occur by advection and longitudinal dispersion in the fractures along 1-D transport paths, retarded by diffusion into the porous rock matrix and sorption on rock matrix pore surfaces. Dispersion was modelled as a diffusion-like process, described by Fick's Laws (referred to as "Fickian dispersion" in the present study). Heer and Hadermann (1996) were able to use this model to fit the experimental breakthrough curves, with parameters consistent with independent information. They were also able to make acceptable predictions for a different dipole flow field.

The 2-D advection-dispersion model differs from the 1-D model in its representation of the flow field and its inclusion of transverse dispersion. Additionally, it allows the inclusion of known artificial structures (e.g. the tunnel) in the modelled domain and the use of more complicated regional boundary conditions (e.g. regional hydraulic gradients).

Both the 1-D and 2-D advection-dispersion models can, if required, explicitly represent the process of matrix diffusion and should more accurately be referred to as advection-dispersion-matrix diffusion models, although, for conciseness, the shorter names are used in this report. The non-Fickian dispersion model provides a more generally applicable representation of advective and hydrodynamic dispersion processes in highly heterogeneous media. It does not, however, currently include matrix diffusion, and thus can only be applied to tracers that can be assumed not to undergo this processes - namely colloids, as discussed in later sections.

The application of three alternative models in the present study can be seen as a test of the following hypotheses:

1. that a representative 1-D transport path is adequate to represent the transport of tracers between the injection well and the withdrawal well in the CRR *in situ* tests, and
2. that the process of hydrodynamic dispersion for both aqueous solutes and colloids can be adequately represented as a diffusion-like process, governed by Fick's Laws of diffusion.

The failure of the 1-D advection-dispersion model and success of the 2-D advection-dispersion model to represent or predict one or more of the breakthrough curves would constitute a falsification of the first hypothesis. Similarly, the failure of the 1-D and 2-D advection-dispersion models and success of non-Fickian dispersion model to represent or predict one or more of the breakthrough curves would constitute a falsification of the second hypothesis.

2.2 Assumptions and procedures common to all the models

2.2.1 Assumptions regarding the structure of the shear zone

To date, nearly all attempts to model transport in the experimental shear zone at the GTS have been based on a structural model first described in Frick et al. (1992)[10], and this structural model is also used in the present work. Fig. 2-1 gives a sketch of the geological structure of the shear zone (upper part of the figure; note, this is already a simplification of reality), and the simplified conceptualisation for transport modelling (lower part). As in Frick et al. (1992), the complex and highly connected network of open and partially filled fractures observed in the actual shear zone is replaced by a set of parallel, open fractures, separated by a homogeneous porous rock matrix, representing the heterogeneous mixture of fault gouge, adjacent rock and dead-end pores between the actual fractures.

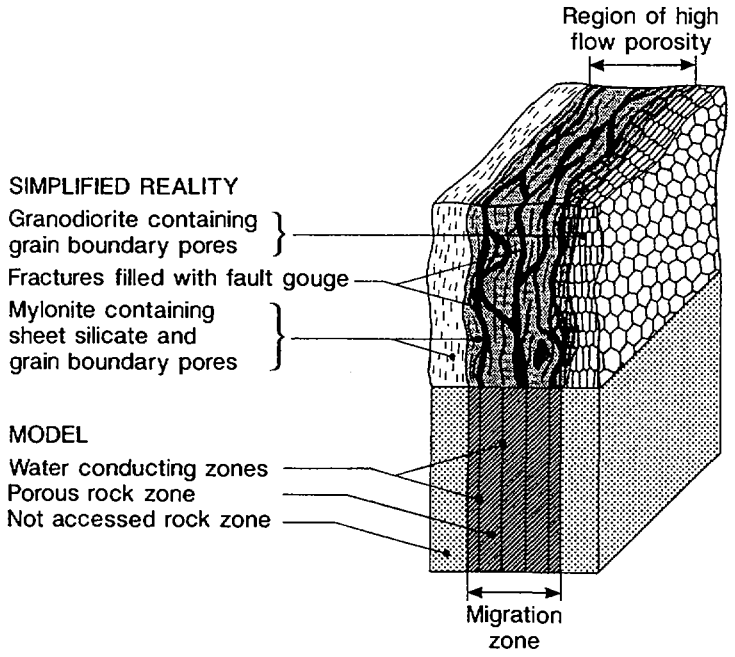

Fig. 2-1: Sketch of the geological structure of the shear zone (upper part) and the simplified conceptualisation for transport modelling (lower part) - from Heer and Hadermann (1996) after Frick et al. (1992).

[10] The conceptualisation was based on work carried out by Bossart and Mazurek (1990). More detailed work can be found in Möri et al. (2003, 2004).

All transport-relevant properties of the fractures and the rock matrix are assumed to be constant in space and time[11].

The simplification of the complex structure of the shear zone is carried out in order to formulate tractable equations for flow and transport, which, in the case of the 1-D and 2-D advection-dispersion models, are based on the consideration of mass balance in structurally simple representative elementary volumes (REVs) (see, e.g. Bear, 1972). The success of such an approach is highly dependent on the scale of the problem in relation to the size and structure of any heterogeneities not explicitly represented in the model. In general, if the size of the heterogeneities is much smaller than the scale of the problem, the use of effective hydraulic and transport properties to represent the effects of heterogeneities is justified for modelling purposes. Otherwise heterogeneities have to be included explicitly into a model or model approaches have to be used that, like the non-Fickian dispersion model, are not based on REVs.

2.2.2 Assumptions regarding flow

All three models used in the present study assume that a steady-state dipole flow field exists in the shear zone, controlled by the injection and withdrawal flow rates. The small fluctuations in flow rate that actually occurred in the course of individual tests were assumed to be insignificant. In principle, the computer code used to solve the equations of the 2-D advection-dispersion model would have allowed the fluctuations to have been included, but this would have resulted in much longer computational times.

2.2.3 Assumptions regarding transport processes

All three models were originally developed to predict the transport of solutes. In the present study, the following additional assumptions are made in order to model the transport of cocktails of tracers that can include both solutes and colloids.

Firstly, it is assumed that the transport of each component of the cocktails can be calculated independently. This implies the following additional assumptions.

- Tracers in aqueous solution do not interact (chemically) with each other.
- Colloids are stable, and do not interact with each other or with tracers in aqueous solution – radionuclide tracers may be associated with colloids at the time of injection, but no further interaction takes place, i.e. the colloid-bound fraction of each tracer remains constant during migration.
- There is no competition for sorbing sites on rock matrix pore surfaces, and sorption coefficients measured on fault gouge material in the laboratory can be applied directly to sorption on rock matrix pore surfaces.

Both solutes and colloids are assumed to be transported by advection and dispersion in the fractures illustrated in Fig. 2-1. Advective transport in the rock matrix is assumed to be negligible. Solutes may undergo limited matrix diffusion and sorption on matrix pore surfaces. Sorption is assumed to be a linear, equilibrium process, described by an element-dependent sorption coefficient K_d [m^3 kg^{-1}]. Colloids are, however, assumed to be excluded from matrix pores as a result of their size and/or charge effects (this assumption is discussed further in Chapter 5). The non-Fickian dispersion model used in the present study does not, as yet, include matrix diffusion, and so is only applied to colloid transport and the transport of radionuclide

[11] See Möri et al. (2003, 2004) for the limitations of these assumptions.

tracers associated with colloids. Immobilisation processes, such as colloid filtration, or interactions of any kind with the fracture walls, are not explicitly included in the models. The total recoveries of injected colloids at the withdrawal well do, however, indicate that colloid filtration takes place. This is treated by applying an appropriate scaling factor to the modelled breakthrough curves (see below).

At the injection well, the models assume time dependent aqueous tracer and colloid concentrations that are based on the experimentally measured concentration of uranine at the well, scaled according to injected tracer mass.

Finally, radioactive decay is assumed to be negligible for all the radionuclide tracers over the timescale of the experimental runs. This assumption is readily justified for all tracers apart from ^{85}Sr and ^{131}I, which have half lives of about 1560 and 190 hours, respectively. Even for these tracers, however, the concentration changes due to decay are small.

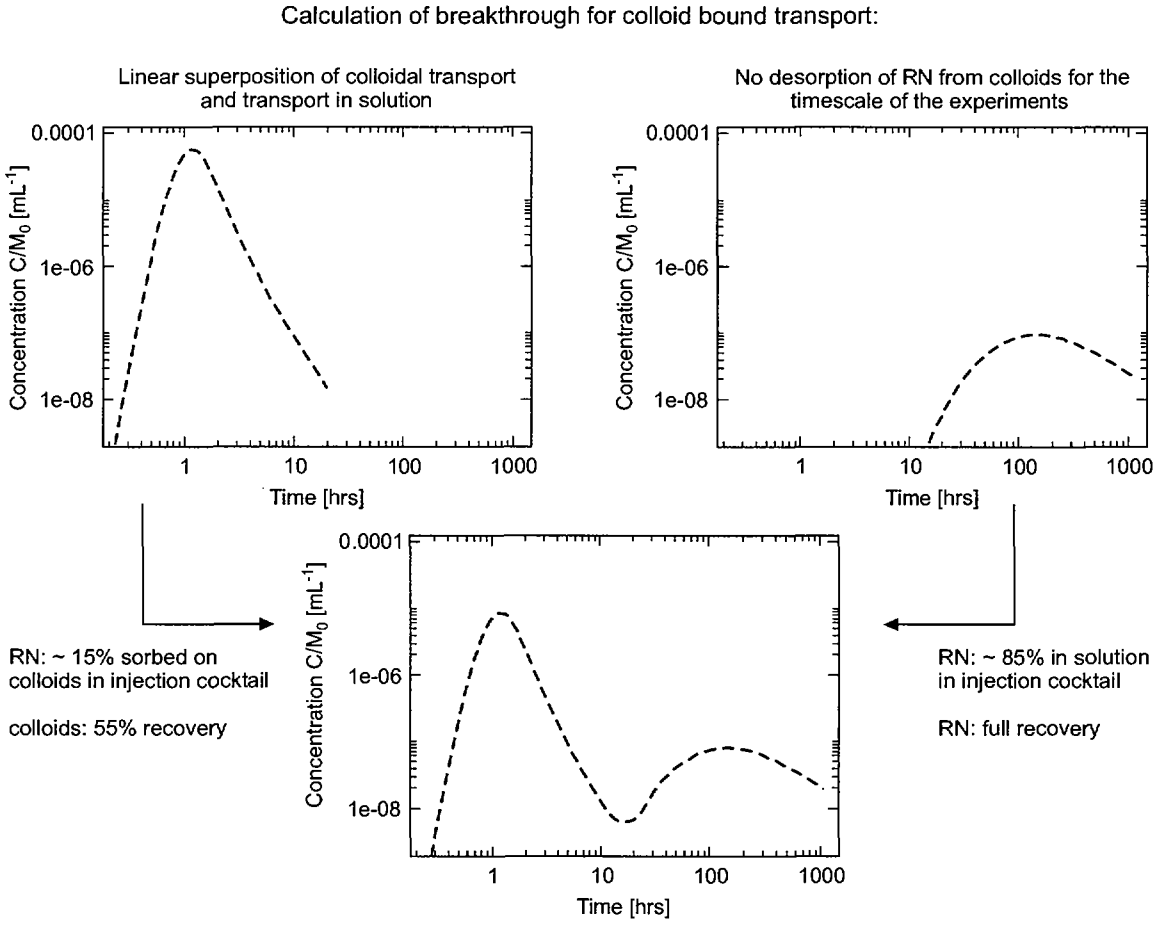

Fig. 2-2: Schematic example of the superposition of breakthrough curves for a radionuclide (RN) tracer transported both in aqueous solution and by colloid facilitated transport, in order to obtain an overall breakthrough curve for the tracer.

2.2.4 Procedure for the generation of breakthrough curves

Since it is assumed that the transport of each component of the tracer cocktails can be calculated independently, the generation of breakthrough curves for colloids, for radionuclide tracers

bound entirely to colloids (i.e. a 100 % colloid bound fraction) and for radionuclides tracers that are transported entirely in the aqueous phase (i.e. a 0 % colloid bound fraction) is straightforward. In the case of radionuclides tracers that are transported entirely in the aqueous phase, the models are simply run for each individual tracer, and the calculated concentration at the withdrawal well as a function of time gives the breakthrough curve. In the case of colloids and colloid-bound radionuclides, the fact that colloid filtration is not included in the models means that the calculated breakthrough curves must be multiplied by the observed or expected colloid recovery, or the experimentally measured data must be normalised to 100 % recovery.

In the case of tracers that are partially associated with colloids and are partially transported in the aqueous phase, separate model runs are carried for the colloid bound fraction and the aqueous fraction. Since it is assumed that no further sorption on or desorption from colloids takes place during transport, the two resulting breakthrough curves (corrected for recovery in the case of the colloid curve) can then be superimposed to give the overall breakthrough curve for the tracer, as illustrated in Fig. 2-2 for a tracer with a 15 % colloid bound fraction, with a 55 % recovery of colloids.

2.3 The 1-D advection-dispersion model

The 1-D advection-dispersion model is based on the model developed during the MI experiment and described in detail by Heer and Hadermann (1996) and Hadermann and Heer (1996). Here, only a brief description is given in order to provide a general understanding of the model.

Heer and Hadermann (1996) divided the dipole flow field into several stream tubes, each carrying an equal part, Q [$m^3 s^{-1}$], of the total flow (Fig. 2-3). Within each stream tube, a characteristic streamline is chosen, separating the stream tube flow into two halves.

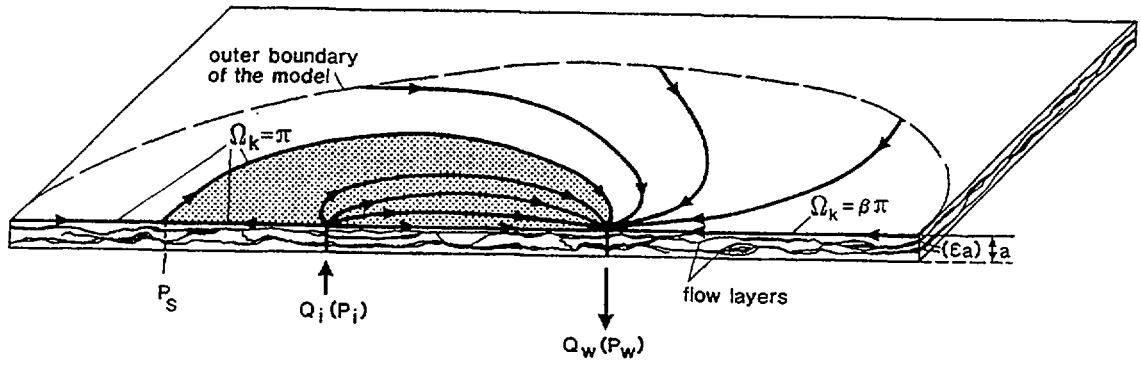

Fig. 2-3: Dipole flow field in the shear zone. Q_i and Q_w represent the injection and withdrawal flow rates. A few streamlines are drawn and the shaded area represents the capture zone, i.e. the region containing streamlines that run from Q_i to Q_w (from Heer and Hadermann, 1996).

The mean water velocity, $\bar{v}_i$ [$m\ s^{-1}$], along streamline i is given by:

$$\bar{v}_i = \frac{Q}{2NbB_i} \qquad (2\text{-}1)$$

where B_i, [m] is the average width of the stream tube in the plane of the shear zone, N is the number of fractures across the shear zone (see the lower part of Fig. 2-1) and $2b$ [m] is the fracture aperture.

Each stream tube flow can be represented approximately by a 1-D transport path, which coincides with the characteristic streamline. Tracers are advected along the transport path with a constant velocity $\bar{v}_i$. They undergo longitudinal dispersion, characterised by a longitudinal dispersion length a_L [m], and may diffuse into the rock matrix separating the fractures.

Tracers are injected into the shear zone at the injection well, where water is pumped at a rate Q_i [m^3 s^{-1}]. Each individual transport path conveys a fraction Q/Q_i of the injected inventories. For each path, the resulting concentration at the withdrawal well is calculated as a function of time. The breakthrough curve is then constructed by superimposing the time-histories of concentration of all the individual transport paths. For the narrow dipole flow fields used in CRR, however, only a single 1-D transport path has been considered.

The governing equations for transport along a 1-D transport path in a fractured porous medium are given, for example, in Heer and Hadermann (1996) and are not reproduced here. These equations are solved numerically (see Section 2.5) in order to generate the model breakthrough curves for the 1-D advection-dispersion model in the present study. It is, however, also informative and useful for later discussions to consider some approximate solutions that illustrate the effects of matrix diffusion and sorption on the form of the breakthrough curves (see Hadermann and Heer, 1996).

The peak arrival time in a breakthrough curve, t_{mi} [s], is given approximately by:

$$t_{mi} \approx \frac{L_i R_f}{\bar{v}_i} + \frac{2}{3}\tau_0, \tag{2-2}$$

where L_i [m] is the transport path length and the retardation factor R_f accounts for the retardation due to sorption on the fracture surfaces (this is set to zero in the calculations carried out in the present study since it is assumed that no interactions take place at fracture walls). τ_0 [s] is a shift in the peak arrival time caused by matrix diffusion, and is given by:

$$\tau_0 = \left(\frac{\varepsilon_p}{b}\right)^2 \left(\frac{L_i}{\bar{v}_i}\right)^2 \frac{D_p R_p}{4}, \tag{2-3}$$

where ε_p is the porosity in the rock matrix, D_p [m^2 s^{-1}] is the pore diffusion constant in the matrix and R_p is a retardation factor due to sorption on matrix pore surfaces. R_p is related to the sorption coefficient K_d [m^3kg^{-1}] for a given tracer via the equation:

$$R_p = 1 + \rho K_d \frac{1-\varepsilon_p}{\varepsilon_p} \tag{2-4}$$

where ρ [kg m^{-3}] is the dry solid density of the porous rock.

The concentration C_{fi} [kg m^{-3}] at the withdrawal well at sufficiently late times (i.e. where $t >> t_{mi}$) is:

$$C_{fi}(L_i,t)=\frac{M_0}{Q_w}\frac{\sqrt{\tau_0}}{\sqrt{\pi}}t^{-3/2}, \qquad (2\text{-}5)$$

where M_0 [kg] is the (injected) total tracer mass and Q_w [m^3 s^{-1}] is the extraction rate at the withdrawal well.

The effect of matrix diffusion and sorption in the porous matrix on the breakthrough of solutes, as described by these relationships, is illustrated in Fig. 2-4. The breakthrough curves shown in the figure are for illustrative purposes only, and do not relate to any actual CRR runs. They are, however, obtained from numerical solutions of the governing equations of the 1-D advection-dispersion model and represent (i), the case of advection-dispersion only (the black curve), (ii), advection-dispersion + matrix diffusion (the red curve) and (iii), advection-dispersion + matrix diffusion + sorption on matrix pore surfaces (the green curve). This shows how matrix diffusion alone broadens and retards breakthrough curve, and how sorption causes further broadening and retardation.

The figure also shows the late time $t^{-3/2}$ slope of the breakthrough curve (Eq. 2-5) that is a signature of matrix diffusion[12].

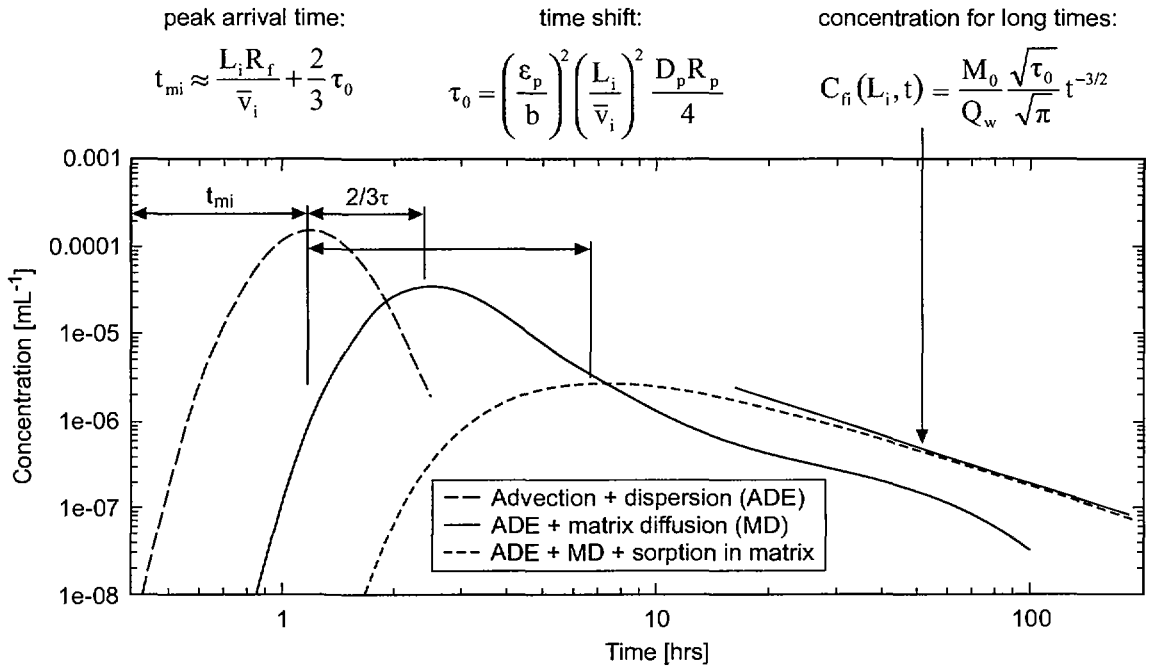

Fig. 2-4: Schematic representation of the influence of matrix diffusion and sorption on matrix pore surfaces on the breakthrough of solutes in a fracture. A tracer transported by advection and dispersion will be delayed and the breakthrough curve broadened if matrix diffusion takes place, with further delay and broadening if sorption on matrix pore surfaces also occurs. The peak time delay due to matrix diffusion is, in this example, exaggerated for illustrative purposes. For the experiments discussed in this document, the effect is significantly smaller.

[12] More precisely, it is a signature of diffusion in a matrix that is sufficiently thick that, for modelling purposes, it can be treated as unlimited. If, at sufficiently long times, the finite thickness of the matrix affects diffusion, then the breakthrough curve deviates from the $t^{-3/2}$ slope and displays a so-called "tail-end perturbation", as shown by the red curve in Fig. 2-4.

2.4 The 2-D advection-dispersion model

In the 2-D advection-dispersion model, flow and transport in the shear zone are evaluated using a finite element approach, thus avoiding the approximations associated with the discretisation of the flow field into stream tubes and transport paths that are a feature of the 1-D model.

Fig. 2-5 shows the initial discretisation of a fracture in the plane of the shear zone into 2-D finite elements (the code used is adaptive, so this discretisation changes with time). At the start of each model run, the mesh is refined around the injection and withdrawal wells in order to represent the flow field adequately in areas where velocity gradients are highest. The dimensions of the model are 40 × 40 m in the plane of the shear zone and a constant head boundary condition is applied at the outer boundaries. The finite dimensions of the injection and withdrawal wells are not considered in the model and two single nodes spaced 2.5 m apart (for dipole 1) in the centre of the model are chosen to represent the wells. The chosen model dimensions and the boundary conditions ensure that the flow field near the wells mimics the theoretical dipole field for an infinite plane as closely as possible.

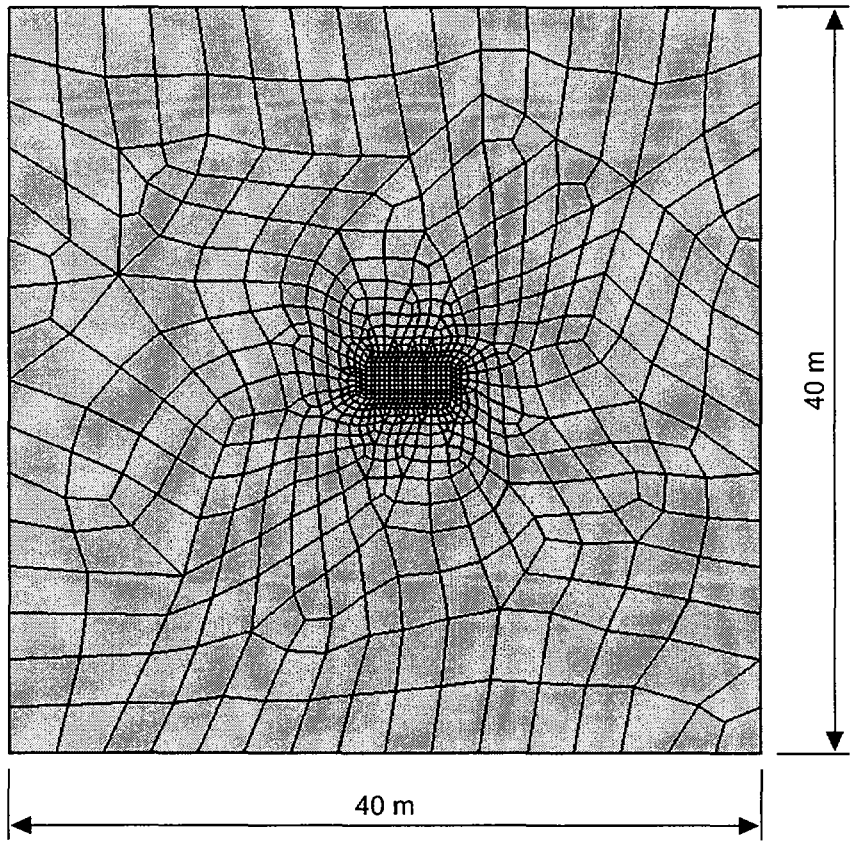

Fig. 2-5: Model dimensions and initial discretisation of a fracture in the plane of the shear zone. The inner region is composed of regular rectangular elements. This mesh is adaptively refined during the calculations.

Fig. 2-6 shows an example of the adaptive refinement of finite elements in the course of a model run in areas of high tracer concentration gradient, and the corresponding concentration distributions.

The porous rock matrix is represented by parallel layers of 3D elements on top of the 2-D elements in the fracture plane (the symmetry of the modelled system means that the region below the fracture plane does not need to be explicitly represented). Fig. 2-7 shows a cross-section through the matrix perpendicular to the fracture plane. The left part of the figure shows the adaptive refinement of rock matrix elements corresponding to the concentration distribution in the right part of the figure.

For modelling transport, a free outflow boundary condition for both flow and transport is applied to the outer model boundaries, although the large distance between the model boundaries and the dipole flow field means that the boundary condition has a negligible impact on the results. The concentrations of tracers at the withdrawal well are calculated as functions of time to obtain breakthrough curves.

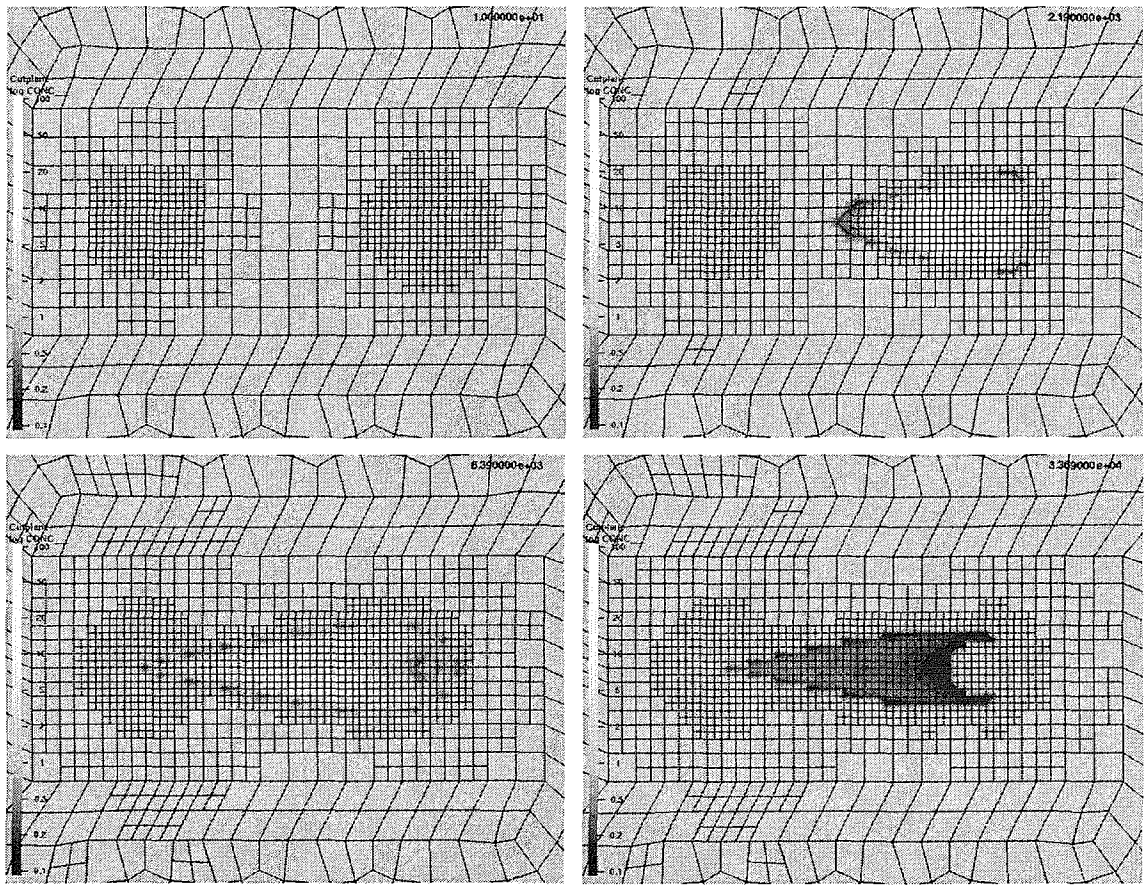

Fig. 2-6: Concentrations of a conservative tracer (uranine) and the corresponding adaptive discretisation of finite elements in the fracture plane at four different times after start of injection: upper left: 10 seconds, upper right: 2190 seconds (36.5 minutes), lower left: 6390 seconds (106.5 minutes), lower right: 33690 seconds (9.4 hours). The shading represents logarithmic concentrations over three orders of magnitude.

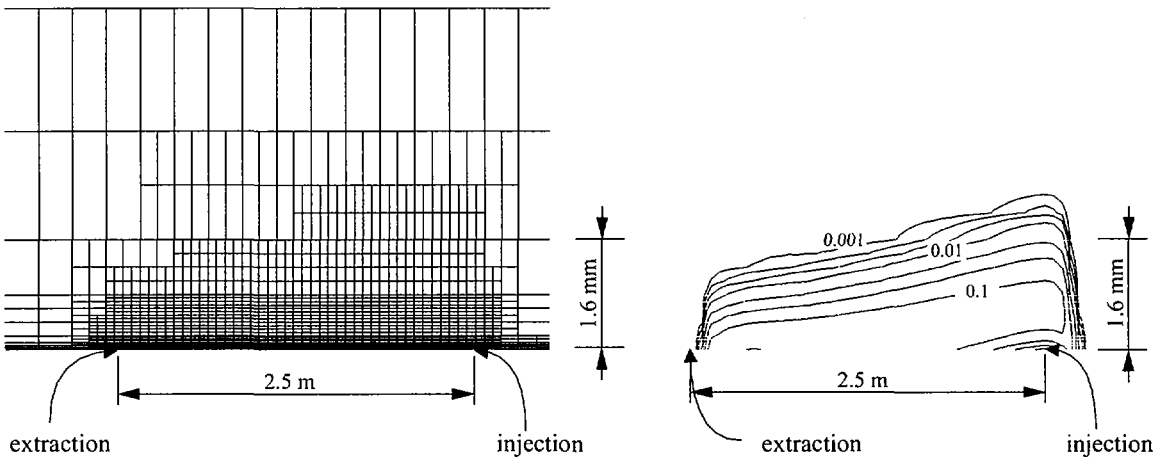

Fig. 2-7: Example of the normalised concentration distribution in the porous rock matrix (right picture) and the corresponding adaptive discretisation of matrix elements (left picture) for a conservative tracer after 6390 seconds following injection. A cross-section through the porous rock matrix perpendicular to the fracture plane is shown. The positions of the injection and withdrawal (extraction) wells are marked.

2.5 The non-Fickian dispersion (CTRW) model

Tracer transport in heterogeneous geological media with strongly varying groundwater flow fields can be envisaged in terms of particles moving along different paths with spatially varying velocities. Different paths are traversed by different numbers of particles. Typically, highly heterogeneous media show a broad distribution of velocities, and thus a greater degree of dispersion, than more homogeneous media. Heterogeneities can occur over a broad range of spatial scales, and can consist, for example, of fractures (joints and/or faults), variations in the porous rock matrix (i.e. grain sizes, mineralogy, layering, and lithology) and/or large-scale geological structures.

The advection-dispersion models assume that dispersion can be modelled as a diffusion-like process, described by Fick's Laws. A more general representation of dispersion, in which Fickian dispersion is a special case, is provided by the CTRW approach, a robust and easily applicable method introduced by Berkowitz and Scher (1995). The formalism of the CTRW approach is well documented and described in Berkowitz et al. (2001) and only the important points relating directly to the CRR analyses are summarised below. The justification for considering this model as an alternative to the more commonly used Fickian model of dispersion is discussed at length in Chapter 5.

Transport through heterogeneous media can be described by a joint probability density function, $\psi(s,t)$, which gives the probability for a particle displacement, s, with a difference of arrival times, t. The challenge is to map the important aspects of the particle motion onto $\psi(s,t)$. Identification of $\psi(s,t)$ lies at the heart of the CTRW approach. It can be shown that the principal characteristics of tracer movements are dominated by the behaviour of $\psi(s,t)$ at large (or asymptotic) times. As discussed by, for example, Berkowitz *et al.* (2001), non-Fickian transport arises in cases where the long-term behaviour of $\psi(s,t)$ is a power law, i.e. $\psi(s,t) \sim t^{-1-\beta}$, with the constant exponent $\beta > 0$.

As in the present study, tracer test measurements often consist of breakthrough curves; i.e. tracer concentrations as functions of time t at a given distance from the tracer source. In the context of the CTRW model, the breakthrough curve corresponds to a First Passage Time Distribution (FPTD) of particles through a plane within the medium. The FPTD is defined as the probability per unit time of a tracer particle reaching a location s at a specific time t for the first time.[13]

The shape of the FPTD functions (and hence the tracer breakthrough curves), including the time of occurrence of the peak, varies strongly as a function of β (Berkowitz *et al.* 2001). For $0<\beta<1$, dispersion is highly non-Fickian, and the concentration peak moves much more slowly than the average fluid velocity, with a longer forward advance of particles. For $1<\beta<2$, the mean particle plume moves with the average fluid velocity (as in the case of Fickian dispersion), but the tails remain broader ("heavier") than those of the Fickian case. For $\beta>2$, the dispersion becomes Fickian.

The FPTD solution for $0<\beta<1$ requires the specification of two parameters: β, which characterises the dispersive process, and x_{shift}, which characterises the effective tracer velocity at a given distance. By contrast, the FPTD solution for $1<\beta<2$ involves three parameters: β, t_{mean} and b_β. The mean fluid velocity can be calculated from t_{mean} by dividing by the transport distance L. For the case of $\beta=2$, it can be shown that the solution is equivalent to the 1-D advection-dispersion solution and that b_β is directly related to the longitudinal dispersion length, a_L, in the Fickian representation of dispersion: $b_\beta = a_L v/L$, where v is the fluid velocity in a Fickian advection-dispersion model.

As discussed in Kosakowski et al. (2001), convolution of the FPTD solutions can be used to deal with experimental systems in which either the input boundary condition is something other than pulse or step input, or transport occurs through regions with distinctly different properties.

2.6 Computer codes

The governing equations of the three models used in the present study can be solved using the computer code PICNIC in the case of the 1-D advection-dispersion model, RockFlow in the case of the 2-D advection-dispersion model, and GRACE in the case of the non-Fickian dispersion or CTRW model. It should be noted that, in the case of PICNIC and RockFlow, only small subsets of the features of the codes are required for the present study.

The PICNIC code (PSI/Quantisci Interactive Code for Networks of Interconnected Channels) can be used to calculate transport in fracture networks (or one or more parallel fractures, as in the present application), with one- or two-dimensional matrix diffusion in a homogeneous or heterogeneous rock matrix. A detailed description the code can be found in Barten (1996) and Barten and Robinson (2001).

RockFlow is based on the finite element method (FEM) in a hybrid approach, in which a 3-D model domain can contain a mix of 1-D, 2-D and 3-D structural elements. Thus, it is possible to simulate fractures as 2-D elements embedded in a matrix of 3-D elements. A detailed description the code can be found in Kolditz et al. (1999)

---

[13] This concept is identical to the concept of the 1-D advection-dispersion model. The "injection" or source plane is the surface of the injection borehole and the exiting plane is essentially the surface of the extraction borehole. Transport between both planes (surfaces) is treated as one-dimensional. Dispersion in the measurement equipement is assumed to be negligible.

GRACE is a graphical analysis package that can access external functions present in either system or third-party shared libraries or modules specially compiled for use with GRACE. The CTRW software library for use with GRACE can be downloaded from the CTRW homepage[14]. The capabilities of the library are described in Berkowitz et al. (2001). The library includes not only the CTRW solutions for different parameters, but also convolution functions that enable arbitrary injection functions to be taken into account. GRACE itself can also be downloaded[15].

2.7 Application of the models

2.7.1 Strategy

The strategy for applying the 1-D and 2-D advection-dispersion models was:

(i) to fit the models to the breakthrough curves from the preliminary experiments carried out prior to the main runs (#31 and #32) by adjusting the model parameters until as good a fit as possible is obtained,

(ii) to use fitted parameters describing the material and transport properties of the dipole, together with laboratory sorption data and data on injection concentrations, to make predictions of the breakthrough curves for the main runs, in advance of the runs being carried out, and

(iii) to modify the models or their parameter values as necessary in the light of the comparison between model predictions and experimental predictions.

In addition to providing parameters for step (ii), step (i) provides a first test of the applicability of the advection-dispersion models. This is achieved by examining the quality of the fits and assessing the plausibility of the values of the free parameters that are adjusted in the fitting procedure - e.g. by comparing with independently derived data and parameter values obtained from MI. Step (ii) was intended to assist in the planning of the main runs by indicating whether it would be possible to detect the breakthrough of the different radionuclides with the combination of planned input concentrations and given detection limits. It was also intended to provide a more stringent test of the models by comparing the actual breakthrough data with the predicted curves[16].

The non-Fickian dispersion model (CTRW) was used where steps (i) or (iii), above, suggested that the advection-dispersion models are inadequate. This was found to be the case for colloid breakthrough, as discussed in Chapter 3 (see, in particular, Fig. 3-1).

2.7.2 Fitting the models to the breakthrough curves

The following procedure was applied for fitting the breakthrough curves from the preliminary experiments and estimating the (material) parameters. The aim is to fit colloid, conservative tracer (uranine) and reactive tracer (Sr) breakthrough curves with one consistent set of material parameters, and to minimise the number of free parameters that must be fitted for each of the curves. This procedure assumes that it is appropriate to use the same material and transport parameters for all tracers in a given run, with the exception of the sorption coefficient[17].

---

14 http://www.weizmann.ac.il/ESER/People/Brian/CTRW/

15 http://plasma-gate.weizmann.ac.il/Grace/.

16 In other words, the Blind Predictive Modelling (BPM) approach. See Pate et al., (1994) for a discussion of BPM.

17 In principle, radionuclides show different effective diffusivities, but these differences have a negligible impact compared to other model simplifications and uncertainties.

(1) It is assumed that colloids are excluded from matrix pores, and not subject to the retardation processes of matrix diffusion and sorption, either on matrix pore surfaces or on the surfaces of fractures. In order to model colloid breakthrough, parameters associated with matrix diffusion and sorption are therefore set to zero, and breakthrough curves are fitted by adjusting parameters associated only with advection and dispersion. The assumption that colloids are excluded from matrix pores is discussed more in detail in Section 5.1.2.

Under these assumptions, the peak arrival time t_{mi} in a breakthrough curve for colloids is given approximately by Eq. 2-2, with R_f set to unity and τ_0 set to zero. Thus, $t_{mi} = L/\bar{v}$. The transport length L is fixed by the distance between the wells. The mean velocity $\bar{v}$ is a function of the injection/withdrawal flow rates, which are fixed by the experimental set-up, and the aperture of the fracture or, if multiple parallel fractures are present across the shear zone, the summed aperture of all the fractures. The fracture aperture (or summed aperture) can thus be fixed in such a way that the experimentally measured peak arrival time is reproduced[18].

The width of the measured breakthrough curves reflects heterogeneity within the dipole field, which, in the 1-D and 2-D advection-dispersion models, is taken into account via longitudinal and, in the case of the 2-D model, transverse dispersion lengths. In the present study, the longitudinal dispersion length is obtained by fitting the measured breakthrough, while, in the 2-D model, the transverse dispersion length is arbitrarily fixed at a value of 0.001 m. Earlier calculations with a very similar 2-D model demonstrated that the calculated breakthrough curves are not sensitive to the value assigned to the transverse dispersion length (Smith et al., 2001).

(2) It is assumed that the advection and dispersion parameters estimated from the breakthrough of the colloids are also applicable to conservative tracers, which are additionally retarded by matrix diffusion. Under this assumption, for a given dipole flow field, the breakthrough curves for these tracers can be fitted by adjusting parameters associated with matrix diffusion, but using parameters associated with advection and dispersion that were obtained from the colloid breakthrough curves.

The effective matrix diffusivity, the product of porosity and pore diffusion coefficient, can be obtained from the differences in the breakthrough curves (and, in particular, the delay in peak arrival time) for conservative tracers such as uranine compared to colloids. This delay is τ_0, which appears in Eq. 2-2 and is defined by Eq. 2-3. For a conservative tracer, R_p is equal to unity. b, L and $\bar{v}$ are already fixed by modelling colloid breakthrough. If the porosity of the rock matrix is known from independent measurements, then the effective matrix diffusivity can be obtained from the delay.

(3) Similarly, the breakthrough curves for sorbing tracers can be fitted by adjusting the parameter R_p, which is a retardation factor due to sorption on matrix pore surfaces, and is defined by Eq. 2-4. In this case, the parameters associated with advection, dispersion and matrix diffusion that were obtained from the colloid and conservative tracer breakthrough curves are assumed to be applicable to a sorbing tracer. If the porosity and the density of the rock matrix are known from independent measurements, then the distribution coefficient K_d can be obtained from the fitted value of R_p. If, on the other hand, it is the density of the rock matrix and the distribution coefficient that are known from independent measurements, then the porosity can be obtained from the fitted value of R_p. It is not possible to extract unique values for either the

[18] These 'modelled' apertures can then be compared with reality (e.g.Möri et al., 2004) to assess the appropriateness of the model reproduction.

distribution coefficient or the matrix porosity solely from fitting the breakthrough curves, and independent information on one or the other is always required.

2.7.3 Predictive modelling for run #31

Main run #31 involved a cocktail of conservative and sorbing tracers. Fitted parameters describing the material and transport properties of dipole 1, together with laboratory sorption data and data on injection concentrations, were used to make predictions of the breakthrough curves for the run with the 1-D advection-dispersion model, in advance of the run being carried out. Laboratory sorption data for the tracers used are given in Tab. 2-1.

Tab. 2-1: Laboratory sorption data for the tracers in the cocktail used for run #31. Note that the data refer to experiments with 2 hours contact time between the radionuclides and the fracture filling material. A full discussion on the applicability of the data, including errors, potential kinetic effects etc, is provided in Missana and Geckeis (2004).

Run #31 tracers	**K_d (fracture filling material)** $[m^3\ kg^{-1}]$
^{243}Am	46×10^{-3}
^{242}Pu	8×10^{-3}
^{238}Pu	8×10^{-3}
^{237}Np	1×10^{-3}
^{238}U	5.6×10^{-3}
^{232}Th	not measured
^{85}Sr	8×10^{-3}
^{131}I	0

It was initially assumed that, since bentonite colloids were not included in the injection cocktail, *all radionuclides tracers were transported only in solution* in run #31. This implies that there is no production of colloids due, e.g. to oversaturation or precipitation (see, e.g. Kosakowski and Baeyens, 2001), and the effects of natural groundwater colloids are negligible – i.e. all radionuclide tracers are subject to matrix diffusion and (in the case of sorbing tracers) sorption on matrix pore surfaces. This assumption had to be revised after the runs had been carried out, as described in Chapter 3.

2.7.4 Predictive modelling for run #32

Main run #32 involved bentonite colloids, in addition to a cocktail of conservative and sorbing tracers. Fitted parameters describing the material and transport properties of dipole 1, together with laboratory sorption data and data on injection concentrations and colloid bound fractions, were used to make predictions of the breakthrough curves for this run, again in advance of the run being carried out. As mentioned above and discussed further in Chapter 3, it had been found necessary to use the non-Fickian dispersion model (CTRW) in order to obtain satisfactory agreement with experimental breakthrough curves for colloids and for radionuclides associated with colloids in the preliminary experiments, and the non-Fickian dispersion model was used for colloids in the predictive modelling of main run #32.

It was assumed that the same material and transport parameters can be used for all tracers injected in run #32, with the exception of the sorption coefficient and the colloid bound fraction. Laboratory sorption data and data on colloid bound fractions for the tracers used in the run are given in Tab. 2-2. In the case of Cs, it is known that sorption is, in reality, non-linear. In principle, therefore, the overall Cs concentration, due not only to the injected Cs but also the natural background Cs concentration in the Grimsel groundwater, which is comparable to that of the tracer solution (Frick et al, 1992), should be taken into account in evaluating sorption. For simplicity, however, the non-linearity of the sorption isotherm and the background concentration of Cs were not considered in the predictive modelling and a linear sorption coefficient K_d was applied instead.

It was also assumed that, at the time of injection, the radionuclide tracers were distributed between the aqueous phase and the colloids according to the colloid bound fractions given in Tab. 2-2, and that these colloid bound fractions remain constant during migration - i.e. there is no further sorption of radionuclides to (or desorption from) colloids.

The colloid experiments in dipole 3 gave a recovery of the injected mass of about 55 % for the bentonite colloids (LIBD detected concentration for run #6a, see Möri, 2004). For the predictive modelling of run #32 in dipole 1, it was assumed that colloids show the same mass recovery. It was also assumed that 55 % of the radionuclides sorbed on the colloids at the time of injection are also recovered. The preferential filtration of larger colloids, as measured by Degueldre and Laube (2000), which may have consequences for the recovery of radionuclides associated with colloids, was not considered in the calculations.

Tab. 2-2: Laboratory sorption data and data on colloid bound fractions for the tracers cocktail used for run #32. The colloid bound fraction of the radionuclides is calculated from the sorption coefficients for bentonite colloids assuming equilibrium between sorbed and aqueous phases. Note that the data refer to experiments with 1 week contact time between the radionuclides and the bentonite colloids. A full discussion on the applicability of the data, including errors, potential kinetic effects etc, is provided in Missana and Geckeis (2004).

Run #32 tracers	**colloid bound fraction in the injection cocktail** [%]	**K_d (bentonite colloids)** [$m^3\ kg^{-1}$]	**K_d (fracture filling material)** [$m^3\ kg^{-1}$]
^{243}Am	97.7	2.1×10^{3}	46×10^{-3}
^{244}Pu	72.2	0.13×10^{3}	8×10^{-3}
^{238}Pu	72.2	0.13×10^{3}	8×10^{-3}
^{137}Cs	14.9	8.75	596×10^{-3}
^{237}Np	9.1	5	1×10^{-3}
^{233}U	1.6	0.824	5.6×10^{-3}
^{99}Tc	0.7	0.361	11.5×10^{-3}
^{232}Th	97.6	2×10^{3}	not known
^{85}Sr	not known	not known	8×10^{-3}
^{131}I	0	0	0

3 Results

This chapter presents the results obtained using the models described in the previous chapter. Section 3.1 deals with the fitting of the breakthrough curves of preliminary tests carried out in advance of the main CRR experimental runs. It is shown that the 1-D and 2-D advection-dispersion models with matrix diffusion provide similarly good fits for tracers conveyed as aqueous species. Assuming, however, that colloids do not undergo matrix diffusion, the non-Fickian dispersion model is required in order to provide an adequate fit in the case of colloids. Section 3.2 describes predictions of breakthrough for the main experimental runs, and compares the predictions and measurements for the breakthrough of Am, Pu, Np, U and Cs with and without the addition of bentonite colloids to the injection cocktail, and suggests reasons for the discrepancies between predictions and measurements.

3.1 Breakthrough curve fitting

3.1.1 The advection-dispersion models

The 1-D and 2-D advection-dispersion models were used to fit breakthrough curves from experiments carried out in dipole 1 using:

- colloids - or, more specifically, Th, Tb and Hf, which are believed to be transported in colloidal form, even without the addition of bentonite colloids to the injection cocktail[19] (see below),
- uranine: a conservative tracer, and
- Sr: a moderately sorbing tracer.

Tab. 3-1 shows the experimental runs that were fitted using the 1-D and 2-D advection-dispersion models and summarises key modelling assumptions.

Tab. 3-1: Tracer breakthroughs that were fitted using the 1-D and 2-D advection-dispersion model and key modelling assumptions.

Tracer	Experimental runs	Models fitted	Key assumptions
Th, Tb, Hf	#14	2-D advection dispersion	Th, Tb and Hf transported in colloidal form, no matrix diffusion
Uranine	#13, #21	1-D advection dispersion	Limited matrix diffusion; no uranine sorption
			Unlimited matrix diffusion; no uranine sorption
	#21	2-D advection dispersion	Unlimited matrix diffusion; no uranine sorption
Sr	#21	1-D and 2-D advection dispersion	Unlimited matrix diffusion; linear, equilibrium Sr sorption

[19] In the case of dipole 1, no experiments were conducted in advance of the main runs #31 and #'32 that specifically addressed bentonite colloid transport.

As explained in Chapter 2, free parameters that are adjusted to fit colloid breakthrough are used to fix some of the parameters required to model conservative tracer breakthrough. Similarly, the remaining parameters that are adjusted to fit conservative tracer breakthrough are used to fix some of the parameters required to model sorbing tracer breakthrough.

Tab. 3-2: Summary of parameters extracted by fitting breakthrough curves with the 1-D and 2-D advection-dispersion models with single and multiple fractures and comparison with values obtained from modelling the MI experiment. The fitting procedure used to calculate the parameters is described in Section 2.7.2 and summarised in Section 3.1.1.

Symbol	Description	CRR modelling study			Heer and Hadermann (1996)	
		Single fracture representation of shear zone		Multiple fracture representation of shear zone		
		1-D	2-D	2-D	MI modelling	Other sources
Fixed-value parameters						
N [-]	Number of fractures	1	1	4	4	
L [m]	Distance between injection and withdrawal wells	2.5	2.5	2.5	4.9	-
α_T [m]	transverse dispersion	-	0.001	0.001	-	-
ρ [kg m^{-3}]	bulk matrix density	2670	2670	2670	2670 (±200)	2670
Parameter values fixed by modelling colloid breakthrough (i.e. Th, Tb and Hf)						
2b [m]	fracture aperture	0.55×10^{-3}	0.55×10^{-3}	0.14×10^{-3}	$9.3\ (+0.046 - 0.03) \times 10^{-5}$	-
v [m s^{-1}]	fluid velocity	7.05×10^{-4}	variable	variable	5.51×10^{-4}	-
α_L [m]	longitudinal dispersion	0.1	0.075	0.075	0.25 (+0.05 - 0.04)	-
Pe [-]	Peclet number	25	variable	variable	19.6	-
Parameter values fixed by modelling conservative-tracer breakthrough						
ε_p [-]	matrix porosity	0.3	0.3	0.15	0.062 (+0.068 - 0.032)	0.15 (+0.12 - 0.07)
D_p [m^2 s^{-1}]	diffusion constant in rock matrix	7.4×10^{-11}	7.4×10^{-11}	1.85×10^{-11}	$2.5\ (+11 -2) \times 10^{-11}$	$5.5\ (+1.9 -0.9) \times 10^{-11}$
D_e [m^2 s^{-1}]	effective diffusion constant in rock matrix	2.2×10^{-11}	2.2×10^{-11}	0.28×10^{-11}	0.2×10^{-11}	0.83×10^{-11}
d [m]	effective matrix thickness	$>3 \times 10^{-3}$	$>3 \times 10^{-3}$	$>3 \times 10^{-3}$	$6.2\ (+7.4 -3.4) \times 10^{-3}$	-
Parameter values fixed by modelling sorbing-tracer breakthrough						
R_p for Sr [-]	retardation factor due to sorption in matrix (Eq. 2-4)	72	72	72	905	136 - 731
K_d for Sr [m^3 kg^{-1}]	sorption coefficient	8×10^{-3}	8×10^{-3}	16×10^{-3}	$21\ (+38 - 14) \times 10^{-3}$	$7.6 - 41 \times 10^{-3}$

Tab. 3-2 shows the fitted parameters values, and compares these values with those obtained by Heer and Hadermann (1996) by fitting MI data, and also the values from other independent sources quoted by Heer and Hadermann (1996). The third and fourth columns give the parameters for the 1-D and 2-D models assuming a single fracture representation of the shear zone. The parameters are nearly identical, as expected from the narrowness of the dipole flow field. Only the fluid velocities and the dispersion parameters are slightly different. Longitudinal dispersion in particular has to be increased in the 1-D model with respect to the 2-D model in order to account for spreading due to the finite width of the dipole flow field and the effects of transverse dispersion. The fifth column gives parameters for the 2-D model assuming four parallel fractures (as in Heer and Hadermann, 1996). This gives rise to some differences in the fitted matrix properties. Nevertheless, with the exception of the retardation factor and sorption coefficient for Sr (discussed further, below), the fitted material and transport parameters for the three model variants fall within the ranges specified by Heer and Hadermann (1996) for the earlier MI experiment. The case with four fractures in particular gives parameter values that are very close to the values estimated during MI.

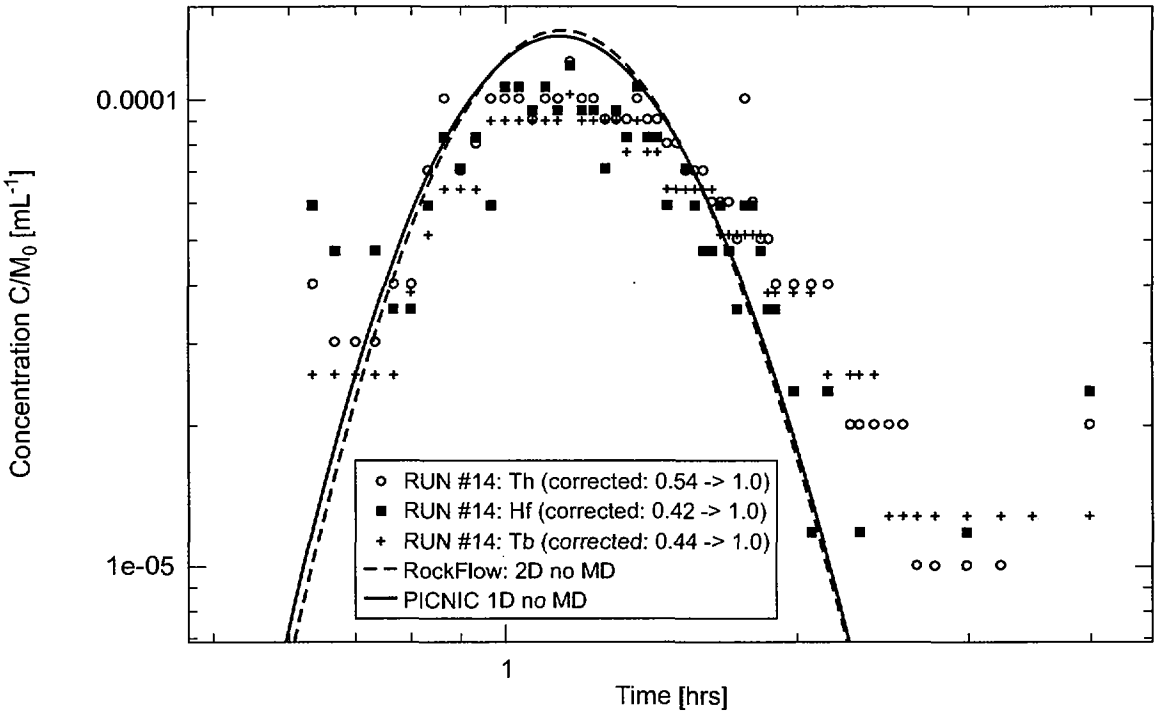

Fig. 3-1: The breakthrough data for Th, Hf and Tb from run #14 and fits of these data using the 1-D and 2-D advection-dispersion models, assuming that the tracers are transported in colloidal form with no matrix diffusion (MD). For ease of comparison, all breakthrough curves are normalised to 100 % recovery.

(i) Fitting Th, Tb and Hf breakthrough

Fig. 3-1 shows the Th, Tb and Hf (homologues for trivalent and tetravalent actinides) breakthrough data from run #14. Th, Tb and Hf are sorbing tracers. Nevertheless, comparing the breakthrough of these tracers with that of non-sorbing uranine (Fig. 3-2), all show a maximum breakthrough at a little over 1 hour, suggesting that sorption does not retard their breakthrough.

In fact, the maximum breakthrough for Th, Tb and Hf occurs slightly before that of uranine, which is the behaviour observed for injected colloids in the case of dipole 3 (see Section 3.1.2, Fig. 3-7). This strongly suggests that Th, Tb and Hf are transported in colloidal form (even in the absence of bentonite colloids in the injection cocktail) and that these colloids, while they can be filtered to some extent during transport, are not retarded by, for example, matrix diffusion or reversible attachment to fracture walls.

The process by which these radionuclide-bearing colloids are formed is not well understood, and it is an open issue whether they are heterogeneous (radionuclides associated with natural groundwater colloids) or homogeneous (formed, e.g. by precipitation during the spiking procedure). As noted by from Möri (2004), Section 3.3.2.2:

"However, even if the homologues were injected without adding bentonite colloids it must be assumed that homogeneous or heterogeneous homologue colloids could have formed in the vial, or later within the dipole flow field, so accentuating the difference in the homologue and uranine breakthrough curves. The formation of heterogeneous homologue colloids can not be ruled out, even if the background concentration of natural colloids in GTS groundwater is quite low (see Degueldre et al., 1990 and natural colloid background studies in this report). On the other hand, even though the homologues were added below their calculated thermodynamic solubility limit, it is also possible that they formed homogeneous oxyhydroxide colloids under 'real' conditions. Whether homogeneous colloids or heterogeneous colloids were formed can not be determined."

The 1-D and 2-D advection-dispersion models without matrix diffusion were fitted to the breakthrough data under the assumption that Th, Tb and Hf are transported as colloids. The fits are also shown in Fig. 3-1. Flow in the shear zone was, in this case, assumed to be confined to a single fracture. The fracture aperture in the models was adjusted to match the peak arrival time for the tracers. For the chosen boundary conditions (fixed injection/withdrawal flow rates), the magnitude of the velocity field depends only on the aperture of the fracture and therefore the time of the breakthrough maximum also depends only on the fracture aperture. The longitudinal dispersion length is used to fit the width of the breakthrough curve. In the case of the 2-D model, the transverse dispersion length was arbitrarily fixed to a value of 0.001 m.

The fit is not entirely satisfactory for either model. In particular, it was not possible to fit both the early concentrations and the late concentrations with one dispersion length. It appears that either the model does not represent all processes, or a process is not represented correctly. These discrepancies provided the motivation for applying the non-Fickian dispersion (CTRW) model to colloid breakthrough curves (see Section 3.1.2). Nevertheless, the aperture and dispersion parameters obtained from the fits were employed as fixed parameters in modelling (conservative) uranine and (sorbing) Sr breakthrough.

(ii) Fitting uranine breakthrough

Fig. 3-2 shows the uranine breakthrough data from runs #13 and #21, and fits of these data using the 1-D advection-dispersion model. Uranine was assumed to be conservative and flow in the shear zone was again assumed to be confined to a single fracture.

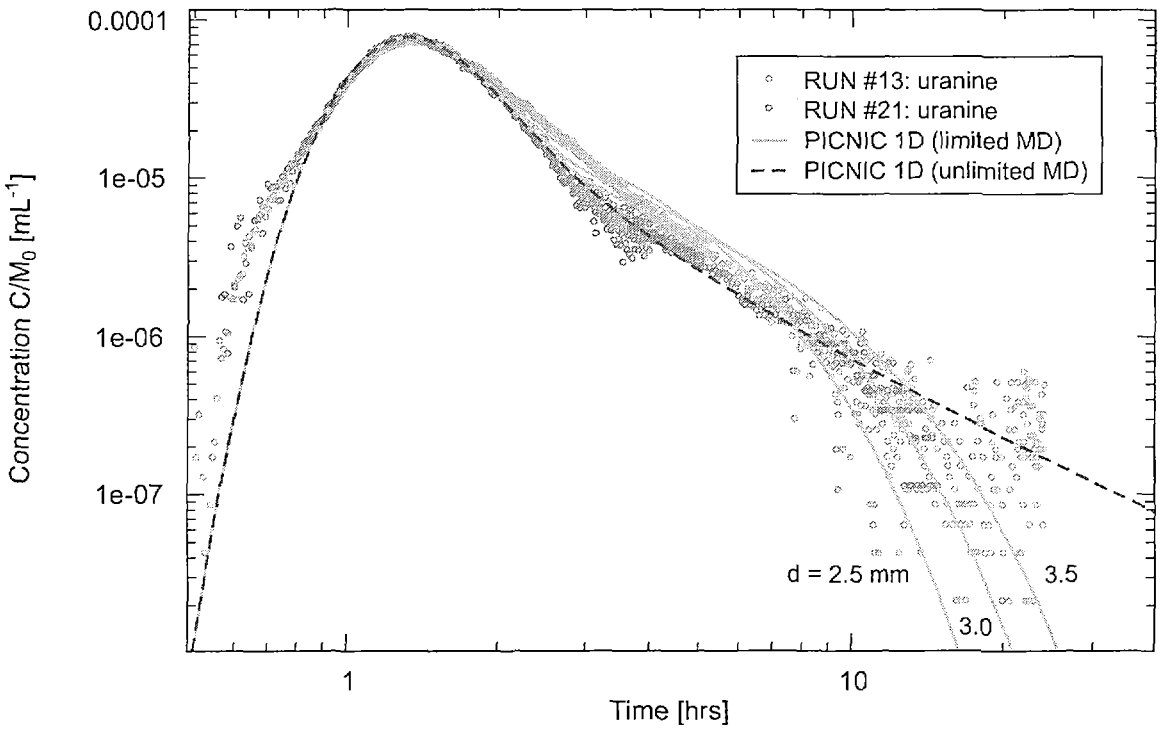

Fig. 3-2: The breakthrough data for uranine from runs #13 and #21 and fits of these data using the 1-D advection-dispersion model, with limited and unlimited matrix diffusion.

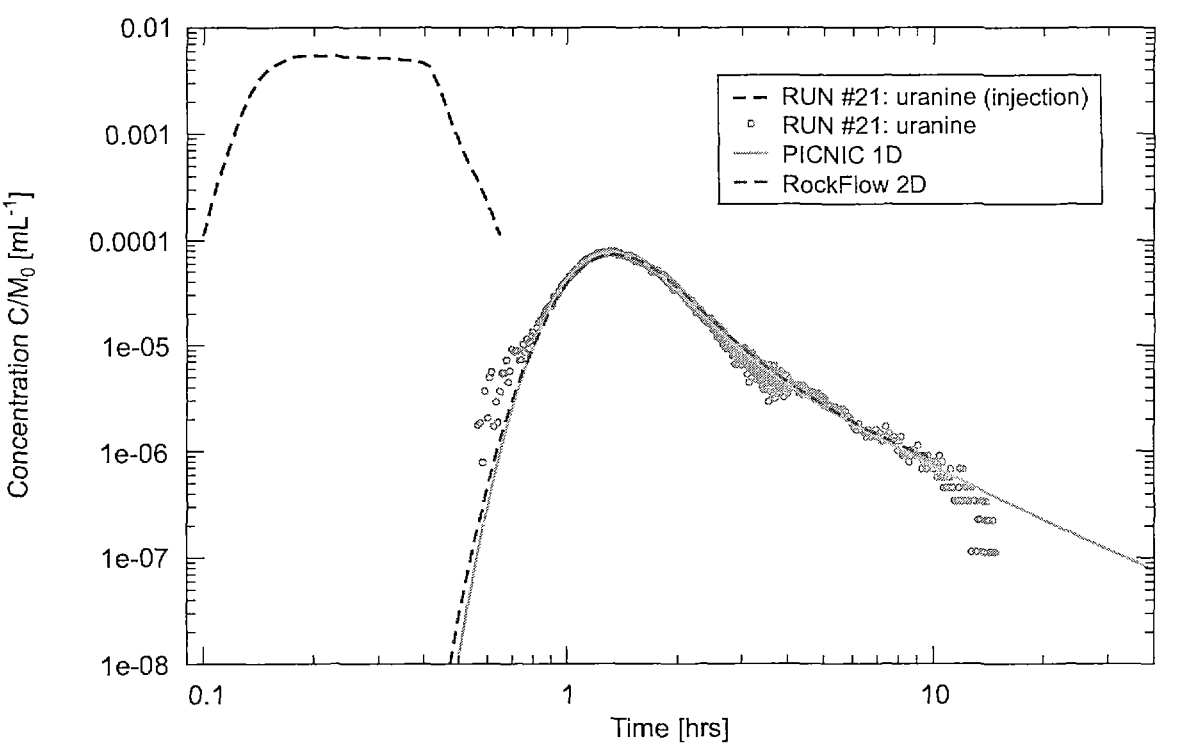

Fig. 3-3: The breakthrough data for uranine from run #21 and fits of these data using the 1-D and 2-D advection-dispersion models with unlimited matrix diffusion.

The breakthrough data show a maximum at a little over 1 hour after injection and a prolonged tail. On the basis of previous modelling studies, it is assumed that the later part of the tail is attributable to matrix diffusion (see, e.g., Heer and Hadermann, 1996, and Fig. 2-4 in the present report). If the depth of the diffusion-accessible rock matrix is modelled as being unlimited, then the later part of the tail displays a $t^{-3/2}$ slope (see Section 2.2, Eq. 2-5). Limited matrix diffusion gives rise to a so-called "tail-end perturbation" - i.e. a perturbation in this slope at still later times. In Fig. 3-2, fits of the data assuming both unlimited matrix diffusion and limited matrix diffusion with different matrix depths (the parameter d in Fig. 3-2) are shown. Unfortunately, the scatter in the data[20] is such that a unique value for the matrix depth cannot be extracted from the fits, although a lower bounding value of about 3 mm is suggested. Nevertheless, the 1-D advection-dispersion model with matrix diffusion provides a good fit to the uranine breakthrough curves, confirming the findings of the earlier MI modelling studies.

Fig. 3-3 shows the breakthrough data from run #21, and fits of these data using both the 1-D and 2-D advection-dispersion models with unlimited matrix diffusion. Similarly good fits can be obtained using either model. It was also observed that good fits could be obtained assuming that the flow in the shear zone is distributed between four parallel fractures, as had been assumed in the modelling of MI, rather than assuming a single fracture[21].

(iii) Fitting Sr breakthrough

Fig. 3-4 shows the uranine and Sr breakthrough data from run #21, and the fit of the Sr data that can be obtained using the 1-D and 2-D advection-dispersion models. Flow in the shear zone was again assumed to be confined to a single fracture, although the case of four fractures was also considered and gave a similarly good fit.

The retardation factor R_p (which was fixed at value $R_p = 1$ for modelling uranine breakthrough) was adjusted until an optimal fit was achieved. The value obtained was 72, which is significantly smaller than the value of 905 obtained by Heer and Hadermann (1996). The retardation factor can be used to obtain (via Eq. 2-4) a sorption coefficient (K_d) using the matrix porosity given in Tab. 3-2 and assuming a bulk matrix density of 2670 kgm^{-3}, as in Heer and Hadermann (1996). This gives $K_d = 8 \times 10^{-3}$ m^3kg^{-1} for the single-fracture models and 16×10^{-3} m^3kg^{-1} for the "4-fracture model", which is within the range obtained by Heer and Hadermann from the evaluation of Sr breakthrough in MI - i.e. 21 (+38 or -14) $\times 10^{-3}$ m^3kg^{-1} - and is within the range quoted Heer and Hadermann (1996) from independent sources - i.e. 7.6×10^{-3} to 41×10^{-3} m^3kg^{-1}.

Finally, it was found that the quality of the fit could be improved by adjusting both the longitudinal dispersion length (or equivalently the Peclet Number, $Pe = L/\alpha_L$) and the retardation factor (or sorption coefficient K_d) simultaneously, rather than the retardation factor alone (Fig. 3-5). The best fit was obtained using a lower Peclet number than in Tab. 3-2 (a Peclet number of 12 rather than 25), and a higher value of R_p (a K_d of 14×10^{-3} m^3kg^{-1} rather than 8×10^{-3} m^3kg^{-1}). One of the findings of Heer and Hadermann (1996) was that, in MI, the longitudinal dispersion length did not depend on the sorption properties of the tracer under consideration. The tentative suggestion of such a dependency in the present study is, however, consistent with the theoretical work of Gelhar (1987), which examined the influence of sorption on dispersion in a heterogeneous fractured medium.

---

[20] The detection limit for uranine is about 10^{-6} mL^{-1}.

[21] Examination of core samples indicates multi-fracture flow in the experimental shear zone (see Möri et al., 2004, for details).

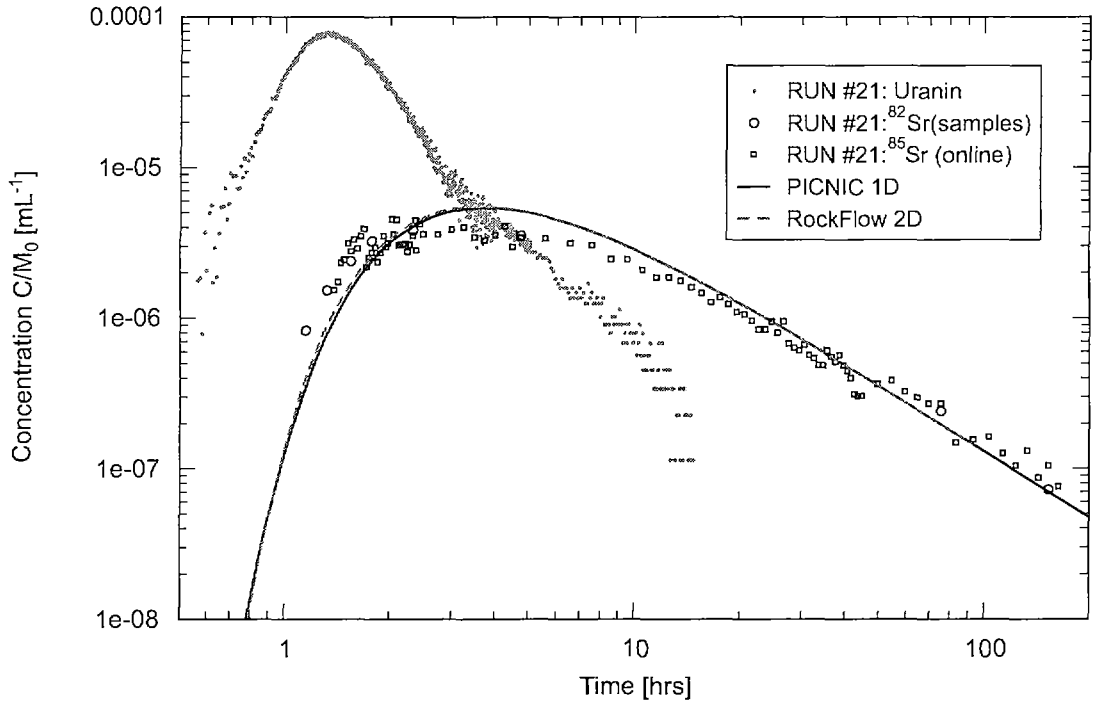

Fig. 3-4: The breakthrough data for uranine and Sr from run #21 and fits of the Sr data using the 1-D and 2-D advection-dispersion models with unlimited matrix diffusion.

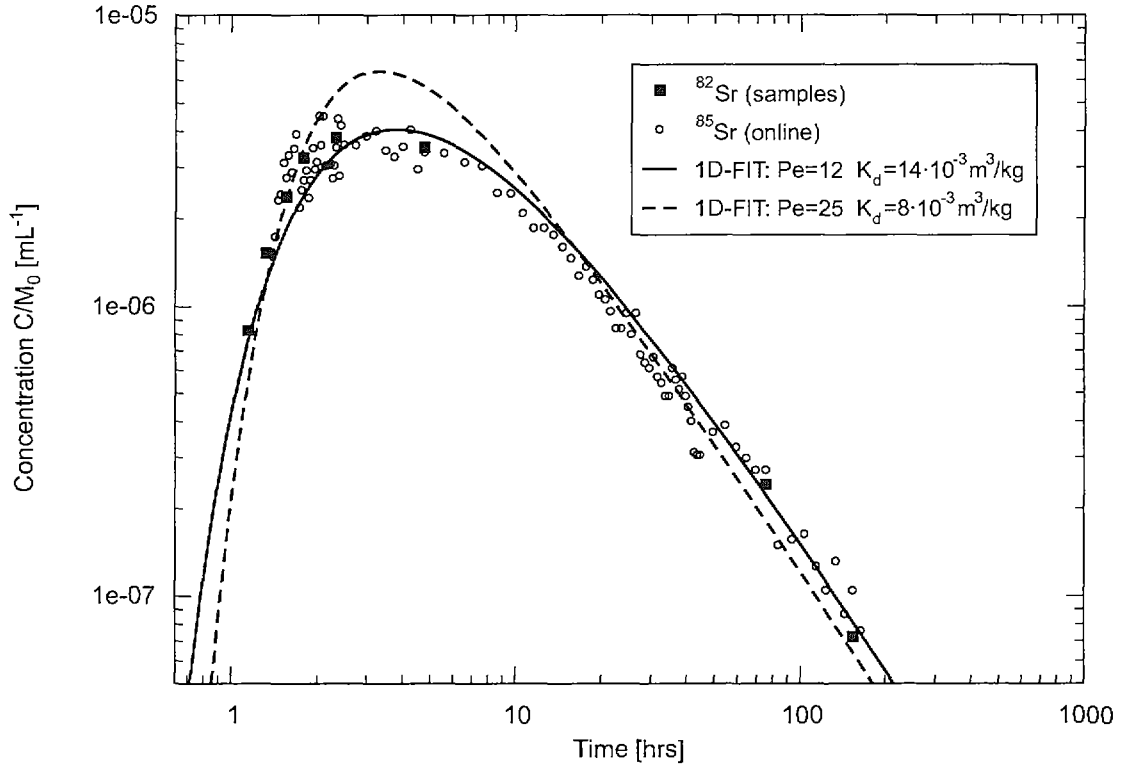

Fig. 3-5: The breakthrough data for Sr from run #21 and fits of the Sr data using the 1-D advection-dispersion model with unlimited matrix diffusion, obtained by varying both the Peclet Number Pe and sorption coefficient K_d simultaneously (solid line) and by fixing Pe at the value for uranine and varying only K_d (dashed line).

3.1.2 The non-Fickian dispersion model

Given that the fit of the advection-dispersion models to the breakthrough data for Th, Tb and Hf was not entirely satisfactory, and given the evidence (especially from dipole 3) that these tracers are transported as colloids that are not retarded by matrix diffusion and sorption (see Chapter 5), it seems reasonable to suggest that it is an inappropriate representation of advection and dispersion that gives rise to the discrepancies. Thus, the non-Fickian dispersion (CTRW) model was applied to the breakthrough curves to see whether an improved fit could be obtained.

The uncertainty in the breakthrough data for Th, Tb and Hf in the case of dipole 1 is relatively large, and it is not possible to obtain unique parameters for the CTRW model from these data by curve fitting. This difficulty was overcome by fitting the bentonite colloid breakthrough data from dipole 3, and assuming that the CTRW dispersion parameter β is the same for bentonite colloids in dipole 3 as for Th, Tb and Hf in colloidal form in dipole 1. This reduces the number of free parameters needed to fit the CTRW model to the breakthrough data for Th, Tb and Hf in dipole 1 to two (t_{mean} and b_β), and a good fit can be obtained, as shown in Fig. 3-6.

The mean particle velocity of the CTRW fit is lower than that of the 1-D advection-dispersion model fit (2.2×10^{-4} ms^{-1} in Fig. 3-6 compared to 7.5×10^{-4} ms^{-1} in Tab. 3-2). This is due to the fact that the stream tube approach matches the velocity for the breakthrough peak, whereas the CTRW approach yields the velocity of the centre of mass of the particle plume.

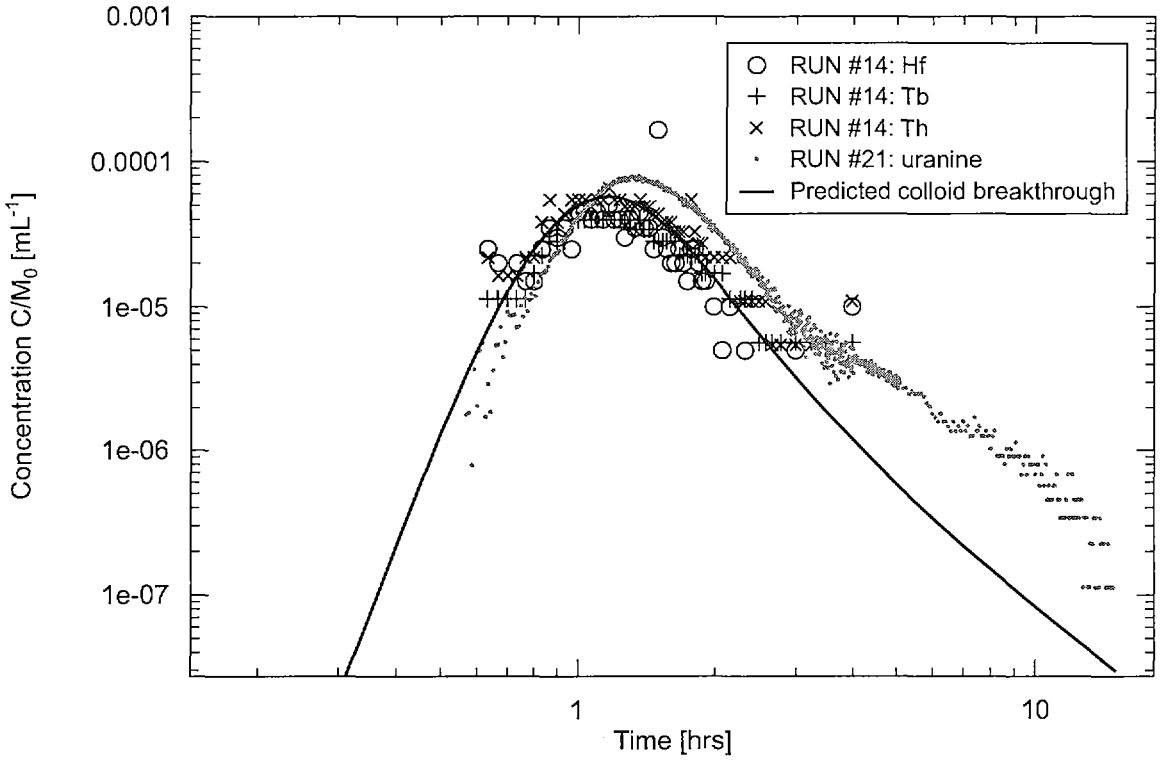

Fig. 3-6: The breakthrough data for Th, Tb and Hf from run #14, and uranine from run #21, and fits of the Th, Tb and Hf data using the non-Fickian dispersion (CTRW) model. CRTW parameters are $\beta = 1.2$ (from dipole 3), $t_{mean} = 2.0$ hours and $b_\beta = 0.335$. The calculated mean particle velocity is 2.2×10^{-4} ms^{-1}.

For fitting the colloid breakthrough data from dipole 3 with the CTRW model, the colloid injection functions[22] for relevant experimental runs were repeatedly convoluted with FPTD[23] solutions for particular combinations of the CRTW parameters, and the parameters were adjusted until optimal fits were obtained. Fits for run #6a (bentonite colloids) and run #7a (bentonite colloids, together with Th, Tb and Hf) are shown in Figs. 3-7 and 3-8, respectively. In each case, a combination of automated non-linear curve fitting and manual selection of fitting parameters was used.

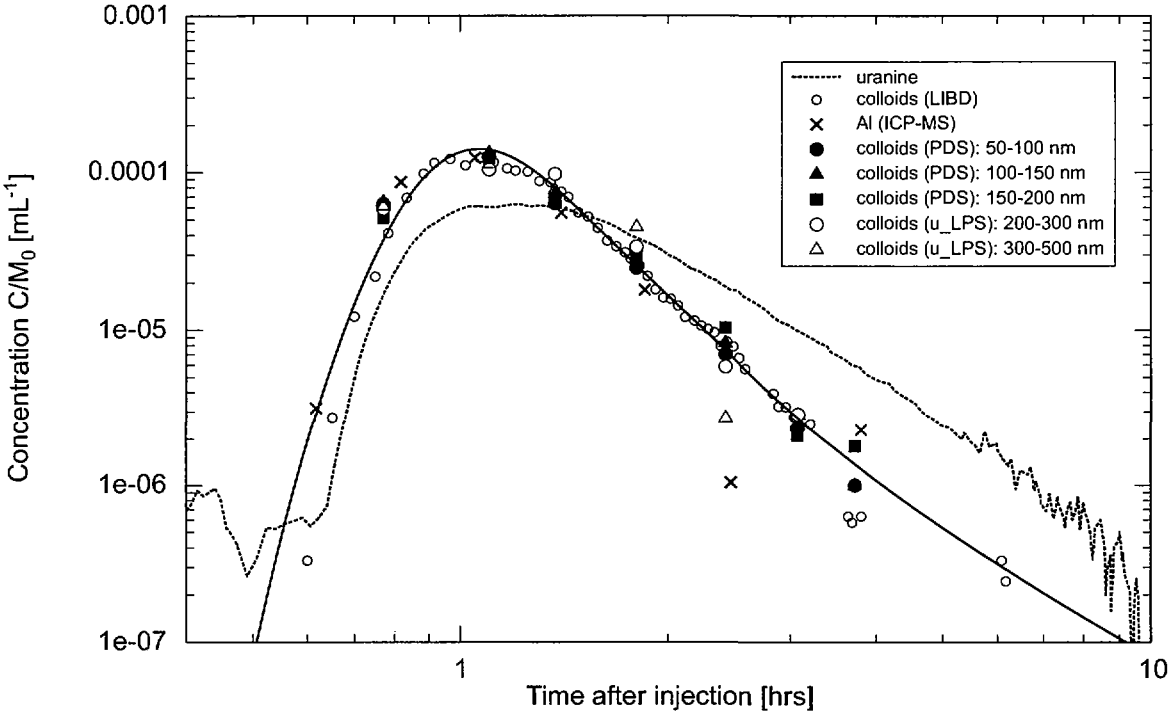

Fig. 3-7: The breakthrough data for bentonite colloids from run #6a, and uranine from run #6, and fits of the bentonite colloid data using the non-Fickian dispersion (CTRW) model. CRTW parameters are $\beta = 1.2$, $t_{mean} = 1.42$ hours and $b_\beta = 0.25$. The calculated mean particle velocity is 9.8×10^{-4} ms^{-1}. Colloid recovery for each size fraction is normalised to 100 %.

In Fig. 3-9, the fits from Figs. 3-7 and 3-8 are superimposed on the breakthrough data for Th and Tb in run #15. Run #15 was intended as an additional check to confirm the migration behaviour of Th and Tb. The CTRW curve from Fig. 3-7 (run #6a) in particular gives a good fit of both early and late time behaviour of the breakthrough data.

If non-Fickian dispersion of colloids occurs, it seems reasonable to suppose that tracers in the aqueous phase may also be affected by non-Fickian dispersion, even if it is not necessary to invoke this effect in order to reproduce the shape of the breakthrough curves. The possibility of non-Fickian dispersion of solutes is discussed in Section 6.4.

---

22 The injection functions for colloids were not directly available. Rather, the normalised measured uranine concentrations in the injection borehole were taken and the assumption made that these also gave the injection function for colloids.

23 First Passage Time Distribution (see section 2.5)

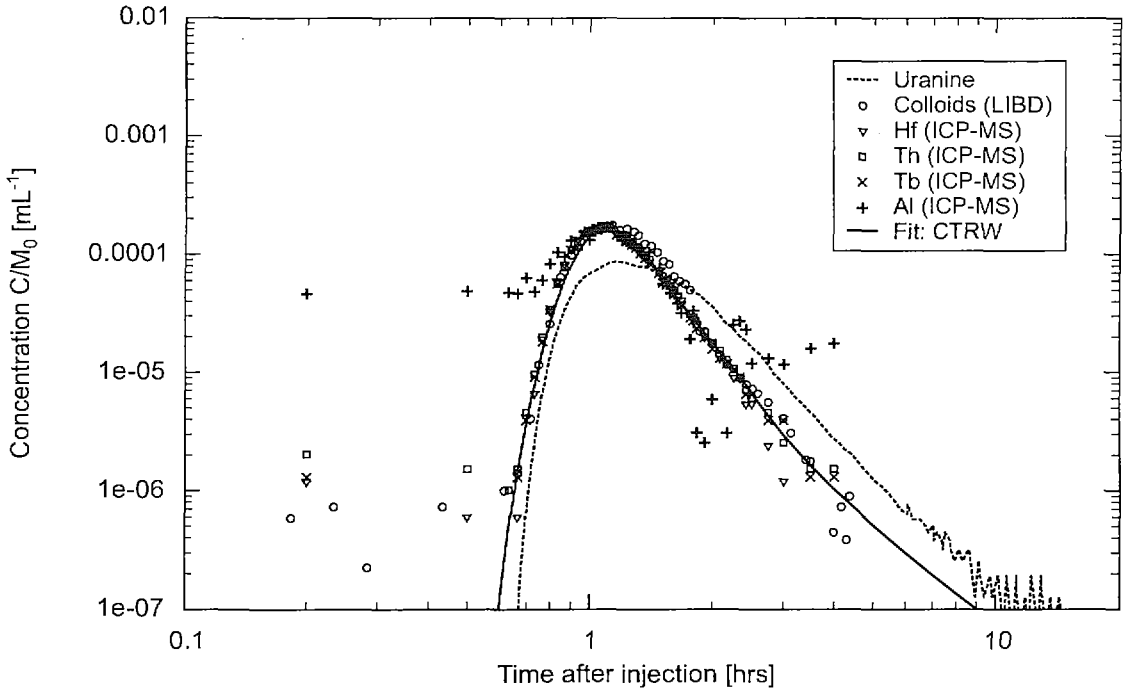

Fig. 3-8: The breakthrough data for bentonite colloids and Th, Tb and Hf from run #7a, and uranine from run #7, and fits of the bentonite and Th, Tb and Hf colloid data using the non-Fickian dispersion (CTRW) model. CRTW parameters are $\beta = 1.2$, $t_{mean} = 1.40$ hours and $b_\beta = 0.25$. The calculated mean particle velocity is 9.9×10^{-4} ms^{-1}. Recovery in each case is normalised to 100 %.

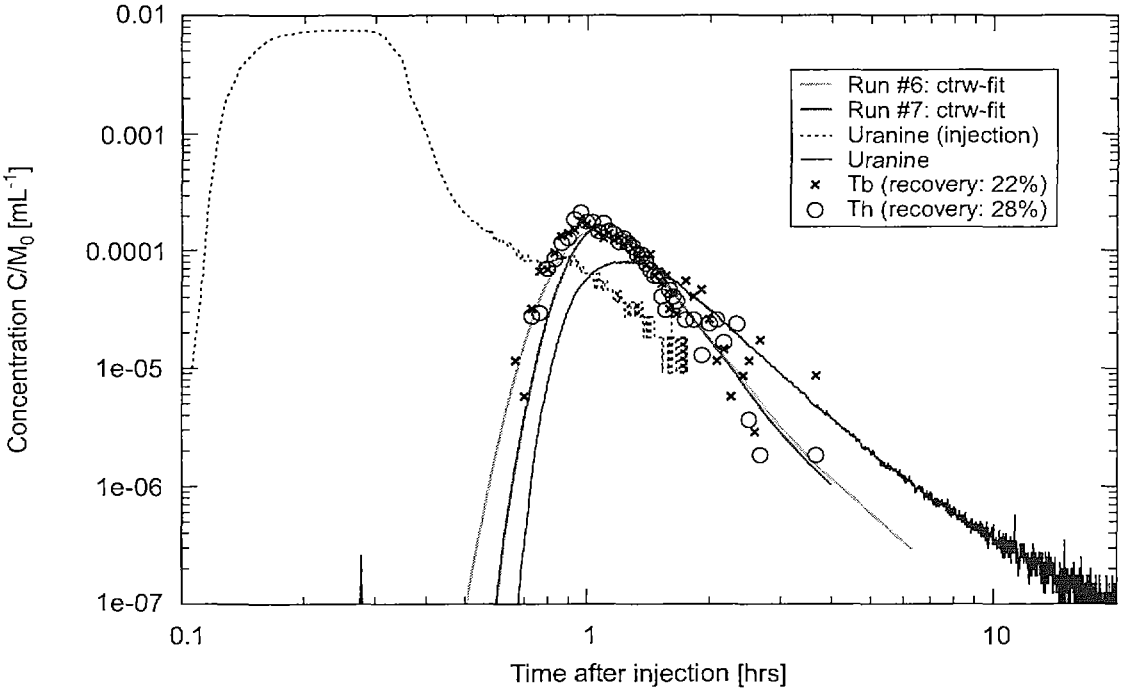

Fig. 3-9: The CTRW fits from run #6a (Fig. 3-7) and #7a (Fig. 3-8), superimposed on the breakthrough data for Th and Tb from run #15. Uranine data from run #16 are also shown.

3.2 Predictive modelling

3.2.1 Models used

Given the similarity between the results of the 1-D and 2-D advection-dispersion models as shown in the previous section, predictive modelling of aqueous tracer transport for the main runs #31 and #32 was carried out using the 1-D advection-dispersion model only. The non-Fickian dispersion model was used for predictions of colloid transport.

3.2.2 Use of predictive modelling for the planning of runs #31 and #32

An evaluation of the predictions made for runs #31 and #32 in advance of the runs being carried out showed that, for the planned injection concentrations, the breakthrough curves would exceed detection limits and, in nearly all cases, it should be possible to measure the full breakthrough in 10 days (240 hours), the planned duration of the experiment. The exception was Cs in run #32. It was predicted that the breakthrough tail for Cs transported in solution would not be detected, and this was confirmed on carrying out the run (see below). The modelling study thus provided a useful planning tool for the experiments.

3.2.3 Predictions and measurements of Am breakthrough

Fig. 3-10 shows the model predictions and measured data for Am breakthrough in runs #31 and #32. There is a marked difference between the predictions for the two runs, due to (i), the relatively high sorption of Am on rock matrix pores, leading to a retardation of Am in solution in run #31, and (ii), the high colloid-bound fraction assumed for Am in run #32, which is not subject to retardation by matrix diffusion and sorption (see Tab. 2-2). The amount of Am predicted to be transported in solution in run #32 is very small and is only visible in the change of the slope for the late time breakthrough curve, as discussed below.

Although the model prediction was that breakthrough for run #31 should be significantly more retarded than that for run #32, the experimental data for run #31 and run #32 in fact coincide closely with each other and with the model prediction for run #32. This strongly suggests that the assumption made in modelling run #31 that Am migrates as an aqueous solute is incorrect, and that it in fact migrates predominantly in colloidal form, even in the absence of bentonite colloids in the injection cocktail.

The predicted breakthrough curve for run #32 is based on the superposition of colloid facilitated transport, which dominates the shape of the breakthrough curve at earlier times, and solute transport, retarded by matrix diffusion and sorption on matrix pore surfaces, which dominates at later times. The change from one dominant transport mechanism to the other is apparent in the change in slope that occurs at about 20 hours after injection. The slope of the breakthrough curve beyond this change is proportional to $t^{-3/2}$, the signature of matrix diffusion. The α-spectroscopy measurements for run #32 and the ICP-MS measurements for runs #31 and #32 match well the predicted curve for run #32 at earlier times, indicating that colloid facilitated transport occurred in both runs. The α-spectroscopy breakthrough curve for run #32 also shows the predicted change in slope, indicating a change in transport mechanism. The change, however, occurs at 3 to 4 hours, rather than the 20 hours predicted. This difference can be attributed to an overestimation of the sorption on rock matrix pores in the predictions. The other measured curves finish too soon to show the change in slope unambiguously. The fact that this change in slope is present in measurements which continue to long enough times is, however, a strong indication that the two different mechanisms do indeed contribute to the transport of Am.

The major part of these tracers is transported in association with (or in the form of) colloids and breaks through at earlier times. A minor part is transported in solution and, because of retardation by matrix diffusion and sorption, breaks through later.

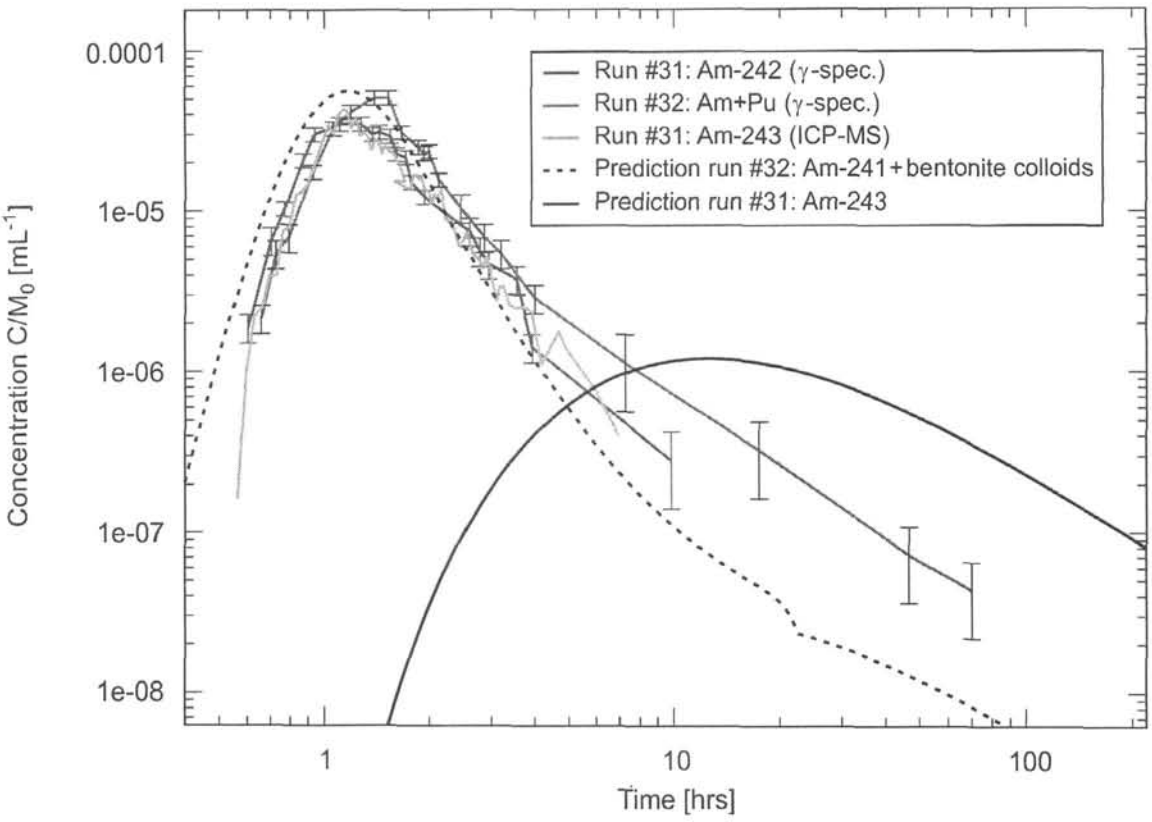

Fig. 3-10: The predictions (black solid and dashed lines) and measured data (coloured lines) for Am breakthrough in runs #31 and #32.

3.2.4 Predictions and measurements of Pu breakthrough

Fig. 3-11 shows the predictions and measured data for Pu breakthrough in runs #31 and #32. Similar observations are made here as in the case of Am. The comparison of predictions with experimental data for run #31 strongly suggests that the assumption of the model for this run, namely that Pu migrates entirely as an aqueous solute, is incorrect, and that, like Am, it in fact migrates predominantly in colloidal form, even in the absence of bentonite colloids from the injection cocktail.

3.2.5 Predictions and measurements of Np breakthrough

Fig. 3-12 shows the predictions and measured data for Np breakthrough in runs #31 and #32. The predictions for the two runs are similar, due the low colloid-bound fraction assumed for Np even in the presence of bentonite colloids. Np is thus predicted to be transported predominantly as an aqueous solute in both runs. The effects of colloids are evident only in the higher predicted breakthrough concentrations at early times in the case of run #32.

The experimental data for run #31 and run #32 coincide closely with each other and with the predictions. The early time breakthrough is not sufficiently resolved in the experimental data to identify the effects of colloids.

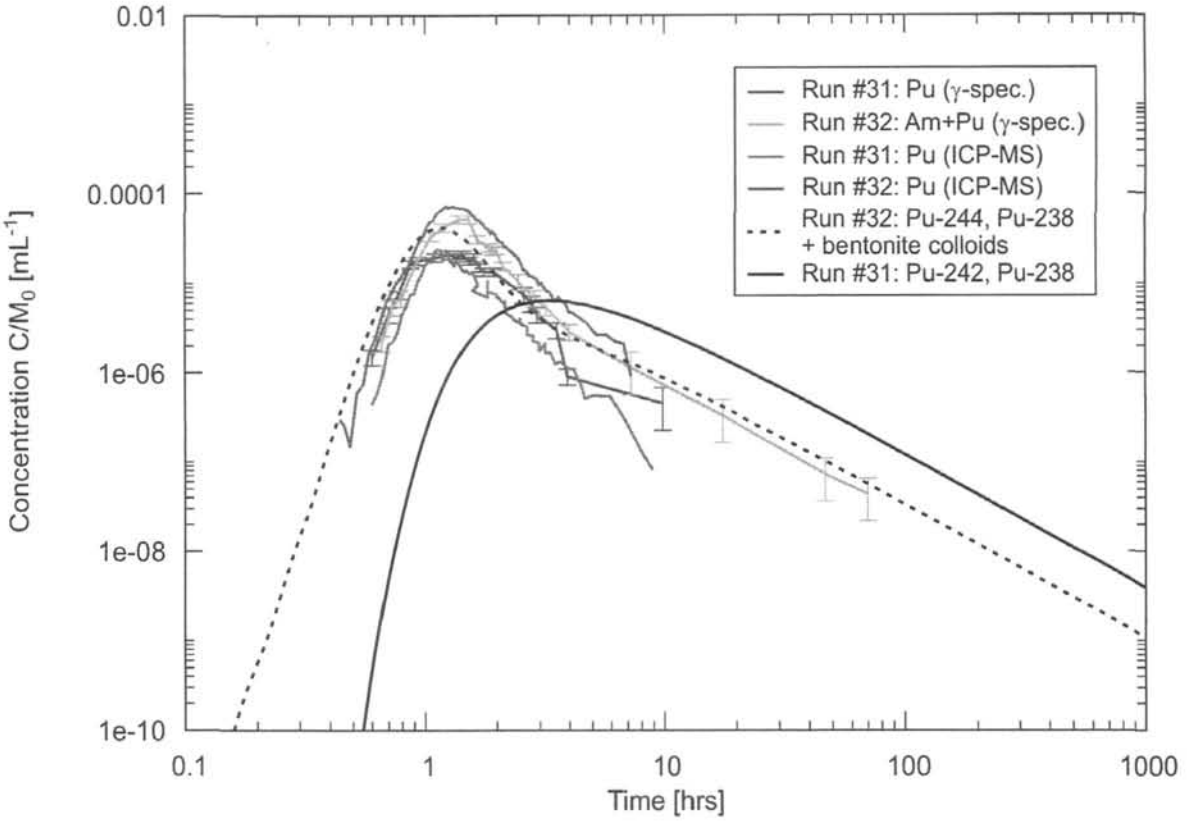

Fig. 3-11: The predictions (black solid and dashed lines) and measured data (coloured lines) for Pu breakthrough in runs #31 and #32.

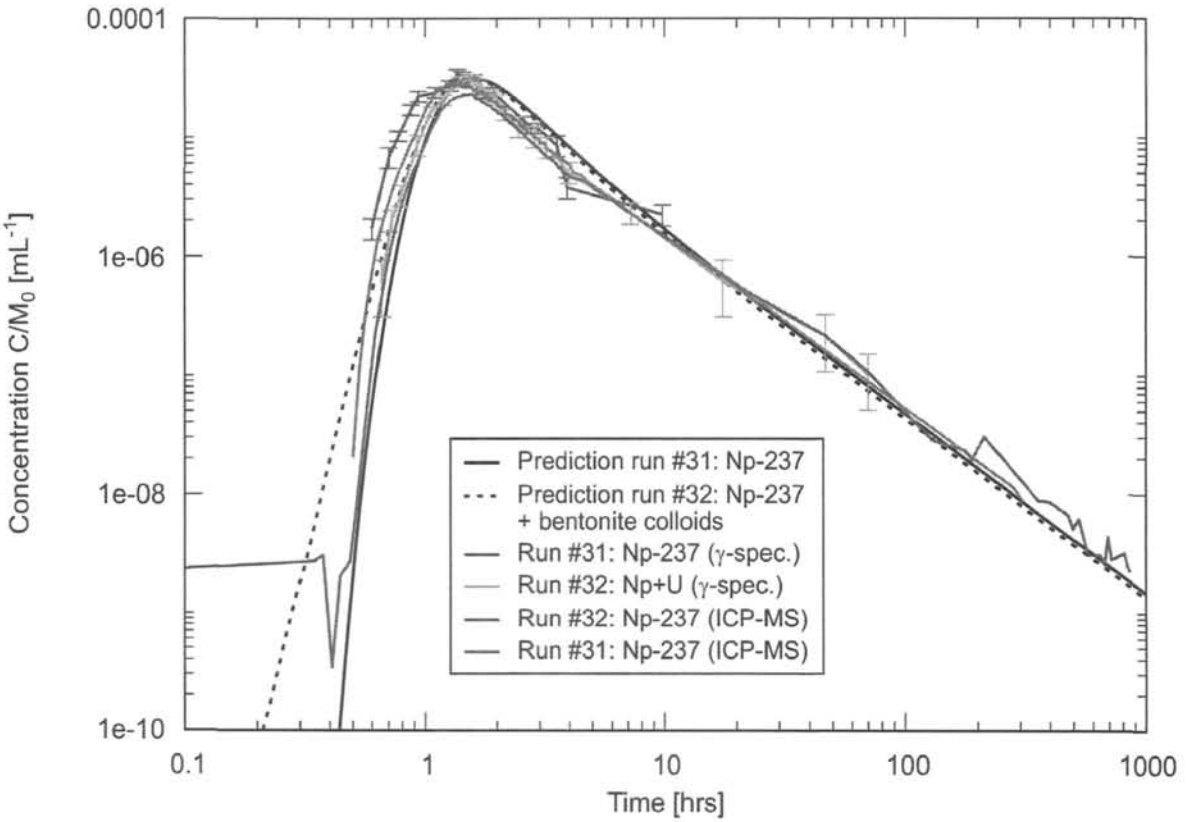

Fig. 3-12: The predictions (black solid and dashed lines) and measured data (coloured lines) for Np breakthrough in runs #31 and #32.

3.2.6 Predictions and measurements of U breakthrough

Fig. 3-13 shows the predictions and measured data for U breakthrough in runs #31 and #32. As in the case of Np, the predictions for run #31 and run #32 are similar due the fact that U is transported predominantly as an aqueous solute in both runs.

The experimental data for run #31 and run #32 coincide closely with each other (again, as in the case of Np), but differ significantly from the predictions. In particular, the peak in the measured data is higher and earlier compared to the predictions. It appears that the sorption of U on the matrix pore surfaces has been overestimated using the sorption coefficients given in Tabs. 2-1 and 2-2. Possible reasons are discussed in detail in Möri (2004) and Missana and Geckeis (2004) [24].

3.2.7 Predictions and measurements of Cs breakthrough

Fig. 3-14 shows the predictions and measured data for Cs breakthrough in run #32; Cs was not used in the injection cocktail for run #31. Cs has a colloid bound fraction (about 15 %) that is intermediate between the high values (98 % and 72 %) for Am and Pu and the much lower values for Np (9 %) and U (2 %). Both colloidal and aqueous phase transport are significant and, since sorption of Cs on matrix pore surfaces is relatively strong, the aqueous component is significantly retarded. This gives rise to two peaks in the breakthrough curves. The first corresponds to the breakthrough of Cs sorbed on bentonite colloids. The second corresponds to the breakthrough of Cs transported in aqueous solution and delayed by matrix diffusion and sorption on the porous rock matrix.

Both prediction and experimental results show two peaks and there is reasonable agreement in their times of occurrence. There are, however, discrepancies in the magnitudes of the peaks, which may be attributed, at least in part, to inaccuracy in assumed colloid bound fraction (see Chapter 4). In the case of the second peak, an additional factor contributing to the discrepancy between prediction and experiment may be the neglection of non-linear sorption and the natural background concentration of Cs in the predictions.

[24] Another possible reason, as discussed in Bradbury and Baeyens (2003), is that scaling effects, experimental procedures or mineralogical variability can lead to sorption coefficients measured in laboratory experiments differing by a factor of about 5 from those applicable *in situ*, although it is unclear why this should be a difficulty in the case of U, but not, say, in the case of Np in the present study. Alexander et al. (2003b) noted kinetic effects in U sorption on Grimsel granite and this may play a role here.

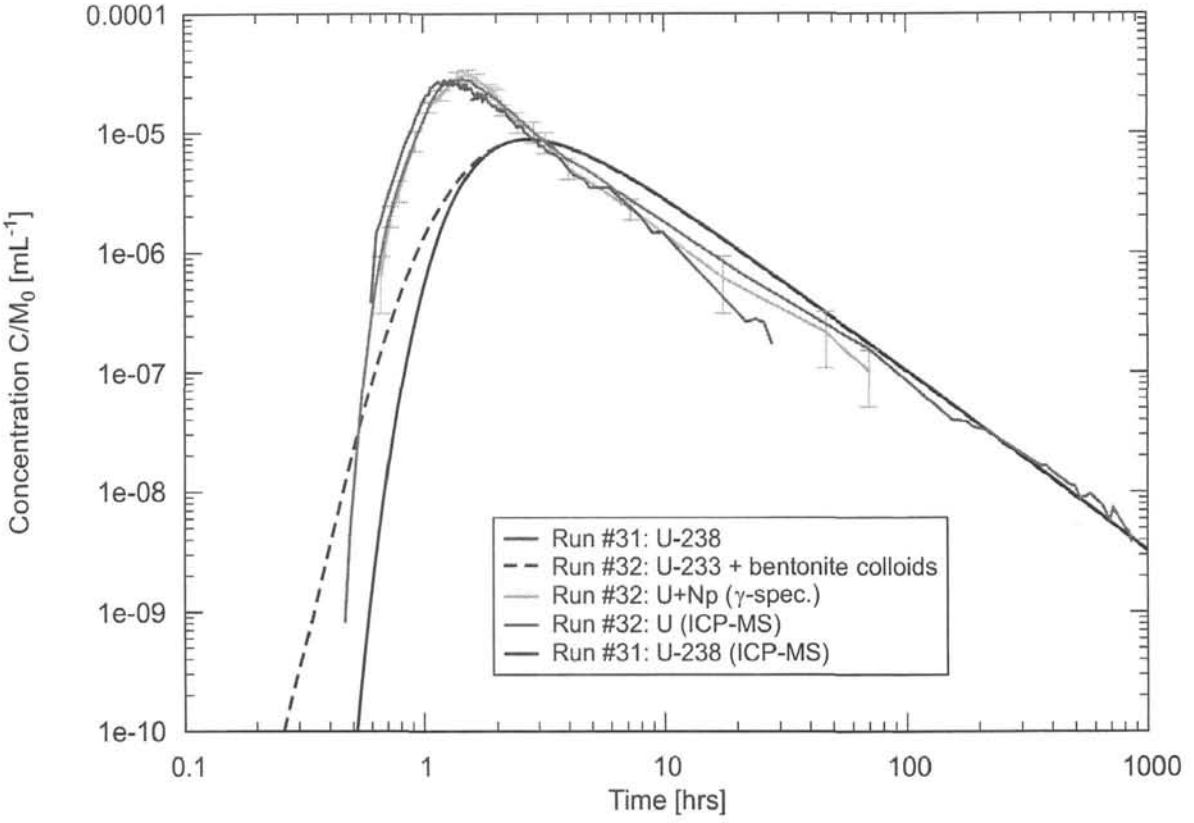

Fig. 3-13: The predictions (black solid and dashed lines) and measured data (coloured lines) for U breakthrough in runs #31 and #32.

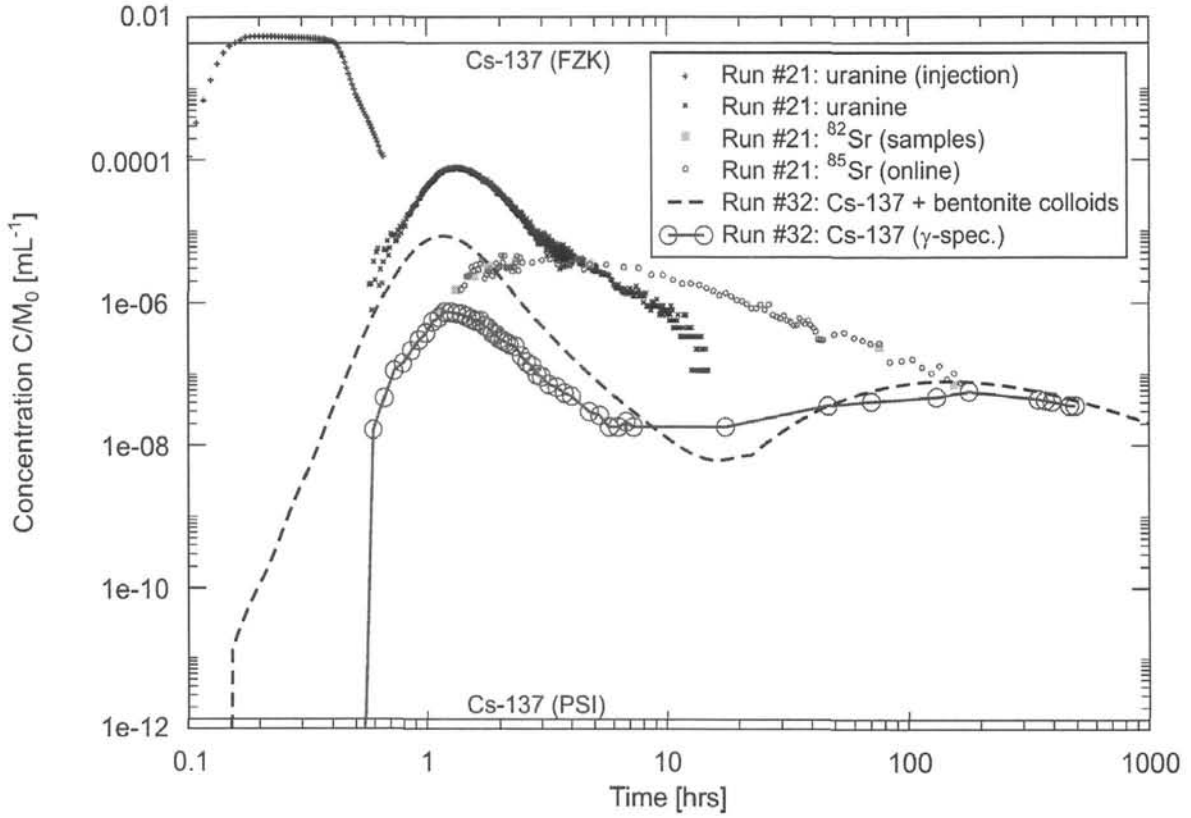

Fig. 3-14: The predictions (black dashed lines) and measured data (coloured lines) for Cs breakthrough in run #32.

4 Review and modification of model concepts and parameters in the light of the measured data and the comparison between predictions and measurements

This chapter presents a review of the model concepts and parameters used in the analyses and predictions of Chapter 3, in the light of the measured data from the main runs, and describes some modifications that improve agreement between theoretical and measured breakthrough curves. Section 4.1 describes some general observations that strongly suggest that at least a part of the injected inventories of Am, Cs, Pu and Th migrates in association with colloids. Section 4.2 discusses the specific influence of bentonite colloids on transport. It is noted that Am, Pu and Th (and also Tb and Hf) are transported in colloidal form, even when no bentonite colloids are added to the injection cocktail, but the addition of bentonite colloids increases the recovery of these tracers. It is also noted that the characterisation of colloids in the injection cocktails (not available at the time that the predictions were made) enables improved agreement to be obtained between calculations and measured breakthrough curves. Section 4.3 describes how a minor adjustment of one of the parameters of the non-Fickian dispersion model improves agreement in the tailing part of the colloid breakthrough curves.

4.1 General observations

As noted in the previous sections, the measured breakthrough data for runs #31 and #32 show clear evidence for the association of a number of radionuclide tracers with colloids. In the case of run #32, Fig. 4-1 shows the breakthrough data for colloids, as well as for Am, Pu, Th and Cs. All are normalised to 100 % recovery, and, in the case of breakthrough curves measured using the colloid detection techniques LIBD, PDS, PCS and Al (see section 1.3 for an explanation of the abbreviations), the background concentration of natural groundwater colloids has been subtracted from the measured colloid concentrations. As noted already in Section 3.2.7, Cs shows two transport mechanisms. Transport in association with colloids is the relevant mechanism for early times up to about 5 hours and transport in solution dominates the later time breakthrough.

It can be seen that the breakthrough curves for colloids coincide closely with those of Am, Cs, Pu, Th, and also with that of the conservative tracer I, although the conservative tracer peaks appear slightly later and, as noted previously, Cs displays a second peak at a much later time. These observations support the model assumption that a part of the inventory of these radionuclides is transported in association with colloids. The discrepancies discussed in Chapter 3 between some measured breakthrough data and the predictions, however, call into question the assumptions regarding the proportions of some tracers that are associated with colloids, as well as the parameters describing the non-Fickian dispersion of colloids, as discussed in the following sections.

Colloid recoveries in main dipole 1 runs show qualitatively similar trends to those observed in the preliminary runs in dipole 3. The small colloid size classes show a nearly complete recovery, as indicated by the breakthrough measured with the LIBD and PDS techniques. The recovery decreases with increasing colloid size. The bulk mass recovery extracted from the normalisation of the breakthrough curves in Fig. 4.1 for all size classes is therefore lower: between 57 % (measured with PCS) and 70 % (Al content measured with ICP-MS). The bulk mass recoveries are not comparable in the two dipoles, because the size distributions of the injected bentonite colloids are different. There are much fewer larger colloids injected in run #32 and the greater degree of filtration of larger colloids means that mass recovery is greater than in the preliminary dipole 3 runs.

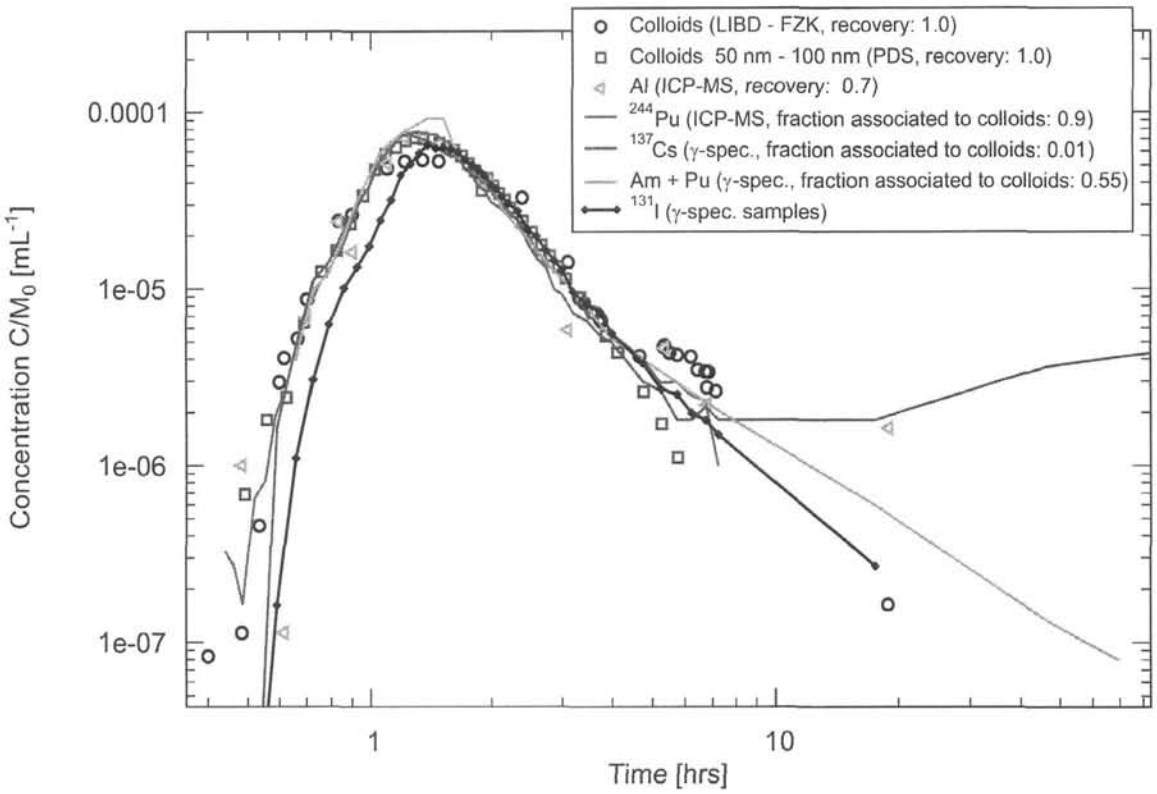

Fig. 4-1: The breakthrough data for colloids and tracers conveyed almost entirely (Am and Pu) or in part (Cs) on colloids from run #32.

4.2 The association of radionuclides with colloids

4.2.1 The influence of bentonite colloids on transport

At first sight, the results in Chapter 3 appear to suggest that the presence of bentonite colloids significantly affected transport only in the case of Cs. U and Np were transported predominantly as aqueous species in both main runs. Am, Pu, Th, Tb and Hf were transported in colloidal form, even when no bentonite colloids were added to the injection cocktail. The addition of bentonite colloids does, however, significantly affect the *recovery* of these tracers.

Fig. 4-2 shows the breakthrough data for Th, Tb and Hf injected together with bentonite colloids in run #7a, as well as data for uranine (complete recovery) and the recovery for each tracer. Fig. 4-3 shows a similar plot for the case where Th, Tb and Hf are injected without bentonite colloids being present (run #15).

A comparison of the recoveries of Th, Tb and Hf in the two cases clearly indicates that the presence of bentonite colloids substantially increases the recovery. This suggests that, without the addition of bentonite colloids, a significant fraction of the injected inventories of these tracers enters the dipole as aqueous solutes. These solutes are then retarded so strongly that they do not break through over the timescale of the experiments. With the addition of bentonite colloids, greater proportions of the injected inventories enter the dipole in association with colloids, and thus experience little or no retardation during transport, increasing the recovery.

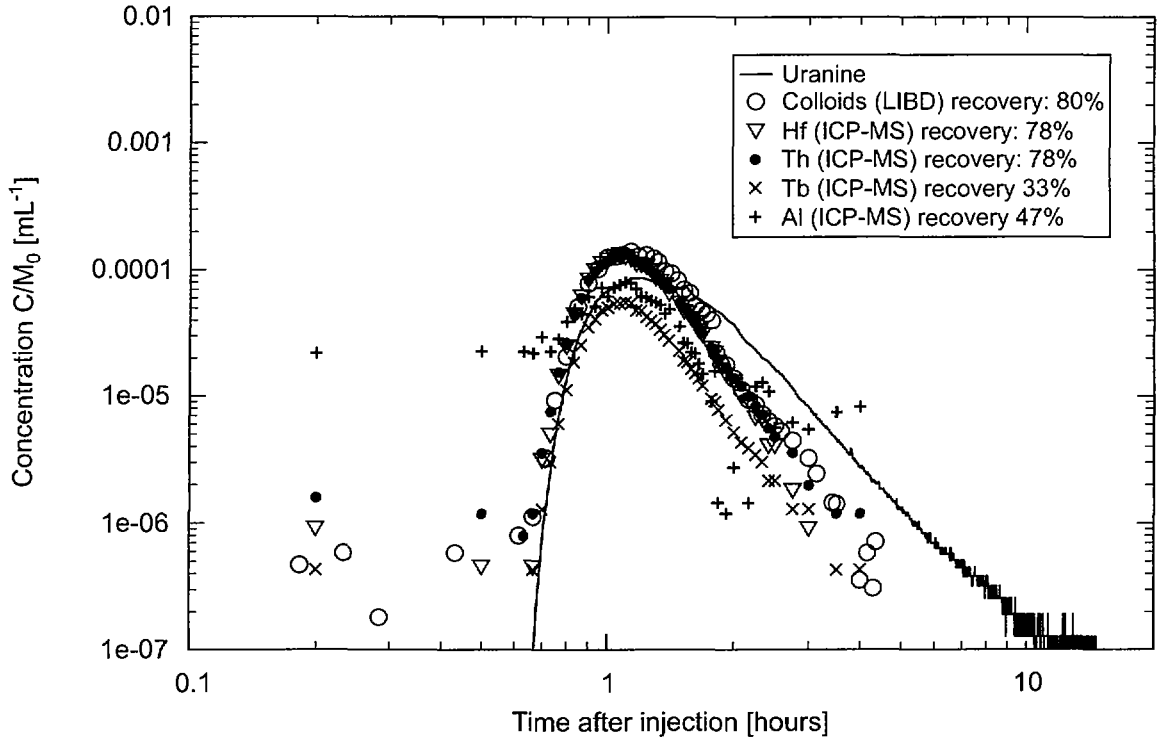

Fig. 4-2: The breakthrough data for Th, Tb and Hf injected together with bentonite colloids in run #7a, and data for uranine from run #7.

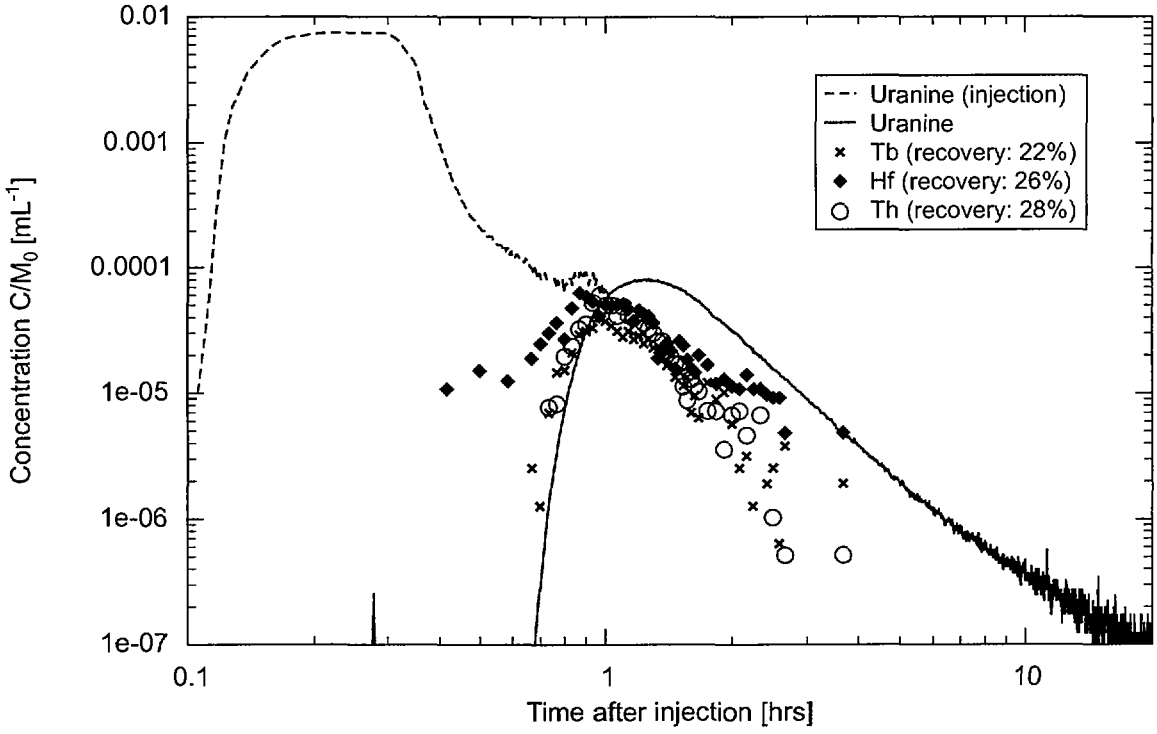

Fig. 4-3: The breakthrough data for Th, Tb and Hf injected with no bentonite colloids in run #15, and data for uranine from run #16 (with normalisation to 100 % recovery).

4.2.2 Characterisation of the colloid bound fractions in the injection cocktails

The injection cocktails for runs #31 and #32 were not completely characterised at the time the predictions were made. Although the fraction of the tracers associated with bentonite colloids could be estimated on the basis of batch experiments (Tab. 2-2), it was not clear if, and to what extent, elements form or become associated with other types of colloids e.g. by the precipitation of hydroxide/oxide colloids and/or sorption on natural groundwater colloids. The proportion of any given tracer transported on colloids (or in colloidal form) was therefore uncertain and, especially in the case of Am and Pu, led to significant discrepancies between predictions and measurements in the case of run #31.

After the predictions had been made, the injection cocktail was analysed, allowing the mass of each element in solution and the mass bound to colloids to be determined directly. LIBD confirmed that radiocolloids were present in the injection cocktail in run #31, even though no bentonite colloids had been added. The difficulty in measuring the colloidal fraction, which was found to vary between 5 and 58 %, suggests the presence of very small colloids or gel like aggregates of Am, Pu and Th. As in the case of Th, Tb and Hf in run #14 (see Section 3.1.1), it remains, however, an open issue whether the colloids associated with Am, Pu and Th are heterogeneous (natural groundwater colloids with associated radionuclides[25]) or homogeneous (formed e.g. by precipitation during the spiking procedure).

Run #32 showed a considerable fraction of Am, Pu and Th (84 – 99 %) and a smaller fraction of Cs and U (8 and 6 % respectively) present as colloids in the injection vial. The mean colloid size in the injection cocktail in the presence of bentonite colloids was determined by LIBD as 109 nm. An extensive discussion on these findings and possible reasons for them can be found in Möri (2004) and Missana and Geckeis (2004).

Tab. 4-1: Comparison of the colloid bound fraction used for predictive modelling of run #32 (see Tab. 2-2) and the measured colloidal fraction in the injection cocktail.

Tracer	**Values used for initial predictions** (calculated fraction sorbed on bentonite colloids [%])	**Values measured in the injection cocktail** (colloidal fraction measured in the injection cocktail [%]; see Möri et al. 2003; Möri, 2004)
Am-241	97.7	99
Pu-244	72.2	84
Pu-238	72.2	84
Cs-137	14.8	8
Np-237	9.1	0-1
U-233	1.6	6
Tc-99	0.7	12
Th-232	97.6	94
Sr-85	Not known	0
I-131	0	0

[25] There is, however, some evidence that the impact of natural groundwater colloids is negligible (see, e.g. Kosakowski and Baeyens, 2001).

The mass bound to colloids as measured in the injection cocktail in the case of run #32 (the right-hand column of Tab. 4-1) was found to show some differences from the values used for initial predictive modelling (the left-hand column). Based on the measured colloidal fraction in the injection cocktail, it was possible to recalculate the breakthrough curves, correcting the relative amounts of radionuclides transported as colloids and the amounts transported in solution. The result was a reasonable agreement with all the measured breakthrough curves. There remains, however, a systematic time difference of a few minutes between predicted and measured breakthrough curves, a possible reason for which is suggested in Chapter 6, as well as a discrepancy between predicted and modelled tailing of colloid breakthrough curves, which required a further modification of the non-Fickian dispersion parameters, as discussed below.

4.3 Advection-dispersion of colloids

The migration of colloids in run #32 was modelled using the non-Fickian dispersion (CTRW) model. It was observed (Section 3.2) that the measured tailing for Am and Pu, which are conveyed predominantly by colloids, is more pronounced than the predictions based on CTRW parameters obtained from the preliminary experiments in dipole 3. This suggests that the main fitting parameter of the CTRW model responsible for tailing (β) needs to be revised for use in dipole 1.

Fig. 4-4 shows the good agreement obtained with the measured data for colloids, and the tracers conveyed almost entirely (Am and Pu) or in part (Cs) on colloids, if β is decreased from 1.2 to 1.1. The fact that β is lower for dipole 1 than for dipole 3 indicates a stronger heterogeneity of the underlying flow field in dipole 1 (see e.g. Kosakowski, 2004; Berkowitz et al., 2001).

The breakthrough data for colloids and for the various tracers shown in Fig. 4-4 have been processed in order to facilitate comparison. The processing takes account of the different amounts of colloids or tracers that have been injected in each case, the fact that some measurement techniques are affected by background colloids, whereas others are not, and the fact that, in some cases at least, a part of the injected mass is not recovered. The processing procedure may be summarised as follows:

- normalise the measured concentrations with respect to the injected mass or colloid number,
- subtract the (normalised) background colloid concentration from the normalised breakthrough if necessary,
- shift the breakthrough curves vertically until they coincide with each other as closely as possible (or, in the case of Cs, until the first peak, which corresponds to colloid-facilitated transport, coincides as closely as possible to the other curves).

Each of these steps is now described in more detail.

In order to normalise the measured concentrations, they are divided by the injected mass or, in the case of the LIBD and PDS measurements, which gave colloid concentrations as numbers of colloids per unit volume of water, by the injected number of colloids.

Colloid concentrations measured using the LIBD, PDS and Al techniques are a superposition of the concentrations of the injected colloids and of natural (background) colloids. At the start of an experimental run, the concentration of background colloids in the groundwater of the experimental shear zone was determined using the three techniques. The breakthrough of injected colloids could then be calculated by subtracting the mean background colloid concentration (given in Tab. 4-2) from the measured concentrations. Note, however, that a

different value of the background concentration is determined by each method because each technique samples a different part of the overall colloid size distribution.

Tab. 4-2: Comparison of the parameters needed to scale the curves in Fig. 4-4 to the same recovery.

Tracer	**Factor *F***	**Normalised background colloid concentration** [mL^{-1}]
LIBD	1	3.4×10^{-6}
PDS (50 nm –100 nm)	1	4×10^{-6}
Al	0.7	6.92×10^{-5}
^{244}Pu (ICMP-MS)	0.9	0
^{137}Cs (γ-spec.)	0.01	0
Am+Pu (α-spec.)	0.55	0

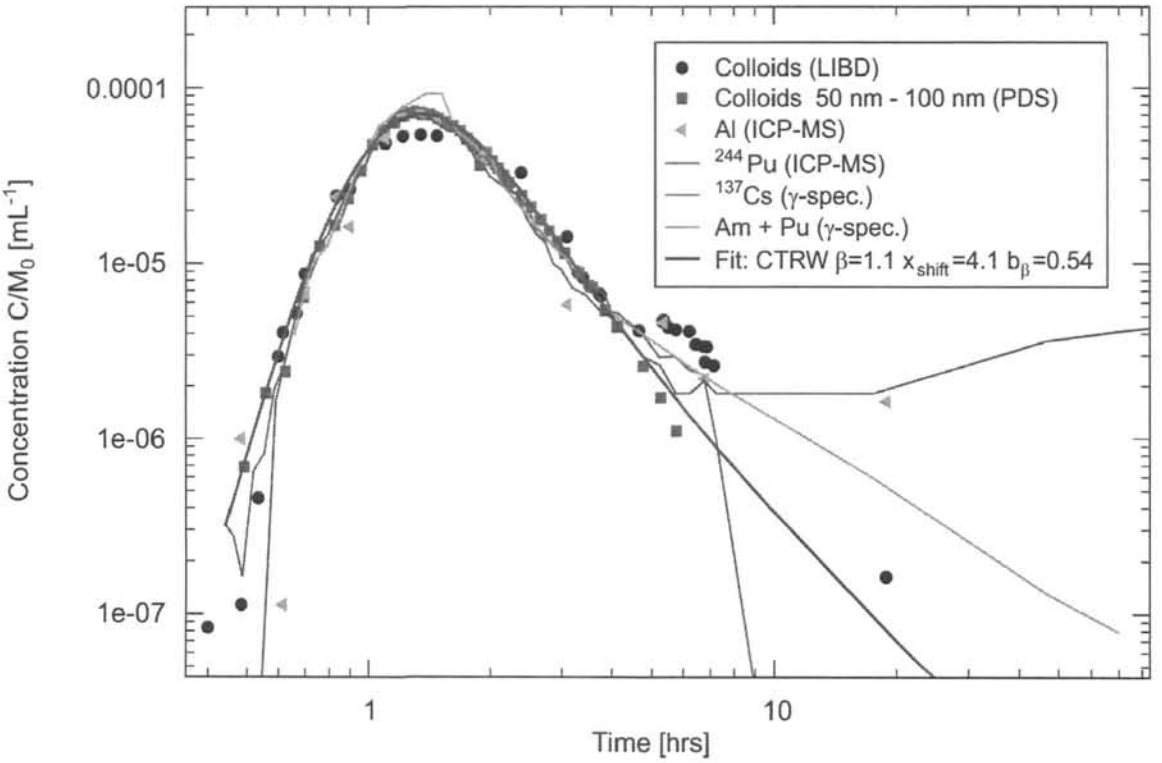

Fig. 4-4: The breakthrough data for colloids and tracers conveyed almost entirely (Am and Pu) or in part (Cs) on colloids from run #32, and a fit using the non-Fickian dispersion (CTRW) model. The breakthrough in each case is normalised to a recovery of 100 %. CRTW parameters are $\beta = 1.1$, $t_{mean} = 4.1$ hours and $b_\beta = 0.45$. The calculated mean particle velocity is 1.7×10^{-4} ms^{-1}.

Finally, the breakthrough curves are shifted vertically. Since the vertical scale in Fig. 4-4 is logarithmic, this is equivalent to dividing by a factor F. LIBD and PDS both sample colloids at the low end of the size distribution, which show a complete recovery. F is set to unity for the breakthrough of colloids measured using these techniques (i.e. no vertical shift is applied). The Al measurements, on the other hand, sample the whole distribution of colloid sizes. The filtration of larger colloid size classes (Möri, 2004) means that colloid breakthrough curves measured using this technique have to be shifted vertically upwards in order to make them coincide with the curves measured using LIBD and PDS. The vertical shift applied to the LIBD and PDS colloid curves corresponds to a value $F = 0.7$, implying a 70 % overall recovery of colloids. Similarly, since Pu and Am are transported principally in colloidal form, the values of F required to make their breakthrough curves coincide with the curves measured for colloids using LIBD and PDS can be interpreted as the recovery of all the colloids (bentonite and others) with which the tracers are associated (see the discussions in Sections 3.1.1 and 4.2.1).

In case of Cs, the value of F of 0.01 required to shift the first Cs peak so that it coincides with the LIBD and PDS colloid peaks implies that 1 % of the injected Cs is associated with colloids and recovered. The rest is either associated (irreversibly, at least on the timescale of the experiment) with colloids that are filtered, or is transported in solution, retarded by matrix diffusion and sorption onto solid surfaces, and gives rise to the second peak.

It should be noted that the values of the colloid bound fractions for Pu and Am derived from the shift in the curves required for full recovery are relatively close to the ones calculated prior to the experiments on the basis of batch sorption experiments, and also close to the colloid bound fractions measured by directly characterising the injection cocktail (see Tab. 4-1). For Cs, F is significantly lower than expected on the basis of the calculated and measured colloid bound fractions. This might suggest that a part of the Cs associated with colloids at the time of injection is desorbed during migration though the shear zone.

5 Justification for the use of the non-Fickian dispersion model for colloid transport

This chapter describes the reasons why advective and hydrodynamic dispersion processes, as represented by the non-Fickian dispersion (CTRW) model, are a likely explanation for the inability of the 1-D and 2-D advection dispersion models to fit colloid breakthrough curves adequately. Possible factors affecting the tailing of colloid breakthrough are reviewed in Section 5.1, including the influence of (i), diffusion processes (and, in particular, the possibility of matrix diffusion of colloids), (ii), the influence of the injection process (i.e. discrepancies between the assumed injection function and the actual injection function), (iii), the finite width of the dipole flow field, (iv), the interaction of colloids with fracture walls, and (v), the velocity profile across the fracture, which could have different effects on the breakthrough of colloids and solutes (i.e. differences in Taylor dispersion). (i) - (iv) do not provide an adequate explanation of the observed tailing. The possible effects of differences in Taylor dispersion remain, however, an open issue. Finally, in Section 5.2, evidence that supports the influence of non-Fickian dispersion on the tailing of colloid breakthrough curves is presented.

5.1 Possible factors affecting the tailing of colloid breakthrough curves

5.1.1 Overview

It was shown in Chapter 3 that the fits of the 1-D and 2-D advection-dispersion models without matrix diffusion to the breakthrough data for colloids, or radionuclides associated with colloids, were not satisfactory. In particular, it was not possible to fit both the early and the late concentrations with a single value for the dispersion length (see Fig. 3-1). The non-Fickian dispersion (CTRW) model, which provides a more generally applicable representation of advective and hydrodynamic dispersion processes in highly heterogeneous media, gave a considerably improved fit. As discussed below in Section 5.2, this is in accordance with increasing evidence of non-Fickian dispersion reported in the literature. Such non-Fickian dispersion gives rise to a scale-dependent spreading of contaminant plumes, as well as earlier breakthrough times or longer late time tails in the breakthrough curves, compared with predictions based on Fickian dispersion.

The similarity of the measured breakthrough data for conservative tracers and colloids (see, e.g. Fig. 4-1), however, raises the question as to whether matrix diffusion of colloids, rather than non-Fickian dispersion of colloids, could provide an equally satisfactory explanation of the tailing behaviour of the colloid breakthrough data. This possibility is considered in Section 5.1.2. A number of other explanations have also been proposed for the tailing of solute and colloid breakthrough curves in fractured geological media (Becker and Shapiro, 2000, 2003), including that it is an artefact of the tracer injection process, the result of the finite width of the dipole flow field, or the result of interactions with the fracture walls. These possibilities, along with the possible effects of Taylor dispersion, are considered in Sections 5.1.3 - 5.1.6.

5.1.2 Influence of diffusion processes

It is certainly possible to fit the breakthrough data for the colloids with the advection-dispersion models if matrix-diffusion is included. This is illustrated in Fig. 5-1 for dipole 3. It is not, however, possible to obtain a fit with a physically plausible combination of values for the matrix porosity, the fracture aperture and the diffusion coefficient.

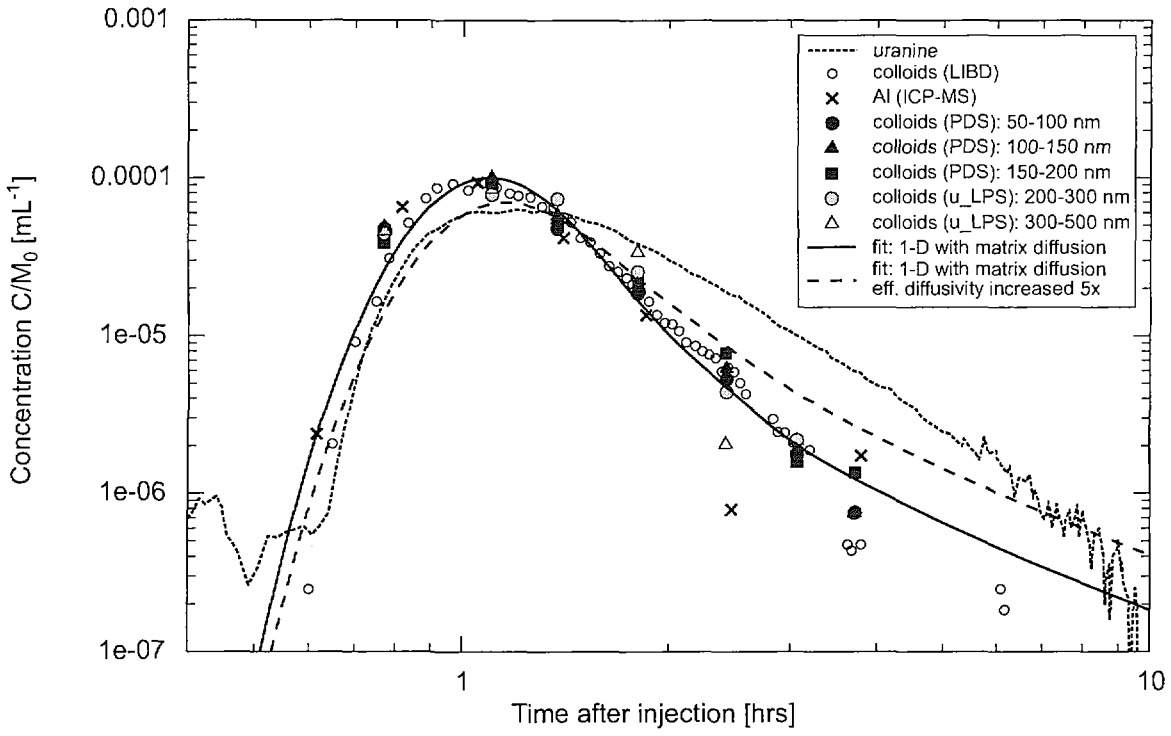

Fig. 5-1: The breakthrough data for bentonite colloids from run #6a, and uranine from run #6, and fits of the bentonite colloid data using the 1-D advection-dispersion model with matrix diffusion.

The fit shown by the solid line in Fig. 5-1, for example, is based on a value for the pore diffusion coefficient of colloids of 10^{-11} m^2s^{-1}. The actual diffusion coefficient for colloids in water, D_0, can be evaluated using the Stokes-Einstein equation:

$$D_0 = \frac{k_b T}{6\pi\mu r}, \qquad (5\text{-}1)$$

where T is temperature, taken to be 283 K, μ = 1.31 mPas is the dynamic viscosity of water at this temperature, $k_b = 1.38 \times 10^{-23}$ Jkg^{-1} is the Boltzmann constant and r [m] is the particle radius. Measured mean colloid sizes ($2r$) range between 75 nm and 4000 nm. Thus, for a mean particle size of 75 nm, $D_0 = 4.2 \times 10^{-12}$ m^2s^{-1} and, for a mean particle size of 400 nm, $D_0 = 8.0 \times 10^{-13}$ m^2s^{-1}. In a porous medium, the pore diffusion coefficient of colloids, like solutes, depends on the structure of the pore space and, in particular, its tortuosity (i.e. the tortuosity of the transport paths through pore spaces), and constrictivity (a measure of the way the cross section of a transport path through pores varies over its length). The pore diffusion coefficient is lower than the diffusion coefficient in free water, typically by a factor of between 0.01 (highly compacted bentonite) and 0.7 (sand) (De Marsily, 1986). Often the pore diffusion coefficient is approximated as the product of the free diffusion coefficient and the porosity of the medium. Thus, the pore diffusion coefficient for the smallest measured colloid size class (50 - 100 nm) and a matrix porosity of 0.3 (see Tab. 3.2) is in fact 1.26×10^{-12} m^2s^{-1}, and is eight times smaller than the pore diffusion coefficient used to fit the colloid breakthrough data in Fig. 5-1.

A further argument against matrix diffusion playing a significant role in the tailing of colloid breakthrough curves is that, according, for example, to Fig. 3-7, when normalised to 100 % recovery, the shape of the breakthrough curves for different colloid size fractions is the same -

the measured late time tailing does not show any dependence on the colloid size. From Eq. 5-1, a significant dependence on size is expected if the tailing is attributable to matrix diffusion[26]. This is consistent with the investigations of James and Chrysikopoulos (1999) on the influence of matrix diffusion on the breakthrough of polydispersed colloids in rough fractures, which showed that larger particles are the least retarded and smaller particles are more slowly transported. The effect of changing the diffusion coefficient by a factor of five on the breakthrough curve calculated using the advection-dispersion model with matrix diffusion is shown in Fig. 5-1. There is a clear shift of the breakthrough curve to the right (i.e. increased retardation). Such a shift is not observed in the measured breakthrough curves for different size fractions. This argument also suggests that diffusion into near-stagnant pore water within the fractures (e.g. in dead-end channels), if such volumes of water exist, is not responsible for tailing. Furthermore, as discussed in Section 5.2, although there are dead-end channels in the shear zone (see Möri et al., 2004, for example), these are not necessarily truly "dead" in terms of fluid flow, and advection may still dominate over diffusion when colloids or solutes enter these volumes.

It can be concluded that diffusion processes have only a minor influence on the transport of colloids in the shear zone.

5.1.3 Influence of the injection process

Often during tracer tests, the tracer is not injected as an ideal step function, but is rather introduced with a significant tailing. In such a case, the observed breakthrough will be influenced by this experimental artefact. The injection device used for the CRR tracer tests is equipped with a sensor for measuring the uranine concentration in the injection borehole. A typical injection function (uranine input) is shown in Fig. 5-2. The duration of the injection tail is much less than the breakthrough tails of the tracers (see the examples of uranine and Sr in Fig. 5-2, noting the logarithmic time scale). Furthermore, a sensitivity study with the CTRW and advection-dispersion models revealed that the tailing of the measured injection function has a negligible impact on the tailing of the breakthrough of conservative and sorbing tracers.

5.1.4 The finite width of the dipole flow field

Even in the absence of heterogeneity, streamlines in a dipole field connecting the injection and withdrawal well are of varying length and particles travelling along the streamlines have different mean velocities. Thus, the shape of a breakthrough curve can be affected by the different travel times of the tracer along different streamlines.

The experiments evaluated in this study use withdrawal flow rates that are 15 times higher than the injection flow rates. This results in a narrow dipole with a nearly radial convergent flow field around the withdrawal well and most of the injected tracer following a nearly direct line from the injection well to the withdrawal well. In such a flow field, the effect of the width of the flow field is minimised, as confirmed by the close agreement between results generated using the 1-D and 2-D advection-dispersion models.

Additional evidence for a relatively small spreading of the tracers due to this effect comes from the results of EP, which was conducted using a similar dipole flow field in the same shear zone. The portion of the shear zone from which tracers were recovered had a maximum width, in the shear zone plane, of about 0.5 m (Möri et al., 2003, Möri, 2004).

---

[26] The impact of pore diffusion coefficient on the form of the breakthrough curves is described, for example, in Heer and Hadermann (1996).

The finite width of the dipole field when coupled to the presence of heterogeneity may, however, give rise to more significant spreading of tracer breakthrough. The effects of heterogeneity on tracer dispersion are discussed in Section 5.2.

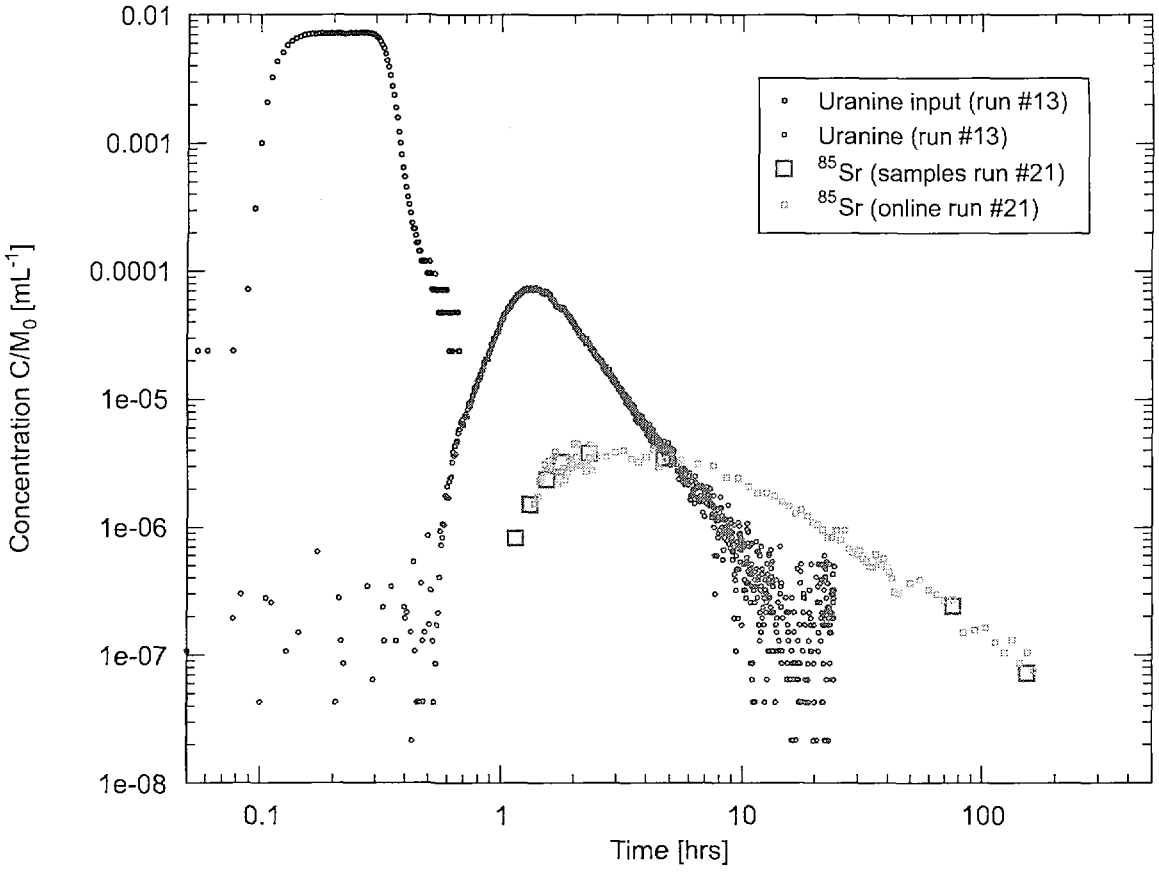

Fig. 5-2: A typical injection function for uranine, plotted with uranine and Sr breakthrough curves for dipole 1.

5.1.5 Influence of the interaction of colloids with fracture walls

Colloids are mobile in the fluid phase, but they can be immobilised as a result of processes that include mechanical filtration, sedimentation (gravitational settling), and electrochemical filtration. Fig. 5-3 shows clear evidence of immobilisation in the CRR shear zone and demonstrates its dependence on colloid size. As discussed in Chapter 6, gravitational settling and/or mechanical filtration, which have a greater effect on larger colloids, are the most likely immobilisation mechanisms operating in the experimental shear zone.

Mechanical filtration includes colloids becoming physically trapped in irregularities in the fracture surfaces, and also straining if the colloid size exceeds the fracture aperture or the pore size of infill material in fractures filled with fault gouge. These processes are insensitive to the diffusivity of the colloids, and hence their influence does not contradict the finding that diffusive processes have only a minor influence on the observed tailing in the colloid breakthrough curves. From currently available data, it is not possible either to differentiate between mechanical filtration and sedimentation, or to identify exactly what types of mechanical filtration may be occurring.

Some filtration processes may, in principle, be reversible - i.e. immobilised colloids may become detached. This would, however, be expected to result in a retardation in the breakthrough peak and a degree of tailing that also depends on colloid size. Such dependence on colloid size is not observed in Fig. 3-7. Colloid size affects the degree of recovery, but, again referring to Fig. 3-7, it does not appear to affect the tailing of the colloid breakthrough curves.

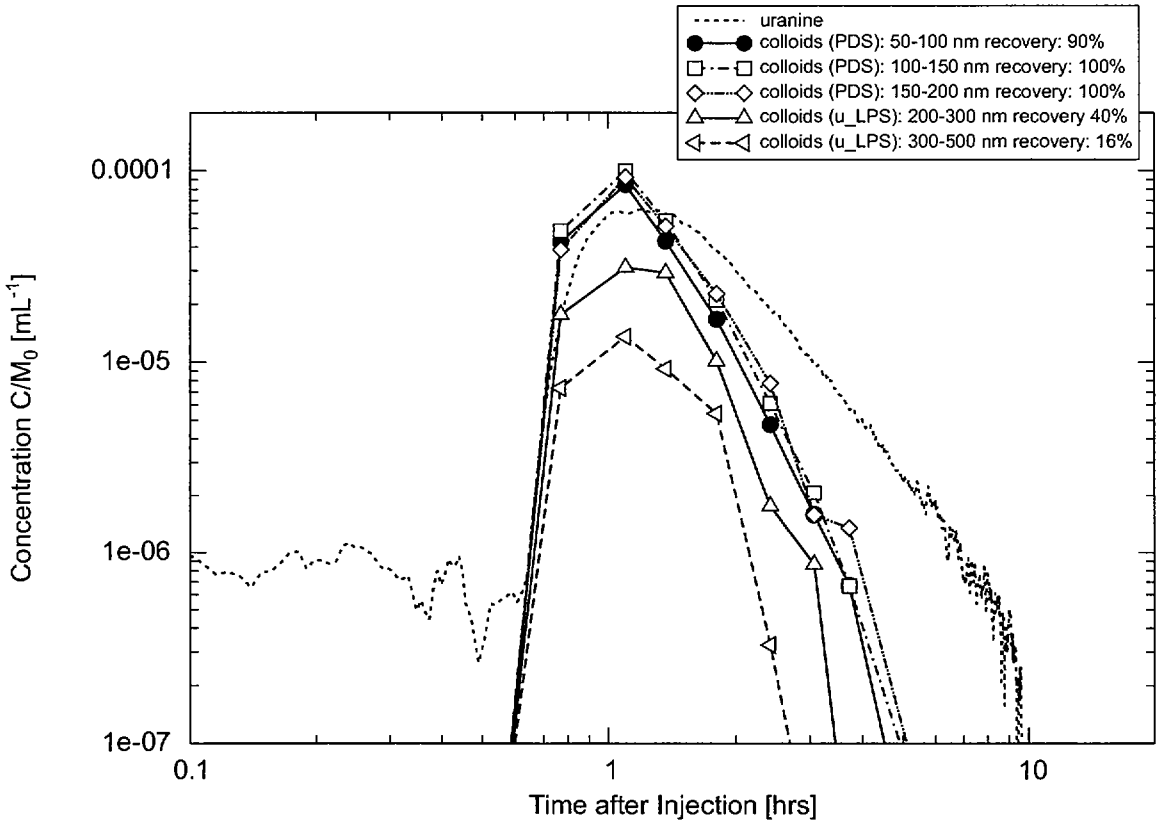

Fig. 5-3: The breakthrough data for bentonite colloids from run #6a and uranine from run #6 (without normalisation to 100 % recovery).

5.1.6 Influence of Taylor dispersion

Taylor dispersion is spreading due to the non-uniformity of flow velocity across the width of a fracture, coupled with diffusion across the fracture, which means that solutes or colloids will spend some time in the low-velocity fluid near fracture walls, and some time in the higher-velocity fluid near the centre of the fracture. If the timescale for diffusion across the fracture aperture is small compared to the timescale for advection along the fracture, then, in the absence of other processes such as matrix diffusion, Taylor dispersion results in a Gaussian breakthrough curve. If this condition is not satisfied, then the velocity profile across the fracture gives rise to a skewed breakthrough curve, with an earlier peak and longer tail. As mentioned in Section 5.1.2, the diffusion coefficient of colloids in water depends on their size, but can be orders of magnitude smaller than that of solutes. It is possible that colloids across a wide range of sizes experience much less Taylor dispersion than solutes, and that this is at least partly responsible for the observed differences in tailing. If the diffusion coefficients for colloids are such that Taylor dispersion is insignificant, then colloid size will not greatly affect the tailing resulting from the velocity profile across the fracture (there will be some effect since small

colloids can sample the very low velocities immediately adjacent to the walls). The possible effects of Taylor dispersion (or its absence) are not investigated further in the present report.

5.2 Evidence for the influence of non-Fickian dispersion on the tailing of colloid breakthrough curves

The observation that the 1-D and 2-D advection-dispersion models are not entirely satisfactory, at least for modelling colloid breakthrough in CRR, is consistent with some previous experimental studies on both solutes and colloids (e.g. Hatano and Hatano, 1998; Sidle et al., 1998; Becker and Shapiro, 2000, 2003). These studies show that advective processes in heterogeneous media can cause tailing of breakthrough curves that is not adequately described using advection-dispersion models based on a Fickian representation of dispersion. There are also more general reasons for questioning the adequacy of the Fickian representation of the dispersion. For example, studies of the breakthrough of solutes transported through geological media, interpreted using the Fickian representation of dispersion, indicate that the longitudinal dispersion length increases with the scale of the system under consideration (see, e.g., Gelhar et al. 1992). This suggests that, while such a model may, to some approximation at least, represent the shapes of breakthrough curves, the spatial distribution of the solutes along the transport paths will be in error. A more detailed study on this topic can be found in Berkowitz and Scher (1995).

The CTRW model used in the present study represents a general, physically based, approach to the quantification of non-Fickian dispersion. Berkowitz and Scher (1998) conducted numerical experiments for particle transport in 2-D networks of fractures. They could show that non-Fickian dispersion does indeed occur, resulting from subtle features of the steady flow-field distribution through the network, and there is good quantitative agreement between their simulations and the CTRW approach. Park et al. (2004) extended this approach to the investigation of particle transport in 3-D fracture networks. Transport simulations at fracture intersections showed that local flow circulations can arise from variability within the hydraulic head distribution along fracture intersections and from the internal no-flow condition along fracture boundaries. They found that local flow cells act as an effective mechanism to enhance the non-Fickian breakthrough tailing in discrete fracture networks. It was also shown that transport in such systems can be modelled by considering advection in the complex flow field using the CTRW approach. Applications of this approach to experimental systems are reported, for example, by Berkowitz et al. (2000) for laboratory flow cells containing heterogeneous porous media, and by Kosakowski et al. (2001) for a medium-scale field experiment in a fractured till.

The EP experiment, described in Ota et al. (2001), Alexander et al. (2003b) and Möri et al. (2004), focused on the detailed investigation of shear-zone structure at the GTS. It was already known that the shear zone used in CRR is highly heterogeneous (see, for example, Smith et al. 2001), and the main result of the EP core analyses was to show that open channels in water conducting features or fractures within the shear zone control tracer migration to a very high degree. Tracers were found in dead-end channels and short cuts between adjacent channels. The merging and bifurcation of transport pathways was observed on the m and cm scale. In both EP and CRR, hydraulic testing and inverse modelling also showed that the shear zone is highly heterogeneous, especially the area around dipole 1 (Smith et al., 2001, Möri, 2004).

In natural fracture networks, dead-end channels are not really "dead" in terms of fluid flow. Small pressure differences set up local flow cells and particles can advectively enter such flow cells and be delayed compared to particles not entering such low velocity zones. In general, the occurrence of low velocity regions causes a delay of some particles. From structural geological

investigations, it is known that the flow channels are partially filled with non-cohesive fault gouge material and water flow is also possible in the highly porous fault gouge material (Smith et al., 2001, Möri et al., 2004, Möri, 2004). Flow and transport processes in the open parts of the shear zone will differ completely from those in the fault gouge filled parts (Lunati et al., 2003). It can be expected that the fluid velocities, and therefore the particle velocities, are higher in the open channels than in the filled parts of the fracture. Furthermore, in the fault gouge filled parts, the transport behaviour is likely to be much smoother, with tracer fronts moving much more regularly than in open rough fractures.

By comparing the findings of EP and other tests on the CRR shear zone with the numerical investigations of Park et al. (2004), it can be inferred that the occurrence of an interconnected network of open channels in conjunction with low velocity regions (e.g. in dead-end channels) is one possible reason for the observed non-Fickian tailing of colloid breakthrough curves.

The Fickian approach to the modelling of dispersion assumes that the scales of heterogeneity affecting the flow field are small compared to the spatial dimensions of the flow field itself (i.e. an elementary volume can be defined that is representative of heterogeneity throughout the flow field). The CTRW approach, as applied in this study, assumes that the transport path in the dipole flow field can be replaced by an equivalent transport path in an uniform flow field. These assumptions are currently impossible to test given the available data, and it remains an open question whether some of the observed non-Fickian tailing is due to larger-scale heterogeneity influencing the dipole flow field.

6 Remaining problems and limitations of the current modelling approach

This chapter describes some unresolved problems associated with the CRR experiment and discusses the limitations of the modelling approaches as used in the present study. Section 6.1 describes the counter-intuitive correlation between extraction flow rate and peak arrival time, which is currently unexplained, but is probably a result of the heterogeneous characteristics of the shear zone. Section 6.2 describes the problem of non-uniqueness of the fits, i.e. different sets of parameters could, in some cases, fit particular breakthrough curves equally well. Section 6.3 discusses the filtration of colloids, which is currently not included in the modelling approaches presented here, although some inferences regarding the most likely mechanisms can be made from experimental observations. Section 6.4 discusses the possibility that non-Fickian dispersion may be an important mechanism for the transport of aqueous solutes, as well as colloids, and the implications for the interpretation of tracer transport experiments. Section 6.5 discusses various artefacts that may have arisen because of the simplified nature of the models.

6.1 Fluctuations in the experimental extraction and injection flowrates and the heterogeneous characteristics of the shear zone

As noted in Chapter 3, there is a systematic time difference of a few minutes between predicted and measured breakthrough curves. This time shift can be attributed to small changes in the experimental extraction and injection rates between the runs. For example, Fig. 6-1 shows how the extraction flow rates and the injection flow rates are related to the differences between the peak arrival time for uranine in dipole 1 and the peak of the injection function. The late arrival times for runs #1, #2 and #3 are strongly (and inversely) correlated to the injection flow rate. Peak arrival times for the other runs show a less systematic relationship to the injection flow rate, but there is an indication that, counter-intuitively, increased extraction flow rates cause later peak arrival times. This behaviour is certainly contrary to the behaviour of an ideal dipole flow field in a homogeneous aquifer, but similar findings have also been described in Guimerà and Carrera (2000). Possible explanations are related to the spatial heterogeneity of the shear zone (see also Chapter 5) or the influence of the hydraulic boundary conditions (e.g. flow field around the tunnel, regional hydraulic gradients).

6.2 Non-uniqueness of the fitted model parameters

Some of the model parameters were set using information from the experimental set-up (e.g. the dipole length, the injection concentrations) and information from independent sources (e.g. sorption parameters). It was not, however, possible to make model predictions purely on the basis of such information. The models had to be calibrated against preliminary tests using curve-fitting procedures. Due, however, to the number of parameters to be calibrated, the limited duration and accuracy of the experiments and the fact that the models provide a highly simplified representation of the actual shear zone system, not all parameters could be uniquely determined in this way. Different sets of parameters could, in some cases, fit particular breakthrough curves equally well. Thus, for example, it was possible to set only a lower bound to the effective matrix thickness, and the single fracture representation of the shear zone and the multiple (four) fracture representation were equally successful in fitting the breakthrough curves.

The latter observation may be understood by considering that, in the absence of retardation processes, the main parameter influencing advective transport is the (mean) fluid velocity. In the

case of the dipole experiments, the volume flow rates through the system are fixed by the injection and extraction flow rates. For such experimental conditions, the fluid velocity in the idealised shear zone depends only on the sum of the fracture apertures. The velocity field in a single fracture of aperture $2b$ is identical to that in a system of four fractures with apertures $2b/4$. Matrix diffusion is a more effective retardation process for a system of four narrower fractures, compared to a single broad fracture. It is, however, relatively easy to adjust the value of the porosity of the matrix rock or the diffusion coefficient (see Eq. 2-2 to 2-4) to compensate for the change in the fracture aperture without changing the quality of the fit. Changes in the matrix porosity also give rise to changes in the (fitted) sorption coefficients. Of course not all combinations of porosity, diffusivity and fracture aperture are possible. All parameters should be reasonable and in the range defined by additional information.

The transmissivity of the system of four narrower fractures is different to that of a single broader fracture. For a given flowrate, this will lead to a different pressure difference between the injection and extraction boreholes in the two conceptualisations. In principle, the measurement of the actual pressure difference could be used to discriminate between the conceptualisations. In practice, however, such discrimination would require a reliable theoretical relationship between transmissivity and aperture. For flow between parallel plates, the so-called "cubic law" can be used (Witherspoon et al. 1980), but this relationship generally fails to hold for the heterogeneous fractures found in geological systems. It was shown by Meier et al. (2001) that the shear zone used in CRR is hydraulically highly heterogeneous and that it is not possible to model the hydraulic behaviour of the shear zone (and hence derive the aperture and number of fractures appropriate for the transport modelling) based on current hydraulic information.

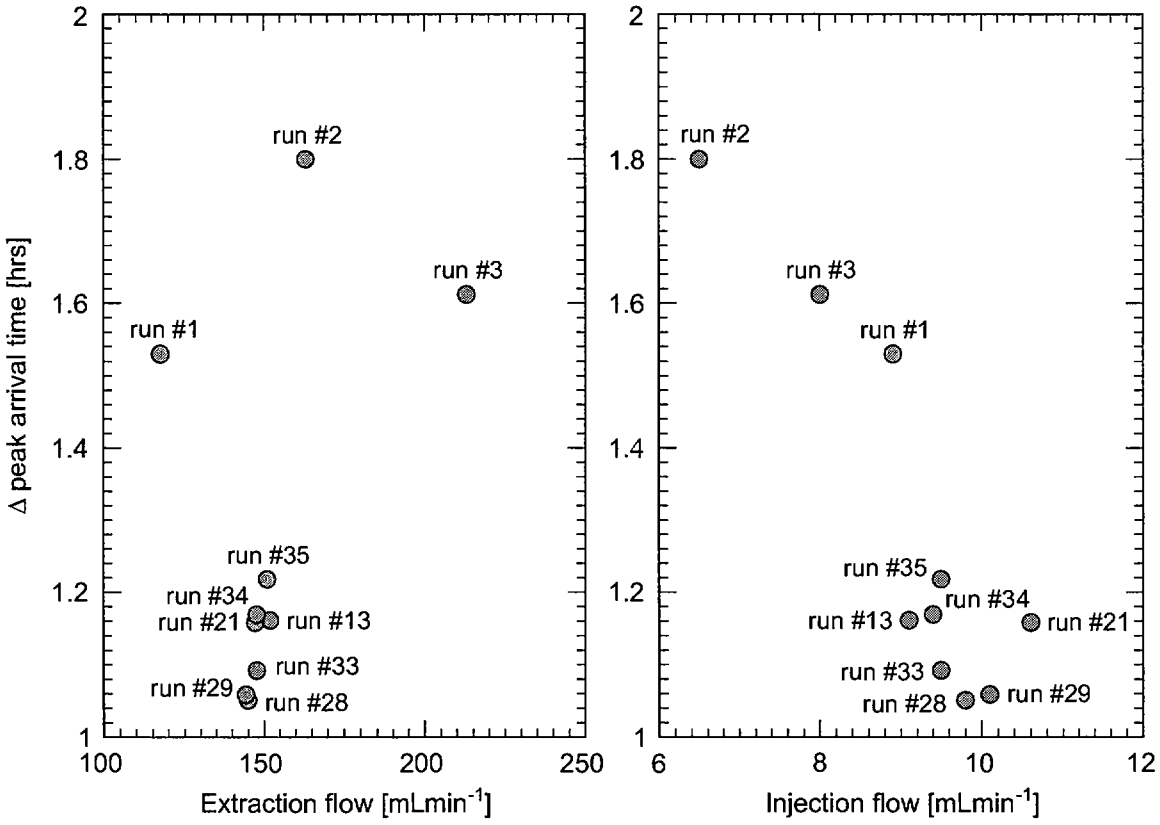

Fig. 6-1: Correlation between extraction flow rate, injection flow rate and peak arrival time for uranine in dipole 1.

6.3 Filtration of colloids

The models used in the present study did not address the issue of colloid immobilisation or filtration during transport. There are, however, clear indications that filtration of larger colloids took place in the CRR *in situ* tests. Fig. 5-3 shows the breakthrough data for colloids of different size fractions, as well as for uranine, indicating the loss of colloids for each size fraction.

The recoveries for the different colloid size classes in Fig. 5-3 decrease systematically with increasing size. PDS measurements for the three smallest colloid size classes yield recoveries of 90 % or more, whereas particles in larger size classes yield lower recoveries.

As discussed in Chapter 5, immobilisation of colloids can occur as a result of mechanical filtration (straining), sedimentation (gravitational settling), and electrochemical filtration. Electrochemical filtration does not explain the observation that it is the larger particles that are immobilised to the greatest extent; James and Chrysikopoulos (1999, 2000) showed that this mechanism would lead to the smallest particles being preferentially deposited onto the fracture walls. Furthermore, at the high pH (~9.6) of the Grimsel groundwater, bentonite colloids, as well as natural groundwater colloids and the rock surfaces, possess a negative surface charge and the attachment of colloids to the rock surface is not favoured electrostatically (Degueldre et al., 1996). The short mean residence time of the bentonite colloids in the shear zone due to the high fluid velocities during the tracer tests also minimises the probability of interactions between colloids and fracture surfaces. Gravitational settling and/or mechanical filtration (straining) are, however, both possible immobilisation mechanisms.

6.4 The possibility of non-Fickian dispersion of solutes

As shown in Chapter 3, it was possible to fit successfully the breakthrough curves of both conservative and sorbing tracers that are transported in the aqueous phase with the advection-dispersion (-matrix diffusion) model already used in MI. Nevertheless, given the evidence for non-Fickian dispersion of colloids (Section 5.2), it seems reasonable to suppose that tracers in the aqueous phase may also be affected by non-Fickian dispersion. Non-Fickian dispersion is unlikely to account fully for the form of all the breakthrough curves; the breakthrough data for Sr in Fig. 3-4 shows the typical behaviour normally associated with matrix diffusion, namely the $t^{-3/2}$ slope of the tail (see Section 2.3, Eq. 2-5, and also e.g. Tsang, 1995; Hadermann and Heer, 1996; Jakob, 1997). Some impact of non-Fickian dispersion cannot, however, be discounted, although the breakthrough curves of sorbing and non-sorbing aqueous-phase tracers were not fitted using the CTRW model, because matrix diffusion effects have not, as yet, been incorporated. Indeed, the fact that the tailing of the breakthrough curves for colloids and conservative tracers is so similar in the experiments in dipole 3 suggests that non-Fickian dispersion is an important contributory process to the tailing of both, at least over the duration of the experiments. The retardation of the conservative solutes compared to the colloids, visible in the differences between the early time concentrations and the peak arrival times, indicates that matrix diffusion is affecting the shape of the breakthrough curves too, although, as discussed in Section 5.1.6, effects related to differences in Taylor dispersion between colloids and solutes cannot be discounted as a factor that also contributes to these observations.

6.5 Artefacts associated with model simplifications

The sorption coefficient for Sr has been obtained by fitting the advection-dispersion models to the breakthrough curves for run #21 (see Tab. 3-2). If part of the tailing attributed in these fits to matrix diffusion is in fact caused by non-Fickian dispersion, then the sorption coefficient may

have been underestimated - i.e., in reality, there may have been less matrix diffusion, but higher sorption in the porous rock matrix.

The overestimation of matrix diffusion (and the associated underestimation of sorption) is a possible partial explanation[27] for the differences between distribution coefficients measured in the laboratory and distribution coefficients extracted from the field experiments in the case of Sr.

A related artefact associated with the modelling of a complex heterogeneous system as a set of parallel fractures is that the effective fracture surface available for matrix diffusion might be underestimated. In a fracture network, the available surface is much larger than in a set of parallel fractures with the same hydraulic transmissivity. In local flow cells, the fluid velocity is smaller and any solutes entering such slow velocity zones have more time to diffuse into the matrix.

All of these effects, i.e. non-Fickian dispersion, different time constants characterising matrix diffusion in slow velocity regions, and a possible underestimation of the available surface area for matrix diffusion, have to be compensated by an appropriate choice of values for the fitting parameters (fracture aperture/effective surface area, fluid velocity, matrix porosity, pore diffusion coefficient for matrix diffusion and sorption coefficients in the matrix) when fitting the breakthrough curves with a matrix diffusion model utilising a parallel planar representation of fractures.

[27] In addition, Bradbury and Baeyens (2003) showed that sorption coefficients measured in laboratory experiments can differ by factors of about 5 from those applicable *in situ* due to scaling effects, experimental procedures or mineralogical variability.

7 Conclusions

7.1 General

This document has described modelling work by PSI to analyse *in situ* experiments carried out at the GTS within the framework of the CRR (see overview in Alexander et al., 2004). The modelling work took as its starting point earlier modelling carried out by PSI in the context of the MI project, and developed and modified the earlier models to take account of the effects of bentonite colloids added to the experimental injection cocktails. A number of alternative modelling approaches were developed for some aspects of the system. In some cases, it was possible to make model predictions in advance of particular experimental runs in order to check the feasibility of the planned experiments. The fitting of models to the experimental breakthrough data and the prediction of experimental breakthrough in advance of the main experimental runs enabled modelling hypotheses to be tested and improvements in the models to be made. The work has certain implications for safety assessment that are discussed at the end of this chapter.

7.2 Aqueous phase transport

The modelling work described in this report showed that it is possible to fit the breakthrough curves of both conservative and sorbing tracers that are transported in the aqueous phase successfully with the conceptual model developed during MI and utilising an advection-dispersion (-matrix diffusion) conceptual model developed during MI (see, however, Section 7.5).

7.3 Colloid-facilitated radionuclide transport

The CRR experiment and the modelling work described in this report show that, in the *in situ* tests with bentonite colloids added to the injection cocktail:

- Am, Pu, Th are transported principally in association with colloids, and
- Cs is also transported in part in association with colloids, although the main part of the injected inventory is transported in solution.

Furthermore, some radionuclide tracers, namely Am, Pu, and Th (and also Tb and Hf) are transported in colloidal form, even when no bentonite colloids are added to the injection cocktail. The addition of bentonite colloids, however, increases the recovery of these tracers.

Colloids showed little or no retardation during transport - there was a marked similarity between the breakthrough of colloids and that of a conservative tracer, although the peak breakthrough for colloids occurred slightly earlier. Hydrodynamic chromatography, the differential retardation of colloids according to their size, was not observed. Some colloids were, however, filtered during transport. The dependence of the degree of filtration on colloid size, with more filtration of larger colloids, suggests that gravitational settling and/or mechanical filtration are the most likely immobilisation mechanisms.

7.4 1-D vs. 2-D modelling of the breakthrough curves

The 1-D and 2-D advection-dispersion models with matrix diffusion provided similarly good fits to the breakthrough curves of tracers conveyed as aqueous solutes. This is because the experiments were conducted in a narrow dipole, with a nearly radial convergent flow field around the withdrawal well and most of the injected tracer following a nearly direct line from the injection to the withdrawal well. In such a flow field, the effect of the width of the flow field is minimised, and a single, 1-D transport path adequately describes the system.

7.5 Non-Fickian dispersion

The experiments showed a significant tailing in the breakthrough of colloids, as well as that of conservative and sorbing tracers. The tailing of the breakthrough curves of tracers transported as aqueous species is generally attributed to a mixture of hydrodynamic dispersion and matrix diffusion. In the case of colloids, an advection-dispersion model with matrix diffusion, where dispersion is modelled as a Fickian process, can reproduce the shape of the observed breakthrough curves, but not with a consistent set of parameters. A number of other possible explanations for the tailing of the breakthrough data for colloids have been reviewed, and it has been shown that non-Fickian dispersion (possibly in conjunction with effects related to the velocity profile across fractures - see Section 5.1.6) is the most likely cause. In the case of solutes, the possibility of non-Fickian dispersion also exists, but, in the present study, it has not been possible to discriminate between the impact of non-Fickian dispersion of solutes and matrix diffusion effects on the shape of the breakthrough curves. The topic of non-Fickian dispersion is currently under further investigation at PSI (e.g. Kosakowski, 2004).

One possible way to differentiate the effects of non-Fickian dispersion and matrix diffusion would be to conduct transport experiments with the simultaneous injection of, for example, bentonite colloids (or other tracers that can be assumed not to diffuse into the porous rock matrix), together with two or more conservative tracers that are expected to undergo matrix diffusion. The conservative tracers should have pore diffusion coefficients in the porous matrix that are different to each other, and have been quantified e.g. from the results of independent experiments. Information on pore diffusion coefficients was unfortunately not available for uranine and I in the CRR experiments. Evaluation of such experiments would allow the quantification of the impact of non-Fickian dispersion on the transport of solutes, and may provide further evidence for non-Fickian dispersion of colloids.

7.6 Implications for safety assessment

The models used in the present study are highly simplified representations of reality, and may only be applicable, or "valid", over the spatial and temporal scales of the CRR experiments. The main limitation lies in the assumption that the fraction of a tracer that is bound to colloids remains constant during migration - i.e. there is no further sorption of radionuclides to (or desorption from) colloids. For the relatively short transport times of the colloids in these experiments, it may be reasonable to assume that sorption on and/or desorption from bentonite colloids is sufficiently slow that it can be neglected. For repository safety assessment, on the other hand, the relevant transport times are much longer and this assumption may not hold.

The modelling approach used in the present study may therefore not be directly applicable to safety assessment problems and the direct implications of the results of this study for safety assessment are limited. It can, however, be said that the study has demonstrated the high degree of mobility of bentonite and other colloids in a system that is at least in some ways comparable to those of interest in safety assessment, and has shown that bentonite colloids can *at least*

potentially affect the transport of some safety relevant radionuclides over longer temporal and spatial scales than those addressed here. It has also shown that parameters for safety assessment (and especially sorption coefficients) derived by fitting field tracer transport experiments using advection-dispersion models based on Fickian dispersion with matrix diffusion need to be viewed with caution.

For these reasons, future experiments conducted over longer time scales using flow velocities that are closer to the slow, unperturbed velocities expected in a repository host rock would certainly be beneficial. This would possibly allow more pronounced effects of processes such as colloid filtration, the desorption of radionuclides from colloids and matrix diffusion of solutes to be observed. Other processes such as non-Fickian dispersion may become less important in their effects on breakthrough curves as timescales increase. Transport tests in natural flow fields with low flow velocities would be a good opportunity to apply and test, under realistic conditions, the conceptual models which were successfully applied in this study.

8 Acknowledgements

The authors thank Res Möri for many helpful discussions, and Andreas Jakob and Ralph Mettier for useful comments and various corrections. Special thanks go to Paul Reimus for his careful review, which resulted in several improvements to the report. Thomas Fierz, Claude Degueldre, Horst Geckeis and Tiziana Missana kindly provided the data from the CRR experiments. The CRR project is conducted in the framework of Phase V of the Grimsel Test Site investigations and the funding partners, ANDRA (France), ENRESA (Spain), FZK-INE (Germany), JNC (Japan), Nagra (Switzerland), and USDOE/SNL (USA), are thanked for their collaboration in this study.

This work reported here was partially funded by NAGRA.

9 References

ALEXANDER, W.R., BRADBURY, M.H., MCKINLEY, I.G., HEER, W., EIKENBERG, J. & FRICK U., 1992. The current status of the radionuclide migration experiment at the Grimsel underground rock laboratory. Sci. Basis Nucl. Waste Manag. XV, 721-728.

ALEXANDER, W.R., FRIEG, B., OTA K. & BOSSART P. 1996. The RRP Project: Investigating Radionuclide Retardation in the Host Rock. Nagra Bulletin No. 27 (June, 1996), 43-55, Nagra, Wettingen, Switzerland.

ALEXANDER, W.R., SMITH, P.A. & MCKINLEY, I.G., 2003a. Modelling radionuclide transport in the geological environment: a case study from the field of radioactive waste disposal. Ch.5 *in* E.M.Scott (*ed*), Modelling Radioactivity in the Environment, Elsevier, Amsterdam, The Netherlands.

ALEXANDER, W.R., OTA, K. & FRIEG, B., *(eds)* 2003b. The Nagra-JNC *in situ* study of safety relevant radionuclide retardation in fractured crystalline rock II: the RRP project methodology development, field and laboratory tests. Nagra Technical Report Series NTB 00-06, Nagra, Wettingen, Switzerland.

ALEXANDER, W.R., MÖRI A. & SMITH, P.A., 2004. The CRR final project report series: 4 – project overview and synthesis of results. NTB 03-04, Nagra, Wettingen, Switzerland.

BARTEN, W., 1996. Linear response concept combining advection and limited rock matrix diffusion in a fracture network transport model. Wat. Resour. Res., 32, 3285-3296.

BARTEN, W. & ROBINSON, P. C., 2001. Contaminant transport in fracture networks with heterogeneous rock matrices: The PICNIC code. PSI Report 01-02, Paul Scherrer Institute, Villigen, Switzerland.

BEAR, J., 1972. Dynamics of fluids in porous media. Elsevier, New York.

BECKER, M.W. & SHAPIRO, A. M., 2000. Tracer transport in fractured crystalline rock: Evidence of nondiffusive breakthrough tailing. Wat. Resour. Res., 36, 1677-1686.

BECKER, M. W. & SHAPIRO, A. M., 2003. Interpreting tracer breakthrough tailing from different forced-gradient tracer experiment configurations in fractured bedrock. Wat. Resour. Res., 39, 1024,

BERKOWITZ, B., KOSAKOWSKI, G., MARGOLIN, G. & SCHER, H., 2001. Application of Continuous Time Random Walk theory to tracer test measurements in fractured and heterogeneous porous media. Ground Water, 39, 593-604.

BERKOWITZ, B. & SCHER, H., 1995. On characterization of anomalous dispersion in porous and fractured media. Wat. Resour. Res., 31, 1461-1466.

BERKOWITZ, B. & SCHER, H., 1998. Theory of anomalous chemical transport in fracture networks. Phys. Rev. E, 57(5), 5858-5869.

BERKOWITZ, B., SCHER, H. & SILLIMAN, S. E., 2000. Anomalous transport in laboratory-scale, heterogeneous porous media: on characterization of anomalous dispersion in porous and fractured media. Wat. Resour. Res., 36, 149-158, (with a minor correction, published in Wat. Resour. Res., 36, 1371).

BOSSART, P. & MAZUREK, M. (1990) Grimsel Test Site – structural geology and water flowpaths in the migration shear zone. Nagra Technical Report NTB 91-12, Nagra, Wettingen, Switzerland.

BRADBURY, M. & BAEYENS, B., 2003. Near-field sorption data bases for compacted MX-80 bentonite for performance assessment of a high-level radioactive waste repository in Opalinus Clay host rock. PSI Bericht 03-07, Paul Scherrer Insitute, Villigen, Switzerland.

DEGUELDRE, C., LONGWORTH, G., MOULIN, V., VILKS, P., ROSS, C., BIDOGLIO, G., CREMERS, A., KIM, J., PIERI, J., RAMSAY, J., SALBU, B. & VUORINEN, U., 1990. Grimsel Test Site – Grimsel colloid exercises: An international intercomparison exercise on the sampling and characterization of groundwater colloids. Nagra Technical Report NTB 90-01, Nagra, Wettingen, Switzerland.

DEGUELDRE, C. GRAUER, R., LAUBE, A., OESS, A. & SILBY, H., 1996. Colloid properties in granitic groundwater systems. II: Stability and transport study. Appl. Geochem., 11, 697-710.

DEGUELDRE, C. & LAUBE, A., 2000. Bentonite colloid migration in a granitic fracture at the Grimsel Test Site. Unpubl. internal Technical Report TM-44-00-07, Paul Scherrer Institute, Villigen, Switzerland.

DE MARSILY, G., 1986. Quantitative Hydrogeology: Groundwater Hydrology for Engineers. Academic Press, New York, USA.

FRICK, U., ALEXANDER, W.R., BAEYENS, B., BOSSART, P., BRADBURY, M.H., BÜHLER, CH., EIKENBERG, J., FIERZ, TH., HEER, W., HOEHN, E., MCKINLEY, I.G. & SMITH, A., 1992. Grimsel Test Site – The Radionuclide Migration Experiment: Overview of investigations 1985-1990. Nagra Technical Report NTB 91-04, Nagra, Wettingen, Switzerland.

GELHAR, L. W., 1987. Applications of stochastic models to solute transport in fractured rocks. SKB Technical Report 87-05, SKB, Stockholm, Sweden.

GELHAR, L.W., WELTY, C. & REHFELDT, K.R. (1992): A critical review of data on field-scale dispersion in aquifers. Wat. Resour. Res., 28, 1955-1974.

GUIMERÁ, J. & CARRERA, J., 2000. A comparison of hydraulic and transport parameters measured in low-permeability fractured media. J. Contam. Hydrol, 41, 261-281.

GUIMERA, J., KOSAKOWSKI, G., IIJIMA, K., PUDEWILLS, A. & SMITH, P.A. (2004): The CRR final project report series: III - results of the supporting modelling programme. Nagra Technical Report NTB 03-03, Nagra, Wettingen, Switzerland.

HADERMANN, J., & HEER, W., 1996. The Grimsel (Switzerland) migration experiment: integrating field experiments, laboratory investigations and modelling. J. Contam. Hydrol,, 21, 87-100.

HATANO, Y. & HATANO, N., 1998. Dispersive transport of ions in column experiments: An explanation of long-tailed profiles. Wat. Resour. Res., 34(5), 1027-1033.

HAUSER, W., GECKEIS, H., KIM, J.I. & FIERZ, TH., 2002. A mobile laser-induced breakdown detection sytem and its application for the in situ-monitoring of colloid migration. Coll. Surf., A 203, 37-45.

HEER, W. & HADERMANN, J., 1996. Modelling Radionuclide Migration Field Experiments. PSI Report 94-13, Paul Scherrer Institute, Villigen, Switzerland, Nagra Technical Report 94-18, Nagra, Wettingen, Switzerland.

HSK, 1998. Unpublished internal note. HSK, Villigen, Switzerland.

JAKOB, A., 1997. Modelling solute transport using the double porous medium approach. In: Grenthe, I., Puigdomenech, I. (*eds*), Modelling in Aquatic Chemistry. OECS/NEA, Paris, France.

JAMES, S.C. & CHRYSIKOPOULOS, C.V., 1999. Transport of polydisperse colloid suspensions in a single fracture. Wat. Resour. Res., 35, 707-718.

JAMES, S.C. & CHRYSIKOPOULOS, C.V., 2000. Transport of polydisperse colloids in a saturated fracture with spatially variable aperture. Wat. Resour. Res., 36, 1457-1465.

KOLDITZ, O., HABBAR, D., KAISER R., ROTHER T. & THORENZ, C., 1999. RockFlow - Theory and Users Manual. Release 3.4, Institut für Strömungsmechanik und Elektr. Rechnen im Bauwesen, Universität Hannover.

KOSAKOWSKI, G. & BAEYENS, B., 2001. Sorption capacity of FEBEX bentonite and natural groundwater colloids. Unpublished internal Report AN-44-01-19, Paul Scherrer Institute, Villigen, Switzerland.

KOSAKOWSKI, G., BERKOWITZ, B. & SCHER, H., 2001. Analysis of field observations of anomalous transport in a fractured till. J. Contam. Hydrol, 47, 29-51.

KOSAKOWSKI, G., 2004. Anomalous transport of colloids and solutes in a shear zone. J. Contam. Hydrol, 72, 23-46, doi: 10.1016/j.jconhyd.2003.10.005.

LUNATI, I., KINZELBACH, W., SØRENSEN, I., 2003. Effects of pore volume-transmissivity correlation on transport phenomena. J. Contam. Hydrol, 67, 195-217.

MCKINLEY, I. G., ALEXANDER, W. R., BAJO, C., FRICK, U., HADERMANN, J., HERZOG, F. A. & HOEHN, E., 1988. The Radionuclide Migration Experiment at the Grimsel Rock Laboratory, Switzerland, Sci. Basis Nucl. Waste Manag. XI, 179-187.

MEIER, P. M., MEDINA, A. & CARRERA, J., 2001. Geostatistical inversion of cross-hole pumping tests for identifying preferential flow channels within a shear zone, Ground Water, 39, 10-17.

MISSANA, T. & GECKEIS, H., *(eds)* (2004): The CRR final project report series: 2 - results of the supporting laboratory programme. Nagra Technical Report NTB 03-02, Nagra, Wettingen, Switzerland.

MÖRI, A., 2001. Radionuclide Retardation Project at the GTS - An overview of lessons learned and ongoing experiments. In: Svensk Kärnbränslehantering, First TRUE Stage - Transport of solutes in an interpreted single fracture. Proceedings from the 4th International Seminar Äspö, September 9-11, 2000. SKB Technical Report TR-01-24, 181-201, Swedish Nuclear Fuel and Waste Management Co, Stockholm, Sweden.

MÖRI, A., ALEXANDER, W. R., GECKEIS, H., HAUSER, W., SCHÄFER, T., EIKENBERG, J., FIERZ, TH., DEGUELDRE, C. & MISSANA, T., 2003. The colloid and radionuclide retardation experiment at the Grimsel Test Site: influence of bentonite colloids on radionuclide migration in a fractured rock. Coll. Surf. A: Physicochemical and Engineering Aspects, 217 (1-3), 33-47.

MÖRI, R., FRIEG, B., OTA, K. & ALEXANDER W.R., 2004. The Nagra-JNC *in situ* study of safety relevant radionuclide retardation in fractured crystalline rock III: the RRP project final report. Nagra Technical Report NTB 00-07 *(in prep)*, Nagra, Wettingen, Switzerland.

MÖRI, A. *(ed)* 2004: The CRR final project report series: 1 - description of the field phase - methodologies and raw data. Nagra Technical Report NTB 03-01. Nagra, Wettingen, Switzerland.

OTA, K., ALEXANDER, W. R., SMITH, P. A., MÖRI, A., FRIEG, B., FRICK, U., UMEKI, H., AMANO, K., COWPER, M. M. & BERRY, J. A., 2001. Building confidence in radionuclide transport models for fractured Rock: The Nagra/JNC Radionuclide Retardation Programme. Sci. Basis Nucl. Waste Manag. XXIV, 1033-1041.

PATE, S.M., MCKINLEY, I.G. & ALEXANDER, W.R. (1994) Use of natural analogue test cases to evaluate a new performance assessment TDB. CEC Report EUR15176EN, Brussels, Belgium.

PARK, Y.-J., LEE, K.-K., KOSAKOWSKI, G. & BERKOWITZ, B., 2003. Effects of fracture intersection characteristics on transport in three-dimensional fracture networks. Wat. Resour. Res. 39, 1215-1224.

SIDLE, C.R., NILSSON, B., HANSEN, M. & FREDERICIA, J., 1998. Spatially varying hydraulic and solute transport characteristics of a fractured till determined by field tracer tests. Funen, Denmark. Wat. Resour. Res., 34(10), 2515-2527.

SKB, 1999. Deep Repository for Spent Nuclear Fuel, SR 97 - post-closure safety. SKB Technical Report TR-99-06, Stockholm, Sweden.

SMITH, P. A., ALEXANDER, W. R., HEER, W., FIERZ, T. MEIER, P. M., BAEYENS, B., BRADBURY, M. H., MAZUREK, M. & MCKINLEY, I. G., 2001. The Nagra-JNC in situ study of safety relevant radionuclide retardation in fractured crystalline rock I: Radionuclide Migration Experiment – Overview 1990-1996, Nagra Technical Report NTB 00-09, Nagra, Wettingen, Switzerland.

TSANG, Y. W., 1995. Study of alternative tracer tests in characterizing transport in fractured rocks. Geophys. Res. Lett., 22, 1421-1424.

UMEKI, H., HATANAKA, K., ALEXANDER, W.R., MCKINLEY, I.G. & FRICK, U. (1995) The Nagra/PNC Grimsel Test Site radionuclide migration experiment: rigorous field testing of transport models. Sci. Basis Nucl. Waste Manag. XVIII, 427-434.

WINBERG, A., ANDERSSON, P., HERMANSON, J., BYEGÅRD, J., CVETKOVIC, V. & BIRGERSSON, L., 2000. Äspö Hard rock Laboratory, Final report of the first stage of the tracer retention understanding experiments. SKB Technical Report TR-00-07, SKB, Stockholm, Sweden.

WITHERSPOON, P.A., WANG, J.S.Y., IWAI, K. & GALE, J.E, 1980. Validity of cubic law for fluid flow in a deformable rock fracture. Wat. Resour. Res., 16, 1016-1024.

Paul Scherrer Institut, 5232 Villigen PSI, Switzerland
Tel. +41 (0)56 310 21 11, Fax +41 (0)56 310 21 99
www.psi.ch